Frequency and Voltage Control of a Grid of Microgrids

by

Baheej Alghamdi

A thesis
presented to the University of Waterloo
in fulfillment of the
thesis requirement for the degree of
Doctor of Philosophy
in
Electrical and Computer Engineering

Waterloo, Ontario, Canada, 2021

Examining Committee Membership

The following served on the Examining Committee for this thesis. The decision of the Examining Committee is by majority vote.

Supervisor:	Claudio Cañizares Professor, Department of Electrical and Computer Engineering, University of Waterloo
Internal Member:	Kankar Bhattacharya Professor, Department of Electrical and Computer Engineering, University of Waterloo
Internal Member:	John Simpson Adjunct Assistant Professor, Department of Electrical and Computer Engineering, University of Waterloo
Internal-External Member:	Roydon Fraser Professor, Department of Mechanical and Mechatronics Engineering, University of Waterloo
External Examiner:	Amir Yazdani Professor, Department of Electrical, Computer, and Biomedical Engineering, Ryerson University

Author's Declaration

I hereby declare that I am the sole author of this thesis. This is a true copy of the thesis, including any required final revisions, as accepted by my examiners.

I understand that my thesis may be made electronically available to the public.

Abstract

The rapid proliferation of Distributed Energy Resources (DERs) in recent years has resulted in significant technical challenges for power system operators and planners, mainly due to the particular characteristics of some of these systems that are interfaced with converters that alter the dynamic behavior of typically power systems. To accommodate the increasing penetration of DERs in power systems, microgrids have been formed to facilitate their integration. The operation of these microgrids could be further enhanced by interconnecting them to satisfy the overall system demand, and improve their stability if suitable control schemes are implemented. The control of microgrids has been extensively studied; however, coordinated operation, dynamics, and control of a grid that includes interconnected microgrids have not been sufficiently addressed in the literature, and thus this is the focus of this thesis.

In the first stage of the thesis, a new microgrid interface based on Virtual Synchronous Generators (VSGs) is proposed to control the power exchange of interconnected ac and dc microgrids, and provide frequency support, voltage regulation, and virtual inertia for individual microgrids and the host grid as required, to improve both frequency and voltage dynamics for the overall system. Thus, a hierarchical distributed control technique is proposed, where the primary control of interfacing VSGs provides adaptive inertia for the ac systems, while a secondary distributed control of the system regulates the frequency and the voltages of the host grid and the interconnected microgrids, based on a consensus technique with limited information about the overall system. The proposed controller shares the total system load among the grid and microgrids, while minimizing the overall frequency and voltage deviations in all interconnected systems. The proposed interface and the controller are implemented, tested, and validated in detailed simulations for a grid-of-microgrids system.

In the second stage of the thesis, an adaptive active power droop controller and voltage setpoint control in isolated microgrids for optimal frequency response and stability after disturbances is first proposed and presented, and then applied to the coordinated control of interconnected microgrids. The control scheme involves an optimal and model predictive control approach, which continuously adjusts the active power droop gains and the voltage setpoints of Distributed Energy Resources (DERs) to maintain the frequency of the system within acceptable limits, and enhance the primary frequency response of the system, while taking into account the active power sensitivity of the microgrid loads to the system's operating voltage. The proposed approach is also implemented, tested, validated, and compared via detailed simulations in a microgrid benchmark system and the developed grid-of-microgrids test system.

The results demonstrate that the proposed VSG controlled interfaces limit severe frequency deviations during disturbances, and allow proper power sharing among the microgrids without causing significant power transients for the ac/dc systems, compared to existing techniques. Furthermore, the proposed secondary distributed and centralized frequency and voltage controllers maintain the power balance of the interconnected systems and regulate the microgrids' frequencies and dc voltages to nominal values, compared to conventional frequency controllers; however, the distributed control approach shows better overall frequency and dc-voltage dynamics and regulation than the centralized control approach.

Acknowledgements

I would like to express my sincere gratitude to Professor Claudio A. Cañizares for his guidance, patience, and support throughout my PhD studies. It has been a great honor for me to have completed my research under his supervision, where I have learned many valuable skills that will help me in my academic career.

I would like to acknowledge the following members of my PhD thesis Examination committee for their valuable comments and input: Professor Kankar Bhattacharya from the Electrical and Computer Engineering Department at the University of Waterloo; Professor Roydon Fraser from the Mechanical and Mechatronics Engineering Department at the University of Waterloo; Professor John Simpson from the Electrical and Computer Engineering Department at the University of Waterloo; and Professor Amir Yazdani from the Department of Electrical, Computer, and Biomedical Engineering at Ryerson University.

I wish to acknowledge King Abdulaziz University, the Saudi Government, and NSERC for fully funding my PhD studies at the University of Waterloo.

Table of Contents

List of Tables

List of Figures

Nomenclature

Chapter 2

α_{P_l}	Active power load exponent
α_{Q_l}	Reactive power load exponent
Δf	System frequency deviation (Hz)
ΔP_L	Change in the system's demand (pu)
ΔP_V	Change in the voltage dependent loads demand (pu)
ω_{PLL}	Angular frequency obtained from the PLL (rad/s)
ω_{SG}	Angular velocity of diesel generator (rad/s)
ω_{VSG}	Angular velocity of the VSG (rad/s)
θ_R	Virtual rotor angle (rad)
C_f	Inverter output filter capacitor (F)
D	VSG Damping constant (s)
d	Duty cycle of dc DERs
D_{SG}	Damping coefficient of the diesel generator (s)
E_d	Virtual internal field voltage (pu)
f_o	Nominal frequency (Hz)
I_d	d-component of the VSG output current (pu)

I_q q-component of the VSG output current (pu)

J Moment of Inertia (s^2)

K_V Droop parameter of voltage control (pu)

K_{I_I} Integral gain of VSC current control loop

K_{I_Q} AVR Integral gain

K_{I_V} Integral gain of VSC voltage control loop

$K_{I_{Fs}}$ Centralized frequency control integral gain

$K_{I_{Vs}}$ Centralized voltage control integral gain

K_{LP_l} Load scaling factors for active power demand

K_{LQ_l} Load scaling factors for reactive power demand

K_{P_I} Proportional gain of VSC current control loop

K_{P_Q} AVR Proportional gain

K_{P_V} Proportional gain of VSC voltage control loop

$K_{P_{DER}}$ DER Droop coefficient (pu)

$K_{P_{Fs}}$ Centralized frequency control proportional gain

$K_{P_{Vs}}$ Centralized voltage control proportional gain

L_f Inverter output filter inductance (H)

M_{DER} Inertia coefficient of the diesel generator (s^2)

P_o VSG reference power (pu)

P_{DER_o} DER nominal power (pu)

P_{DER_s} Reference value of active power for centralized frequency control (pu)

P_e Output power of the VSG (pu)

P_{gov} Input power obtained from the virtual governor (pu)

P_{SG_m} Mechanical input power into the diesel generator (pu)

P_{SG} Electrical output power the diesel generator (pu)

Q_o VSG reference reactive power (pu)

Q_{DER_s} Reference value of reactive power for centralized voltage control (pu)

Q_{out} VSG reactive power output (pu)

R_f Inverter output filter resistance (Ω)

R_s Virtual Synchronous Resistance (pu)

V_o Reference terminal voltage (pu)

V_{dc} DC microgrid voltage (V)

V_{out} VSG output voltage (pu)

X_s Virtual Synchronous Reactance (pu)

Chapter 3

ΔI_i Local control signal tracking ΔI_{ref} (pu)

ΔI_j Output currents of neighbouring DERs communicated to the local DER i (pu)

ΔI_{ref} Reference current to be used in the inner current control loop of the distributed controller (pu)

ΔP_{MG_i} Local control signal tracking $\Delta P_{MG_{ref}}$ (pu)

ΔP_{MG_j} Output power variation of a neighbouring MG j (pu)

$\Delta P_{MG_{ref}}$ Reference power to be used in the inner power control loop of the distributed consensus controller (pu)

$\frac{\mathrm{d}\Delta I_i}{\mathrm{d}t}$ Tracking current error of local DER

$\frac{\mathrm{d}\Delta P_{MG_i}}{\mathrm{d}t}$ Tracking power error of local VSG interface

γ Actual measured frequency or dc voltage of the MG

$\gamma_i^{'}$	Normalized ac frequency or dc voltage index
$\gamma_o^{'}$	Index value corresponding to the nominal frequency γ_o of the host grid
γ_{max}	Maximum allowable frequency or dc voltage deviations
γ_{min}	Minimum allowable frequency or dc voltage deviations
$\mathcal{E}$	Vector that represents the links from node v_i to node v_j
$\mathcal{V}$	Vector that contains vertices or nodes of the graph
τ_Q	Output reactive power filter (s)
τ_{1_Q}	VFC lead time constant (s)
$\tau_{1_{dc}}$	VSG adaptive damping lag time constant (s)
$\tau_{1_{dc}}$	VSG adaptive damping lead time constant (s)
τ_{2_Q}	VFC lag time constant (s)
τ_{dc}	VSG adaptive damping angular velocity filter (s)
A_G	Connectivity matrix
a_{ij}	Weights of connectivity matrix
a_{LP}	Filtered value of the derivative of the angular velocity of the VSG
b_i	Pinning gain
D_{big}	VSG damping coefficient during faults (s)
D_o	VSG nominal damping coefficient (s)
f_{max}	Maximum allowable system frequency (Hz)
f_{min}	Minimum allowable system frequency (Hz)
G	Bidirectional communication graph
I_{ref}^*	Reference current for the inner current control loop (pu)
I_c	VSG output current before filter (pu)

I_{dc} VSG interface current from the dc side (pu)

I_{max_i} Maximum current capacity of the local DER (pu)

I_{max_j} Maximum current capacities of the neighbouring DER (pu)

$I_{d_{ref}}$ d-component reference current for inner current control loop of dc-link regulator (pu)

$I_{q_{ref}}$ q-component reference current for inner current control loop of dc-link regulator (pu)

J_{big} VSG moment of inertia constant during acceleration (s^2)

J_{small} VSG moment of inertia constant during deceleration (s^2)

K_{dc} VSG adaptive damping controller gain

K_D DC DER droop coefficient (pu)

$K_{I_{AVR}}$ Integral gain of the virtual AVR

K_{Idc} Integral gain of the PI controller of the dc-link regulator

K_I Integral gain of the local PI-controller of the frequency control loop of the distributed controller

$K_{P_{AVR}}$ Proportional gain of the virtual AVR

K_{Pdc} Proportional gain of the PI controller of the dc-link regulator

K_P Proportional gain of the local PI-controller of the frequency control loop of the distributed controller

P_{dc} VSG interface dc side power (pu)

$P_{MG'_i}$ Maximum power capacity of the local MG (pu)

$P_{MG'_j}$ Maximum power capacity of neighbouring MG (pu)

V Load voltage (pu)

$V_{dc_{ref}}$ Reference rated voltage of the dc microgrid (pu)

V_{dc} Measured dc microgrid voltage (V)

V_{DER} DC DER voltage (pu)

V_{max} Maximum allowable dc voltage (pu)

V_{min} Minimum allowable dc voltage (pu)

Chapter 4

β_{BESS_j} Parameter chosen to have a linear relation between the maximum power of BESS j and maximum values of droop constants

$\beta_{DER_{G_i}}$ Parameter chosen to have a linear relation between the maximum power of host grid DER i and maximum values of droop constants

β_{DG_i} Parameter chosen to have a linear relation between the maximum power of diesel generator i and maximum values of droop constants

$\beta_{MG_{ms}}$ Parameter chosen to have a linear relation between the maximum power of MG interface ms acting as sources and maximum values of droop constants

$\Delta P_{DER_{ms_i}}$ The available power in the i^{th} DER of the ms^{th} MG (pu)

Δt MPC sample time (s)

η_C Charge efficiency

η_D Discharge efficiency

$\overline{\Delta f}$ Maximum allowable frequency deviation (Hz)

$\overline{P_{MG_{S_{ms}}}}$ The available power reserve of the ms^{th} microgrid (pu)

k MPC Control interval

K_{DER_G} The droops of the host grid DERs (pu)

K_{DER} DER droop gains (pu)

K_{MGs} The droops of MG interfaces acting as sources (pu)

N_P MPC prediction horizon

P_{BESS_j} Output power of BESS j (pu)

$P_{BESS_{o_j}}$ Reference power of BESS j (pu)

P^C_{BESS} BESS charge power (pu)

P^D_{BESS} BESS discharge power (pu)

$P_{DER_{G_i}}$ The output power of the i^{th} DER of the host grid (pu)

$P_{DER_{G_{o_i}}}$ Reference power of host grid DER i (pu)

$P_{DER_{ml_i}}$ The i^{th} DER power of the ml^{th} MG (pu)

P_{DU_i} Output power of diesel unit i (pu)

$P_{DU_{o_i}}$ Reference power of diesel unit i (pu)

$P_{MG_{L_{ml}}}$ The demand power of the ml^{th} ac/dc MG acting as a load (pu)

$P_{MG_{So_{ms}}}$ Reference power of the ms^{th} ac/dc MG acting as a source (pu)

$P_{MG_{S_{ms}}}$ The output power of the ms^{th} ac/dc MG acting as a source (pu)

$P_{L_{G_l}}$ The l^{th} host grid load (pu)

$P_{L_{ml_l}}$ The l^{th} load of the ml^{th} MG (pu)

SOC BESS State-of-Charge (kWh)

$V_{MG_{ms}}$ The ac voltage of the ms^{th} ac MG (pu)

List of Acronyms

AGC Automatic Generation Control.

B2B Back-To-Back.

BESS Battery Energy Storage System.

CC Centralized Controller.

DER Distributed Energy Resource.

DG Distributed Generation.

DU Diesel Units.

EMS Energy Management System.

EV Electric Vehicles.

MG Microgrid.

MGCC Microgrid Central Controller.

MMG Multi Microgrids.

MPC Model Predictive Control.

NLP Nonlinear Programming Problem.

OPF Optimal Power Flow.

PLL Phase Locked Loop.

PV Photovoltaic.

RES Renewable Energy Resources.

SG Synchronous Generator.

SOC State of Charge.

VFC Voltage Frequency Control.

VSC Voltage Source Converter.

VSG Virtual Synchronous Generator.

VSI Voltage Source Inverter.

WG Wind Generator.

Chapter 1

Introduction

1.1 Research Motivation

Interest in Renewable Energy Sources (RES) has grown exponentially, due to the significant improvement in converter-based technologies, and motivated by initiatives to combat climate change associated with conventional fossil-fuel-based power plants [1]. Due to the cost and technical integration issues associated with RES, these are being widely deployed in distribution systems as part of Distributed Energy Resources (DERs) and in the context of microgrids (MGs) [1]. The proliferation of DERs has altered the dynamic behavior of the power grid, mainly due to the particular characteristics and technologies associated with these systems [2].

The increasing penetration of DERs in distribution networks is resulting in the "nature" formation of MGs, which are a promising solution for large scale integration of DERs. MGs are clusters of loads and DERs located in medium to low voltage networks that are capable of working in both grid-connected mode and islanded mode [1]. Despite the overwhelming benefits of MGs, such as enhanced reliability and carbon emission reductions, there are various technical aspects that need to be addressed for their full deployment and grid integration. For instance, the intermittency associated with RES, and the lack of inertia due to the prevalence of Voltage Source Converter (VSC) interfaces in these systems, make the system prone to frequency, voltage, and power oscillations [1].

MGs have been extensively studied in the literature, both from control and stability perspectives. However, there are limited studies about the dynamics of a grid of interconnected MGs. This is mainly due to the low penetration of MGs in the last decade, which

is changing, and the fact that small MGs working in a grid-connected mode do not affect the main grid. However, as the penetration of MGs increases, their overall impact on the network would be significant in terms of stability, reliability, operation, and security. In general, a single MG working in islanded mode can only satisfy its demand, with proper controllers that account for the intermittent nature of RES and the limited energy storage capacity within the MG. These issues are motivating the interconnection of MGs, and in this context, the coordinated operation of interconnected MGs and the host grid becomes a necessity to ensure a smooth operation and management of the integrated system [1].

A network that consists of multiple microgrids (MMG) offers several benefits such as reduced carbon emissions, and increased energy efficiency through the reduction of power losses and enhanced utilization DERS, particularly energy storage systems and intermittent RES [3]. In addition, an MMG makes it possible to harness different MG architectures to improve the resiliency and flexibility of the system, such as the integration of dc and/or ac MGs. Due to the promising advantages of an MMG system, the research of such an integrated system becomes relevant.

As discussed in details in the next section, most studies in the literature that address technical issues of an MMG system have focused mainly on the development of Energy Management Systems (EMS) and optimization aspects, assuming that the MGs are interconnected together through a host utility grid with a transmission network [4–10]. The few papers that addressed dynamics of an MMG model the system in grid-connected mode, i.e., the MGs are connected to an external network with large inertia [11–14]. In addition, these studies employ several simplifications and assumptions that render their models unsuitable for investigating the actual dynamics of MGs; for instance, the impact of voltage control on the frequency of the MGs has not been addressed in these papers. In addition, most studies related to dc MGs ignore the impact of converter interfaced loads on the voltage oscillations of the system [15–17, 17, 18]. None of the existing literature models a realistic MMG system, considering the effect of low inertia and load characteristics on system controls, employing simplified models that do not adequately represent MG dynamics. Moreover, none of the papers have developed a distributed frequency and dc-voltage control to coordinate an MMG system that consists of both ac and dc MGs. Furthermore, none of the papers utilized Virtual Synchronous Generators (VSGs) for MG interfaces to enhance the frequency and voltage dynamics of ac and dc MGs. Finally, none of the papers utilize voltage control to enhance the frequency stability of the grid, based on the load characteristics in MGs.

Based on the aforementioned discussion, this thesis proposes the use of ac-dc-ac and dc-ac converter interfaces for the interconnection of ac and dc MGs, respectively, introducing a new hierarchical distributed control approach for the proper exchange of power among

the MGs, and considering the overall system frequency and voltage control. Virtual Synchronous Generator (VSG) technologies are applied in the proposed interface converters to adaptively adjusts the inertia and damping constants, while considering Voltage Frequency Control (VFC) to improve the frequency and voltage stability of the overall system.

1.2 Literature Review

The state-of-the-art for MMG systems is discussed and reviewed in this section.

1.2.1 Gird of MGs

The concept of a gird of microgrids or MMG system is a relatively new field of research in power systems, which has gained momentum in recent years due to the rapid proliferation of MGs. It is based on a grid with multiple MGs being utilized to facilitate the integration, control, and coordination of DERs within a power system by adequately managing these resources in each MG.

1.2.1.1 Energy Management

One of the earliest studies in the literature that mentions the concept of an MMG system is [19], where the authors develop a multi-stage stochastic optimization approach to deal with the stochastic nature of DERs and loads in the energy management problem. Most recent studies of MMG systems in the literature focus on the steady-state analysis of these systems, concentrating on Optimal Power Flow (OPF) problems, and the associated Energy Management Systems (EMSs) of interconnected MGs and the host grid. For instance, the authors in [4] discuss a Model Predictive Control (MPC) based power flow control for optimal allocation of power exchanges among interlinked MGs and the main network, while taking into account several factors such as energy prices, the State of Charge (SOC) of batteries, load demand, and power generation forecasts. In [5], the authors present a technique based on Pontryagin's minimum principle to exchange the power optimally among interconnected MGs, while maintaining the energy storage around an optimal value. The authors in [6] develop an algorithm to optimally control and schedule power among interconnected MGs based on a Linear Quadratic Gaussian. In [7], the authors discuss a decentralized control system for the optimal exchange of power among

smart MGs, while taking into account several factors such as the SOC of the energy storage system, energy prices, and Distributed Generation (DG) output power profiles. The authors in [8] present a price-based OPF algorithm for an optimal exchange of charge and discharge power of Electric Vehicles (EVs) among interlinked MGs. In [9], the authors develop a hierarchical OPF algorithm among interconnected MGs that takes into account load variance, energy prices, and energy storage. In [10], the authors discuss a robust distributed control technique for interlinked MGs where the MGs are agents; the mathematical formulation in the paper aims to optimize the power flow among interconnected MGs, while taking into account the stochastic nature of the DERs and loads in the system. In [20], the authors present a distributed-economic MPC for the energy management of a cluster of interconnected MGs; the energy management in this paper mainly focuses on uncertainty and stochastic nature of DERs within each MG to optimize the power sharing among the interlinked MGs. The authors in [21] develop a distributed energy management control scheme for an MMG system that are interconnected by dc and ac interfaces.

Issues such as participation of the MGs in providing ancillary services for the main grid such as voltage and frequency support are discussed in [22–24]. Thus, the authors in [22] present a steady state optimization problem for optimal participation of MGs in frequency regulation markets, while taking into consideration several factors such as DERs ramp-up rates and generation costs. In [23], the authors develop a hierarchical steady-state OPF algorithm for providing frequency regulation to the main grid, while taking into account power flow constraints, uncertainty in loads of the MGs, and energy prices. The author in [24] concludes that as the penetration of MGs increases in low voltage distribution networks, the transmission system would benefit from the presence of an MMG by reducing loading on the transmission system.

1.2.1.2 Frequency and DC-Voltage Control

In the context of isolated MGs, the problem of load sharing among DERs has been addressed with passive droop controllers. For example, the authors in [25] present a control scheme to dynamically adjust the droop parameters of derated Doubly Fed Induction Generator (DFIG) wind turbines, to improve both the frequency response of the MG and its stability, considering a simplified model where the components of the MG are represented by first-order transfer functions. However, this control scheme is limited to the adjustment of the droop gains of wind turbines that have insufficient primary reserves (due to changes in wind speeds) such that the stability of the system is maintained; in addition, it does not coordinate between the various DERs such as diesel generators and Battery Energy Storage Systems (BESS) to improve the primary frequency response of the overall system.

A multi-agent based dynamic droop gain adjustment of DERs is presented in [26], where each DER is an agent that interacts with neighboring DERs to adjust the droop parameters to improve the primary frequency response for grid-connected MGs; such a decentralized scheme presents some challenges for supply-demand balance in isolated MGs, as discussed in [27], that are not considered in the paper. Another study that proposes adaptive droop control is presented in [28], where the droop gain of a DER is regulated so that its output power follows a setpoint. However, the presented controller does not coordinate the adjustment of multiple DER droop gains for optimal frequency regulation.

Optimal and MPC based frequency and/or voltage controls in MGs are presented in [11, 29–34]. Thus, in [29], the authors discuss an MPC approach to minimize frequency deviation of an isolated MG with EVs; the presented control scheme mainly focuses on adjusting the active power setpoints of DERs to satisfy the objective function and the constraints, but does not consider the impact of voltage and droop control on the system's frequency. Similarly, in [30] and [31], the authors propose an MPC-based secondary controller to improve the transient response of isolated MGs, but the studies do not consider droop control nor VFC. In [32], a distributed MPC controller is presented to regulate the operating voltage of the system; however, the control scheme does not consider the impact of droop nor VFC control on the system frequency. In [33], the authors propose an MPC approach to adjust the voltage setpoints of DERs, where the controller receives input signals from a conventional droop controller to minimize the difference between the reference and measured DER voltage; however, the proposed technique does not aim to regulate the frequency nor coordinate the DERs to achieve optimal frequency regulation with proper load sharing, and VFC control is not considered either. Similarly, in [34], an MPC technique is used in DERs to improve their voltage dynamic response, but there is no consideration for DER optimal droop, coordination, nor VFC. Finally, in [11], a linear optimization problem to minimize the generation-load power balance is proposed for frequency regulation in MGs; however, droop and VFC issues are not considered.

In the context of dc voltage control in dc MGs, several control techniques have been proposed in the literature to improve the performance of conventional droop controllers. For instance, the authors in [15] developed adaptive droop controllers for improved stability and power sharing in dc MGs; however, the proposed techniques still inherit the post disturbance voltage deviation issue associated with droop controllers. In [16], a distributed droop-free dc-voltage control approach for dc MGs control is presented. The proposed primary and secondary control method realizes voltage control and accurate reactive power sharing in a distributed manner using minimum communication, with each DER only needing little information from neighboring units. Hence, a sparse communication network is used, including spanning trees, to enhance reliability if a DER or link is lost. However,

a simplified dc MG model is used, which mainly consists of resistive loads without the dynamics of actual dc-dc and dc-ac converter interfaces of loads; Furthermore, the impact of RES variations is not considered on the proposed controller, and there is no comparison with conventional droop controllers.

There are several papers in the literature that address the dynamics and control of a network with multiple dc MGs [17, 18, 35, 36]. Thus, in [17], the authors develop a hierarchical multi-agent distributed control scheme to share the loads among dc MGs by adjusting DER voltage setpoints for each MG in the network. The control scheme consists of two levels: the first level is a global tertiary controller where each MG agent ,i.e., the MG central controller (MGCC), cooperates with neighboring MGs to reach consensus and optimality; the second control level is local within each MG, where DERs are associated with agents that communicate with each other to coordinate the voltage setpoints. However, this paper does not consider coordination among dc and ac MGs. In [18], the authors present a distributed OPF-based control technique for dc MGs; however, similar to [17], the paper does not consider the impact of such a control scheme if ac MGs are present in the system. In [36], the authors discuss a simple PI controller to coordinate the exchange of power among dc MGs only through flyback converters; such a simple controller is not suitable for coordination among MGs, due to the inability of such a controller to account for the numerous constraints associated with MGs. In the aforementioned studies, several simplifications are made, such as ignoring the dynamics of converter-interfaced loads, which have a detrimental impact on the stability of the system by inducing significant voltage oscillations [37, 38].

A novel droop-free frequency control for ac MGs is presented in [39], which has been employed in [40] for frequency control in a cluster of interlinked MGs. In [40], the authors propose a hierarchical multi-agent droop-free control scheme that consists of two levels. The lower level acts on primary and secondary voltage and frequency control within each MG, where each DER is considered an intelligent agent that exchanges data with neighboring agents to generate the required voltage setpoints and active power reference signals. The higher level control is a tertiary control that aims to coordinate the interlinked MGs in the network, through the same multi-agent approach used for the lower level controls to obtain an optimal frequency response. However, the presented tertiary control does not take into account the effects of the voltage setpoints of the DERs on the frequency of the system; in addition, the paper assumes that all the MGs in the system are ac with a single bus that consists of a single load and a DER, and there is no differentiation in the characteristics and operational states among the various MGs except for the load rating.

A hierarchical frequency control for a network consisting of multiple interconnected islanded MGs is presented in [11]. The proposed control scheme consists of two main

layers, with the upper layer comprising of a centralized EMS that obtains data from the whole network and acts similarly to an Automatic Generation Control (AGC) by sending the control signals to each MG to balance supply-demand in the system. In the lower control layer, the MGCC of each MG controls the DERs to allocate the required power generation. The study consists of time-domain simulations that validate the effectiveness of the proposed control scheme for limiting frequency excursions following disturbances in the system. However, the network model does not include local DER controllers in the DERs (primary control or droop controllers). Furthermore, it is assumed that the MGs are connected to a strong host grid, without considering the possibility of the system being formed only by a cluster of isolated MGs that could suffer from fast frequency excursions. Finally, the developed optimization algorithm for coordinating the MGs is a simple linear economic dispatch problem that is not suitable for large networks with nonlinearity voltage dependent load characteristics. A similar study is presented in [12], but with a hierarchical decentralized multi-agent control; however, the study lacks time-domain dynamic considerations, neglecting nonlinearity as in [11].

Other relevant studies that involve dynamic models and time domain simulation of an MMG are presented in the literature. Thus, in [13], the authors conduct a comparative study among several control techniques to coordinate a group of MGs with the main grid. The paper demonstrates that a decentralized multi-agent control system is capable of coordinating the active power output of MGs to limit frequency excursions in the wake of severe disturbances in the main grid. However, the study assumes all MGs as ac systems, and the impact of voltage control on the frequency of the system is not investigated. Moreover, the main host grid which is modeled as a Synchronous Generator (SG) with large inertia, which does not capture the actual dynamics of an MMG network with its inherent overall low inertia. Finally, the network topology in this study assumes that ac MGs are directly interconnected without a power electronic-based interface, which significantly limits the controllability of the power exchanged among the MGs.

A study that involves adaptive control is presented in [41], where the authors present a hybrid cluster of interconnected MGs that consist of dc and ac MGs. These MGs are interlinked through a power exchange unit that includes a set of VSCs and BESSs with a controller to solve synchronization issues among the MGs. The proposed network topology and control scheme in the paper maintains the frequency and the voltages of the interconnected cluster of MGs. However, the system is heavily dependent on adding new BESSs and dc lines to connect the MGs, which would be more suitable for small systems due to the significant costs of such an approach. In addition, the frequency control of the system is done based on droop control, which may become ineffective for system with multiple MGs due to the need for the exchanging information for optimal coordination. Finally,

the impact of VFC and voltage dependent loads on the coordination of the system is not discussed.

Another paper that involves hybrid ac/dc connected MGs is [14], where the authors discuss a unique hybrid point of common coupling that connects each MG in the system with the main grid through an ac interface, and interconnects the cluster of MGs directly through a dc interface with a BESS. This hybrid ac/dc connection offers several benefits, such as mitigation of synchronization issues and better control and power sharing among the interconnected MGs. However, the control schemes presented in the paper do not include frequency regulation through voltage control; furthermore, the proposed interconnection approach would be expensive for large networks of multiple MGs, due to the need to add new dc lines with BESSs. Finally, the study does not consider the impact of such an interface if dc MGs are present in the system, since the dynamics of dc MGs differ from ac MGs.

A comprehensive analysis of different topologies and architecture of networks of multiple MGs is presented in [42], where the authors investigated the impact of the layout and interface technologies of multiple-interconnected MGs on energy costs, reliability, stability, and protection. Several network layouts are discussed in the paper, such as parallel and mixed series/parallel interconnected MGs, concluding that dc interfaced MGs and dc MGs are a promising solution for MMG networks. However, the study does not consider detailed MG models, presenting general arguments without adequately analyzing the impact of the proposed control techniques and topologies.

1.2.1.3 Voltage Control

From a voltage and reactive power control perspective, in [43] and [44], the authors propose a frequency control approach that exploits the sensitivity of the loads to the operating voltage of the system. Furthermore, in [45], the author develops a Non-Linear Programming (NLP) algorithm for optimal DER sizing and placement to enhance the voltage stability of a grid-connected distribution network. A small-perturbation voltage stability analysis is also conducted, showing how the location, size, and type of DER affects the system eigenvalues. A similar study is presented in [46], where a small perturbation voltage stability analysis of a CIGRE benchmark isolated MG is performed, demonstrating that the type of controllers employed by the DERs could positively or adversely affect small-perturbation voltage stability. However, none of the aforementioned studies address the impact of voltage control on the stability of an MMG system, but, the proposed approaches will be taken into consideration in the proposed research work.

In [32], the authors present a distributed voltage control for a cluster of interconnected MGs, which is based on a distributed MPC to account for different dynamic speeds and characteristics of voltage regulators within each MG in the system. However, the developed control scheme relies on offline voltage sensitivity matrices, which are dependent on the topology of the network; thus, if a severe disturbance occurs in the system that alters the topology of the grid, a network wide control failure and a voltage collapse may occur due to improper coordination among the interconnected MGs. Furthermore, the effects of load characteristics on the proposed control and frequency control are not addressed in this paper.

In [47], the authors developed a distributed control system to regulate the voltage of a simplified MG model, but the proposed controller does not regulate the frequency of the system. In [48], the authors also developed a distributed reactive power control scheme that maintains a desired reactive power distribution among DERs in steady-state. However, this voltage control scheme does not consider the coupling between active and reactive power in the system and its effect on the frequency of the system.

In [49], the authors develop a coordinated voltage control of distribution networks with multiple MGs to mitigate the issue of voltage rise in low voltage distribution networks, which are predominantly resistive with a low X/R ratio; the proposed control in this paper is based on a decentralized-hierarchical approach. The presented control model has some limitations, such as representing the MGs with equivalent artificial neural networks (ANNs), which is an issue, since if a severe disturbance occurs within the network that changes the topology of the grid, the ANN equivalent model may not work properly, unless it has been specifically trained for that topology. Furthermore, this paper only focuses on steady state behavior of the system, and the MGs are assumed to be clustered and connected to the main grid through a single Point of Common Coupling (PCC), which does not adequately represent a possible system of MGs that would be connected to a host grid at various points.

1.2.1.4 Stability

From a transient stability perspective, the authors in [50] conduct transient stability studies of a single islanded MG that consist of different DERs, considering that VSC interfaced DERs with PQ controllers worsen the transient stability of the system by shortening the critical clearing time (CCT), compared to DERs with droop controllers; furthermore, the study only focuses on the effects of primary frequency control on transient stability. In [51] and [52], the authors investigated the dynamic impact of a power system with high penetration of distributed generation, identifying several factors that affect the system

stability such as the types of DERs, their controllers, and the DER penetration level, which could positively or adversely affect the transient stability of the system. Thus, it is concluded that if the penetration of VSC-based DERs in the system becomes significant, the system may become more prone to oscillations due to the lack of control and coordination among DERs and centralized thermal power plants. None of these papers nor others, as far as the author knows, have investigated these issues from an MMG system perspective.

The authors in [53] investigate the impact of communication delays on distributed controlled interconnected clusters of DC MGs, based on time-delay stability switching boundary. However, the paper does not examine the impact of the interconnected MGs on the transient stability of the overall system.

1.2.2 Discussion

It can be observed that several of the aforementioned studies focus mainly on the development of OPF, control, and EMS for steady-state MG models, to improve the economy, reliability, and performance of an MMG system while neglecting the dynamic effects of such a network. Other papers mainly focus on different architectures of multiple interlinked MGs to solve synchronization and power sharing issues, while several papers discuss different dynamics and control aspects of a cluster of MGs, with various limitations and assumptions. However, to the best of the author's knowledge, none of the papers in the literature have fully modeled and study dynamics and control aspects of an MMG system that includes different characteristics such as mixed dc and ac MGs with voltage dependent loads. In addition, none of the papers propose control schemes to coordinate the interconnected ac/dc system in the time domain. Finally, no paper, as far as the author knows, has investigated the use of VSGs for stability improvements of an MMG system. Therefore, the following are the main issues with the reviewed literature, in the context of MMG system:

- Many studies mainly focus on the development of EMSs for optimal exchange of power among interconnected MGs in steady state, neglecting the dynamic aspects of such a network.
- Several of the studies investigate the dynamics of interconnected MGs through a main grid with large inertia, and/or significantly simplify the MG models such as representing MGs as a single bus with a load, ignoring the nonlinearity of the system associated with voltage dependent loads, without considering a diversity of ac and dc MGs.

- The network topologies in these studies assume that ac MGs are directly interconnected without a power electronic-based interface, which significantly limits the controllability of the power exchanged among the MGs.
- The impact of voltage control on the frequency of interconnected MG has not yet been discussed.
- Some dynamic studies mainly focused on solving synchronization issues among clusters of interconnected MGs through the development of special network architectures, such as introducing dc links with BESSs to connect the MGs, which are costly solutions.
- Frequency and dc-voltage regulation methods and stability studies based on VSGs have not been discussed in the context of an MMG system.
- Stability analyses and the development of coordinated control systems to improve the overall system stability of a network of MGs are very limited.

1.3 Research Objectives

Based on the aforementioned state-of-the-art review, the following are the main objectives of this thesis:

- Develop a dynamic model of a grid of interconnected MGs that includes both dc and ac MGs, to study the dynamic issues in these types of networks, particularly focusing on interconnected MGs which are not interlinked through a larger host grid with significant inertia, since it is more challenging to coordinate a network of isolated MGs due to the small inertia and limited availability of dispatchable DERs in such a system.
- Develop distributed frequency and voltage controllers to coordinate a cluster of MGs to enhance the stability of the system, limiting severe frequency and voltage excursions.
- Develop a VSG based Back-To-Back (B2B) MG interface, with a new adaptive inertia control technique and VFC to enhance the frequency response of ac MGs and the host grid in an MMG system, limiting severe frequency excursions systems, especially during severe disturbances, and allowing proper power sharing among the MGs without causing significant power transients.

- Propose a novel control of the VSG-based dc-ac interface of dc MGs to improve their dc MG voltage dynamics in the MMG system.
- Develop, test, and demonstrate a new centralized frequency control technique that enhances the frequency response of MGs and MMG systems, ensuring an optimal trade off between load sharing and frequency regulation by optimally adjusting the main active power droop parameters and considering VFC to avoid stability issues associated with the improper tuning of DER droop gains.

1.4 Outline of the Proposal

The rest of the thesis is organized as follows: Chapter 2, provides a brief overview of the background relevant to the thesis, in particular basic control and modelling issues such as control techniques in ac/dc MGs, and VSG controlled VSCs, MMG concepts, layouts, and existing frequency and voltage control techniques are discussed. Moreover, dynamic models of various components of ac/dc MGs, such as diesel generators, BESSs, WTs and dc MGs and loads are presented. Finally, a generic model of inverter-based VSGs is discussed, including a virtual governor, Automatic Voltage Regulator (AVR), voltage, and current control loops.

Chapter 3, first proposes a distributed voltage control of dc MGs based on distributed consensus technique, which is used to regulate the voltage of the dc MGs. The controller is tested and validated based on a dc MG model of a university building in China, and the performance of the controller is compared with conventional decentralized controllers. The second part of the chapter discusses the proposed B2B VSG interfaces with adaptive inertia, and extends the aforementioned distributed controller to coordinate an MMG system. The hierarchical distributed control technique is tested, validated, and compared on an MMG based on a CIGRE benchmark MG system, and the results are discussed to highlight the performance of the proposed control scheme.

Chapter 4 first presents a new centralized optimization based adaptive droop and voltage control for isolated MGs and MMG systems. The control scheme is based on an optimal and model predictive control approach that continuously adjusts the active power droop gains and the voltage setpoints of DERs to regulate the frequency of the system. The second part of the chapter extends the aforementioned controller to coordinate an MMG system by adjusting the droop gains of the interfacing VSGs. The proposed controllers are tested, validated, and compared on the previously defined MMG system, and analyses are

conducted to evaluate their performance compared to the distributed controller proposed in Chapter 3.

Finally, Chapter 5 highlights the main conclusions and contributions of this thesis, and briefly discusses possible future research work. The appendices present data of the test systems and controllers proposed and used throughout this thesis.

Chapter 2

Background Review

2.1 MG Overview

2.1.1 MG Definition and Components

According to [54], an MG is a cluster of loads and DERs located at medium and low voltage distribution networks that has a single PCC with the main grid. MGs are capable of working in grid connected mode or in islanded mode, which increases the reliability of power delivery to consumers if there is a disturbance in the host grid. An example of an MG is shown in Figure 2.1. Thus, the structure of the MG consists of a medium or low voltage network with controllable and uncontrollable loads; dispatchable DERs such as diesel synchronous generators and BESSs; undispatchable and variable distributed resources such as solar PV and wind turbines and a control and communication system that includes an MGCC or a coordinator with decentralized controllers.

2.1.2 Modeling

2.1.2.1 Synchronous Generators (Diesel Units)

Diesel SGs have been widely used in MGs since they are readily dispatchable, thus being used as grid forming DERs to support the frequency of MGs [27]. The frequency dynamics of these generators are mainly described by the swing equation, which relates the frequency

of the MG to the power mismatch of the system as follows [56]:

$$M_{SG}\,\frac{\mathrm{d}\omega_{SG}}{\mathrm{d}t} + D_{SG}\Delta\omega = P_{SG_m} - P_{SG} \tag{2.1}$$

where P_{SG_m} is the mechanical input power into the generator, P_{SG} is the electrical output power, ω_{SG} is the speed of the rotor (the angular velocity), and M_{SG} and D_{SG} are the inertia and damping coefficients of the diesel generator, respectively.

The authors in [55] have developed a dynamic model of a diesel generator suitable for time-domain simulations, which have been validated with an actual field model. This model is used here, which includes the governor and exciter models depicted in Figure 2.2, with properly tuned gains for the test systems used here.

2.1.2.2 BESS

BESSs are used in MGs to properly integrate undispatchable DERs by smoothing frequent and rapid changes in the output power of solar and wind DERs [54]. These systems are usually interfaced through a VSC; therefore, the dynamics of the BESS are much faster than the diesel generator, thus rapidly supplying active and reactive powers to help control the frequency and voltage of an MG. A suitable model of a BESS based on the average model is presented in [57], with a modified version of this model being used in this research work, as per the schematic diagram shown in Figure 2.3. The presented average model ignore the converter switches to increase the speed of the time domain simulations, while preserving the main dynamic characteristics of the VSC.

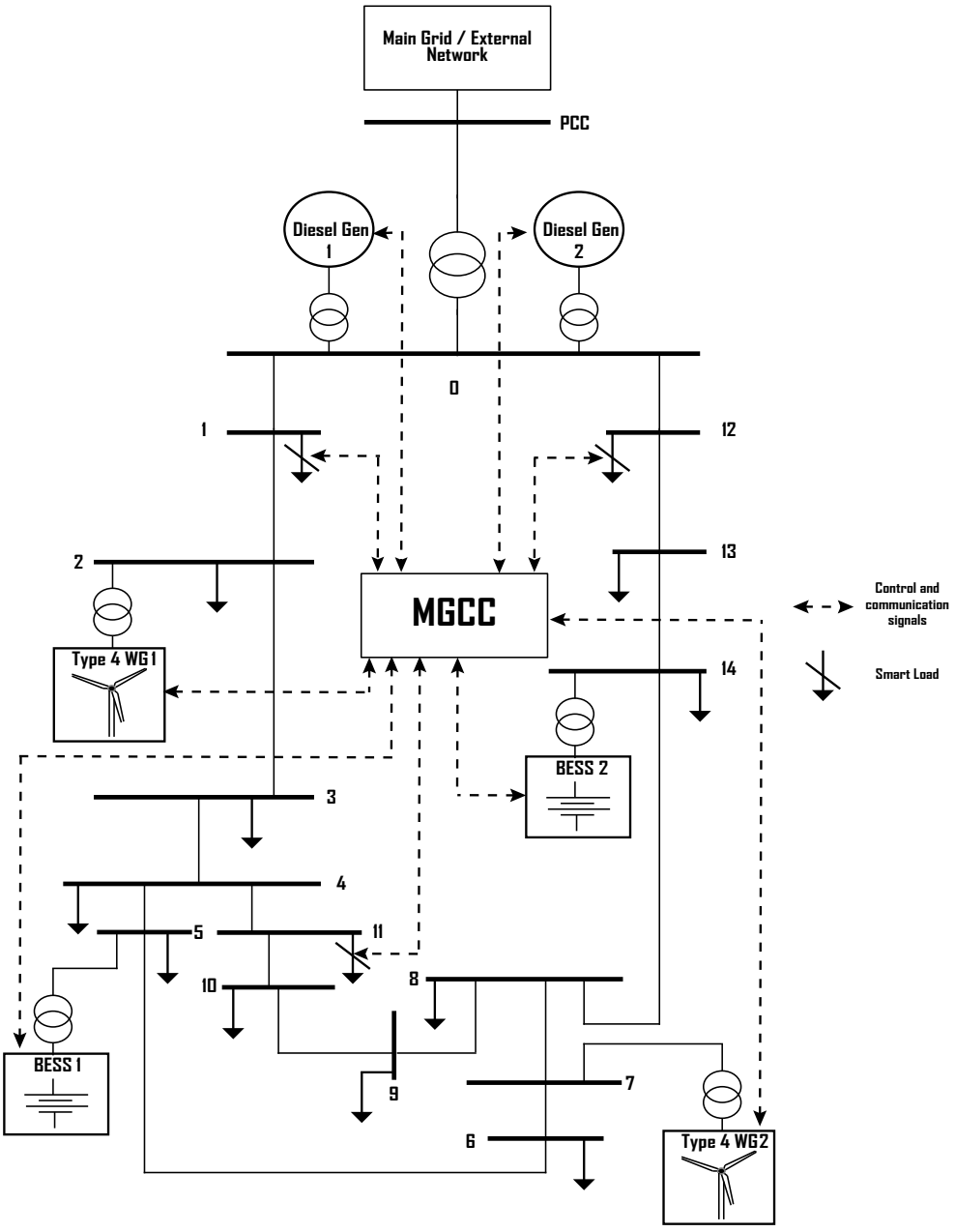

Figure 2.1: Example of an MG.

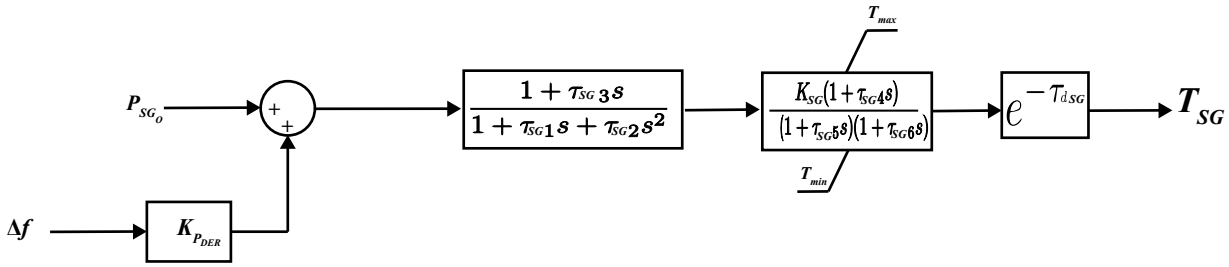

(a)

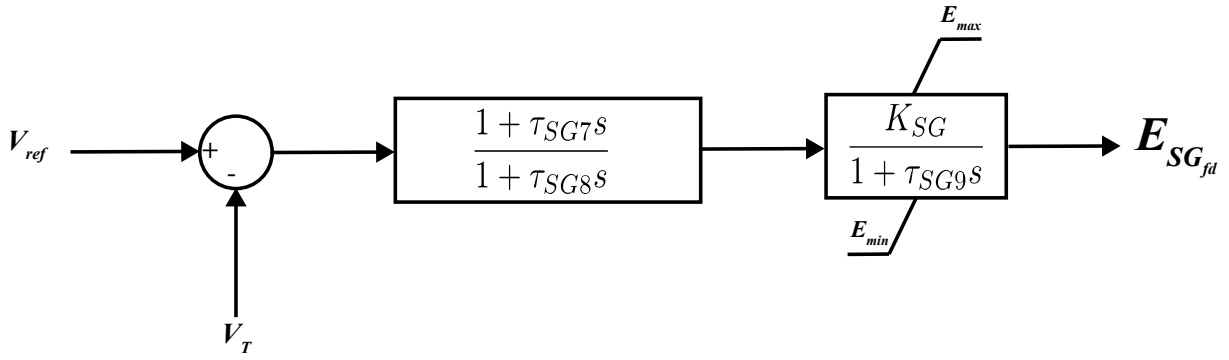

(b)

Figure 2.2: (a) Governor model of a diesel generator and (b) exciter model of a diesel generator [55].

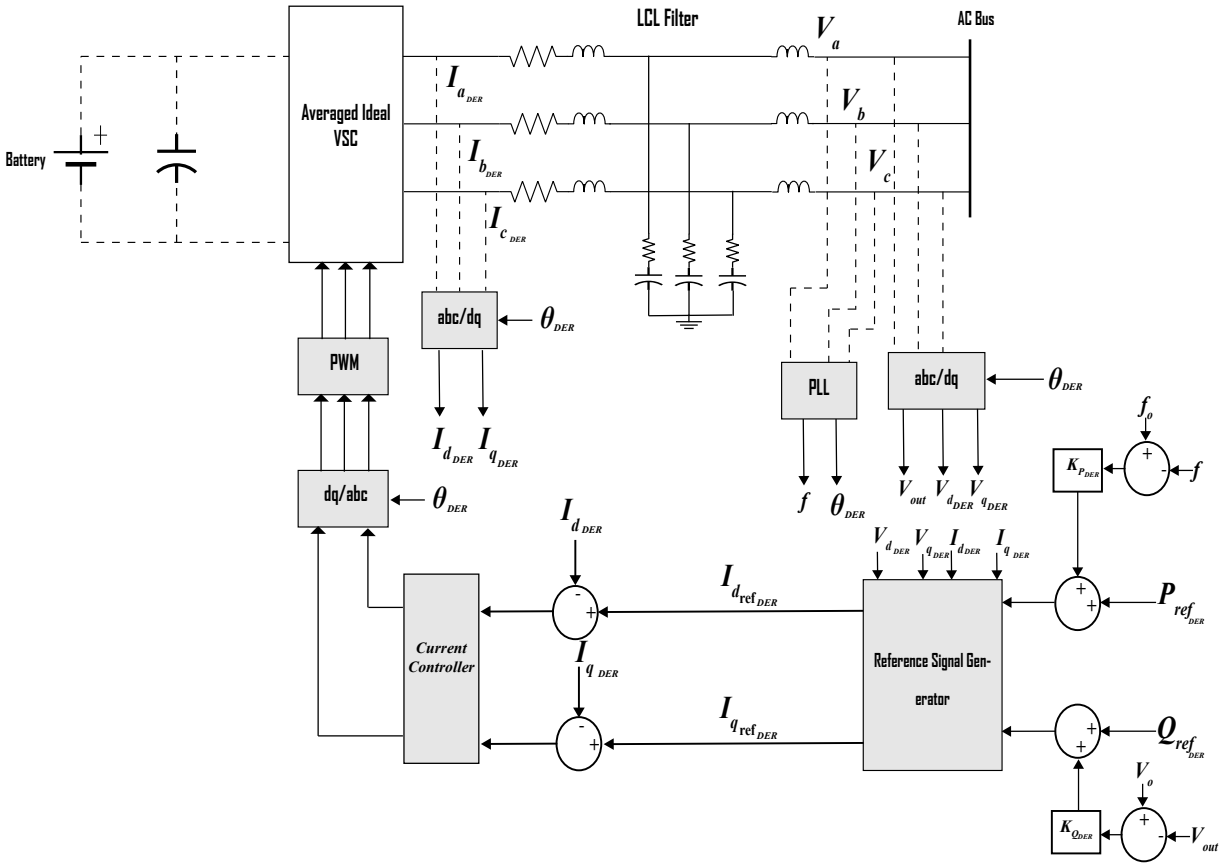

Figure 2.3: BESS and WG VSC average model based on [57].

2.1.2.3 Wind Generator Model

Wind Generators (WGs) are assumed to be Type 4, with full VSC interfaces as discussed in [44] and [57]. The schematic of the model of a VSC-interfaced WG used here is shown in Figure 2.3, with the wind generator and corresponding VSC being modeled as a dc source.

2.1.2.4 Load Model

An exponential model is used to model the loads as follows [44]:

$$P_{L_l} = K_{LP_l}\, V^{\alpha_{P_l}} \qquad \forall l \tag{2.2}$$

$$Q_{L_l} = K_{LQ_l}\, V^{\alpha_{Q_l}} \qquad \forall l \tag{2.3}$$

where V is the MG voltage, which is assumed to be the same as the loads and throughout the MG, as the voltage drops in the network are not significant [44,58]; K_{LP_l} and K_{LQ_l} are load scaling factors for load l; and the coefficients α_{P_l} and α_{Q_l} define the load type (for a constant current load $\alpha_{P_l} = \alpha_{Q_l} = 1$, for a constant impedance load $\alpha_{P_l} = \alpha_{Q_l} = 2$, and for a constant power load $\alpha_{P_l} = \alpha_{Q_l} = 0$), with the values of α_{P_l} and α_{Q_l} chosen here to represent mixed load types.

2.2 MG Control

A communication infrastructure is employed to implement the hierarchical control structure that corresponds to a secondary controller that is handled by the MGCC, as depicted in Figure 2.4. Primary control in isolated MGs is performed by dispatchable DERs through local decentralized droop controllers, to control frequency and voltage through load sharing.

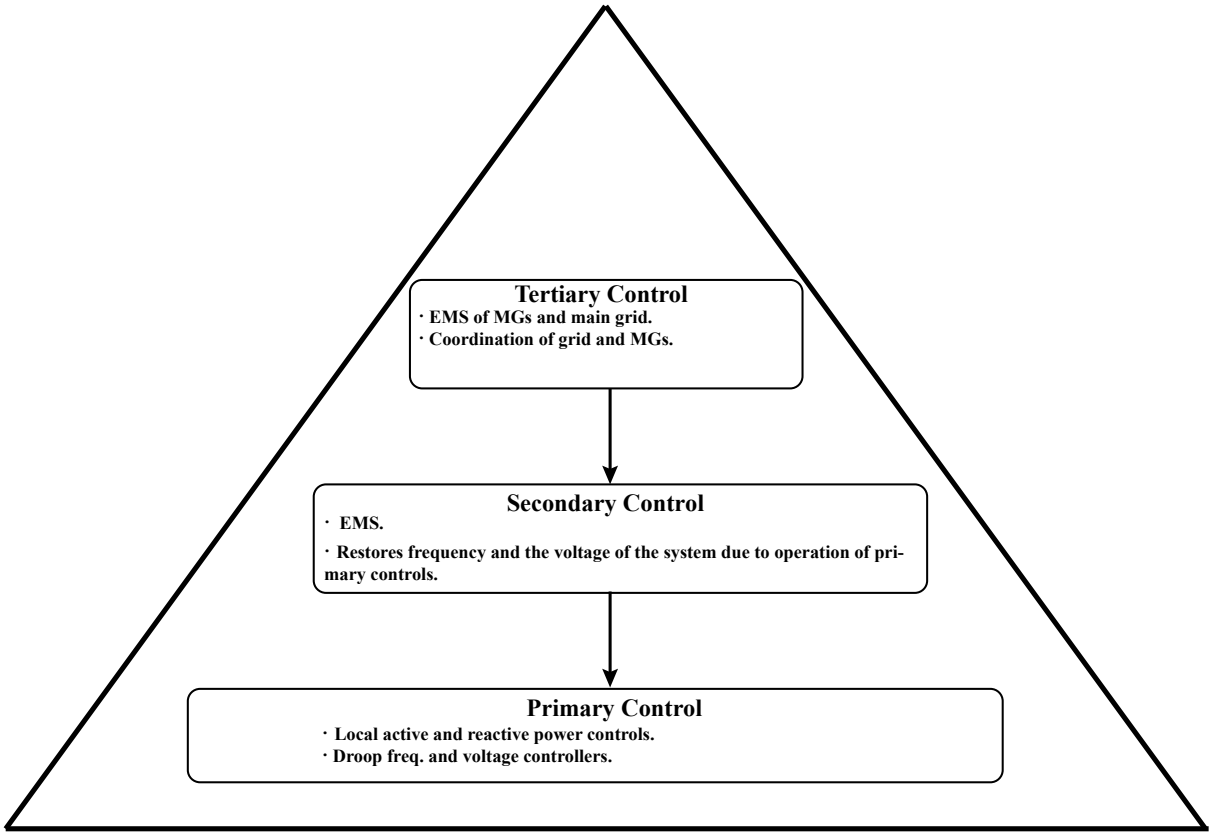

Figure 2.4: Hierarchical control structure for isolated MGs [54].

2.2.1 Frequency Control

2.2.1.1 Decentralized Primary Frequency Control

DERs in MGs usually employ droop control to share power among them, emulating an SG power-frequency relationship. The droop controller modulates the output of DERs as a function of the frequency deviation as follows:

$$K_{P_{DER}} \Delta f = -(P_{DER} - P_{DERo}) \tag{2.4}$$

where P_{DERo} and f_o are the DER nominal active power and frequency, respectively, while $K_{P_{DER}}$ is the droop parameter. Hence, if the frequency of the system deviates due to load

or DER changes or system disturbances, the primary control will attempt to restore power balance in the MG and limit frequency deviations. A suitable value of the droop constant must be selected to ensure a robust frequency response of the system, and it can be defined as:

$$K_{P_{DER}} = \frac{\Delta P_{DER}}{\Delta f} \frac{\text{pu}}{\text{Hz}} \tag{2.5}$$

The droop gains of DERs are selected based on their capability to provide active power. DERs with high ratings tend to have higher gains, since they have more primary reserves and have more capability for regulating the system's frequency. For such DERs, a small change in the system's frequency would result in significant power injection or reduction as illustrated in Figure 3.15 [59].

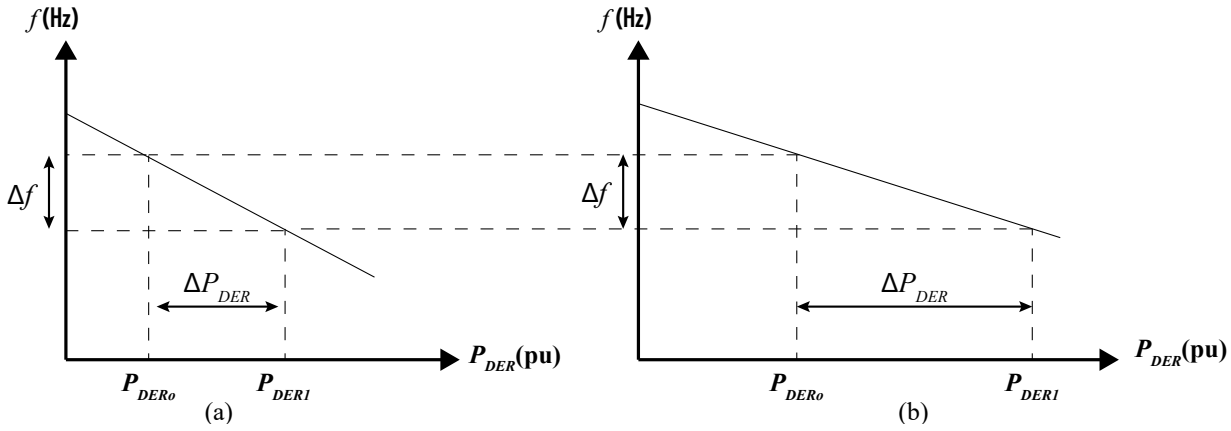

Figure 2.5: Droop characteristics of DERs: (a) 6% droop, and (b) 3% droop [56].

2.2.1.2 Centralized Frequency Control

A centralized control scheme is usually employed in the secondary control layer of MGs, with the main objective of restoring the system's frequency to its nominal value and remove steady-state error from decentralized droop controllers and load changes. A basic secondary controller employs a PI compensator to change the reference value for the active power by ΔP_{DER_s} to be sent to DERs to restore the frequency as follows:

$$\Delta P_{DER_s} = \left(K_{P_{F_s}} + \frac{K_{I_{F_s}}}{s} \right) (f_o - f) \tag{2.6}$$

where $K_{P_{Fs}}$ and $K_{I_{Fs}}$ are the gains of the PI controller, and f_o is the nominal value of the frequency. An alternative secondary frequency control based on optimization techniques to regulate the frequency of the system is proposed in the next chapters.

2.2.2 Voltage-Frequency Control

As discussed in [43], the majority of the loads in MGs are sensitive to system's voltage changes, as per (2.2) and (2.3); therefore, these can have a significant impact on the MG's frequency, directly affecting primary frequency control. Figure 2.6, based on [22], shows the frequency deviations in a MG for changes in DER generation and load demand, with ΔP_{DER} representing the change in the total generation of the MG, ΔP_L corresponding to the change in the system demand, and ΔP_V representing the change in the voltage dependent loads. Thus, a deviation in the frequency of the system due to a demand change will force the governors of the diesel generators and the droop controls of the DERs to adjust their output power, while voltage dependent loads will change with a reverse slope depending on the system voltage. For instance, a frequency drop in the system would result in increased generation from DERs, while a decrease in the DER voltage setpoints of the voltage regulators would decrease the demand of the voltage dependent loads. Thus, with suitable DER voltage control, the MG frequency deviation after a disturbance can be minimized, as discussed in [44].

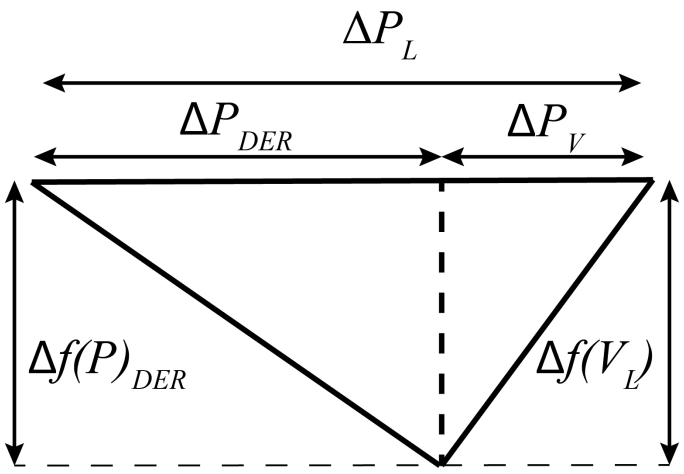

Figure 2.6: Frequency deviation after load and generation changes.

2.2.3 Voltage Control

2.2.3.1 Decentralized primary Voltage Control

The droop controllers in DERs are also capable of voltage control by adjusting the reactive power output as a function of voltage deviation as follows:

$$\Delta V = K_{DER_V} \Delta V = -(Q_{DER} - Q_{DERo}) \tag{2.7}$$

where Q_{DERo} and V_o are the DER nominal reactive power and voltage, respectively, while K_{DER_V} is the droop parameter of the voltage control. Therefore, if the voltage at the PCC of a DER deviates due to a disturbance, the DER would inject or absorb reactive power to limit further voltage deviations, as illustrated in Figure 2.7.

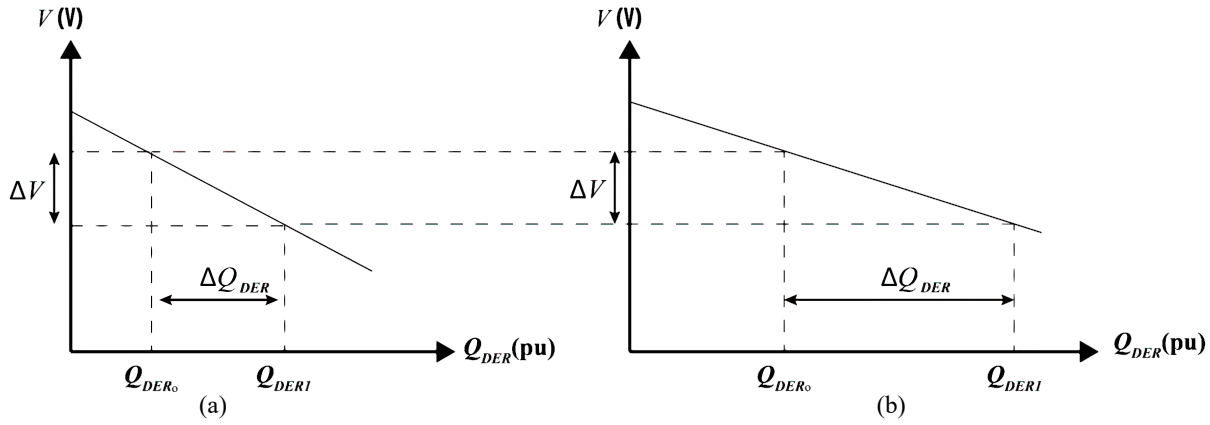

Figure 2.7: Voltage droop characteristics of DERs: (a) 6% droop, and (b) 3% droop [56].

2.2.3.2 Centralized Voltage Control

Similar to secondary frequency control, a basic secondary controller employs a PI compensator to change the reference value for reactive power by ΔQ_{DER_s}, which is sent to DERs to restore the voltage of the system as follows:

$$\Delta Q_{DER_s} = \left(K_{P_{V_s}} + \frac{K_{I_{V_s}}}{s} \right) (V_o - V) \tag{2.8}$$

where $K_{P_{V_s}}$ and $K_{I_{V_s}}$ are the gains of the PI controller, and V_o is the nominal voltage. As discussed in the next chapter, advanced secondary voltage control approaches based on optimal and distributed control techniques are proposed in this thesis.

2.2.4 DC MGs

The use of dc MGs has increased recently, mainly due to their control characteristics, the increased availability of dc loads (e.g., LED lighting), and the fact that it reduces the need for dc/ac conversions in DERs; furthermore, as opposed to ac MGs, the lack of reactive power control in these systems is a significant advantage since the control and operation of these MGs would be simpler, with lower voltage drops across feeders [56]. However, these systems present significant protection challenges [60]. A typical topology for a dc MG is shown in Figure 2.8. Hence, the structure of a dc MG consists of a low voltage network (e.g., 750 V_{dc}), with controllable and uncontrollable dc/ac loads, dispatchable DERs such as BESSs; intermittent DERs such as solar PV and wind turbines, and an MGCC or a coordinator with decentralized controllers [54].

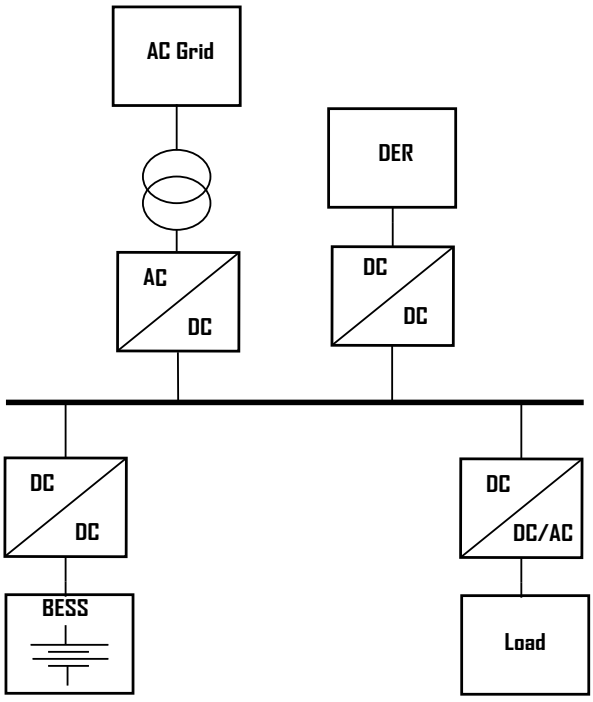

Figure 2.8: Typical dc MG layout [56].

2.2.4.1 DC-DC Converters

DERs in dc MGs are interfaced with dc-dc converters to regulate and control voltage and output power. A typical model of an average bidirectional Buck-Boost converter is shown in Figure 2.9 [56,61]; note that the controller employs a droop approach to ensure adequate voltage regulation and load sharing. A conventional hierarchical control scheme similar to the one shown in Figure 2.4 could be utilized to control dc MGs.

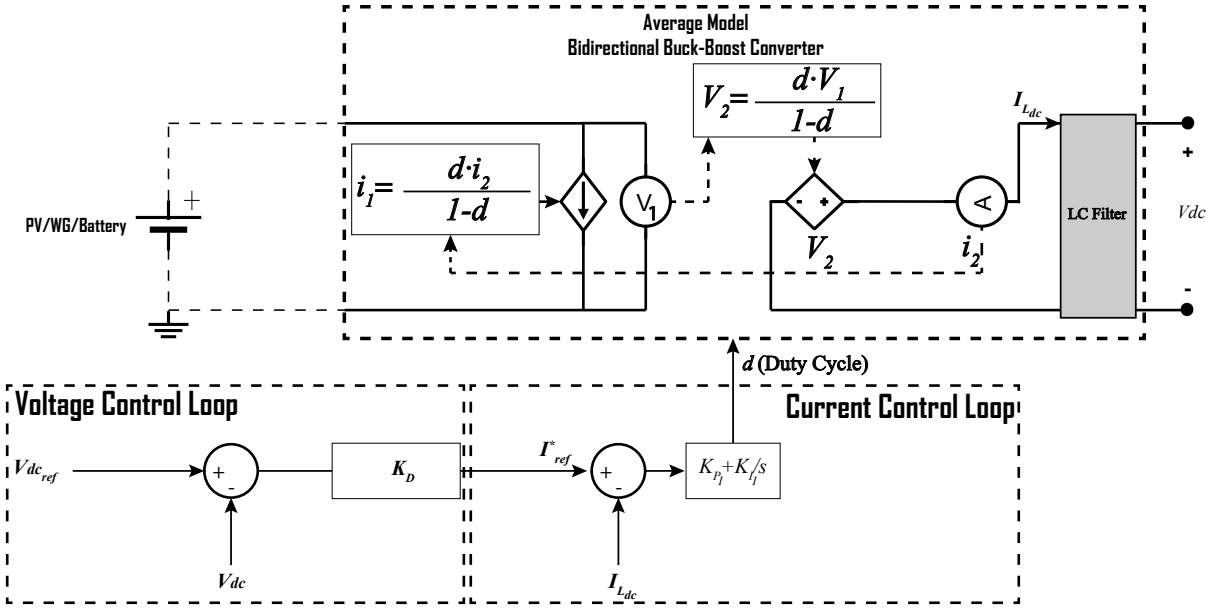

Figure 2.9: Typical average dc-dc converter for DERs [61].

2.2.4.2 DC Loads

Loads of dc MGs could be either dc or ac. If the load is dc, it is interfaced with a buck converter as shown in Figure 2.10, but if it is an ac load, it is connected to the dc MG through an dc-ac converter as shown in Figure 2.3. Thus, the loads behave like constant power loads due to the presence of the converters and their V and I controls, which would have a detrimental impact on the stability of the system if a disturbance occurs in the system, as these loads are not voltage dependent [37,38].

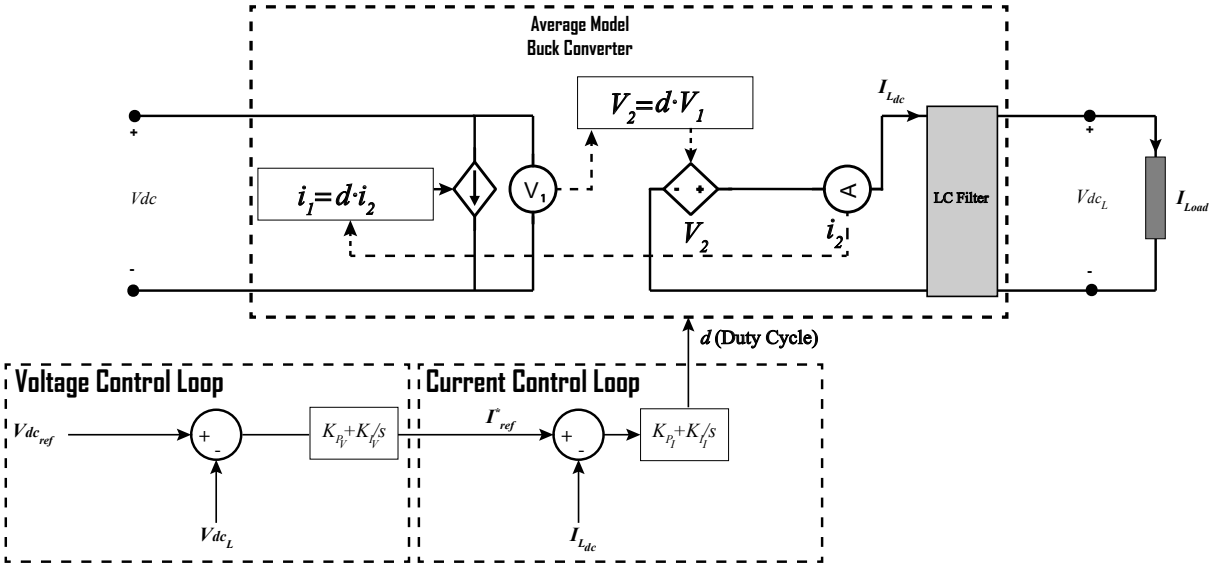

Figure 2.10: DC load model [61].

2.3 MMG System

2.3.1 Architectures and Layouts

An MMG has different layouts, architectures, and technologies (dc and ac systems) as discussed before. Common network architectures of interconnected MGs presented in the literature are [42]:

- Parallel connected MGs with an external entity. This external entity could be the host grid (the main network) or could be a power router that interconnects the MGs, as shown in Figure 2.11(a). This topology is the most realistic one since the microgrids would likely be interconnected through a medium voltage host grid, as observed in most MMG studies [13].
- Series interconnected MGs and host grid, with some MGs having more than one external interconnection, as shown in Figure 2.11(b). It should be mentioned that "MGs" with multiple connections points are not MGs in principle, since the latter have by definition a single PCC.

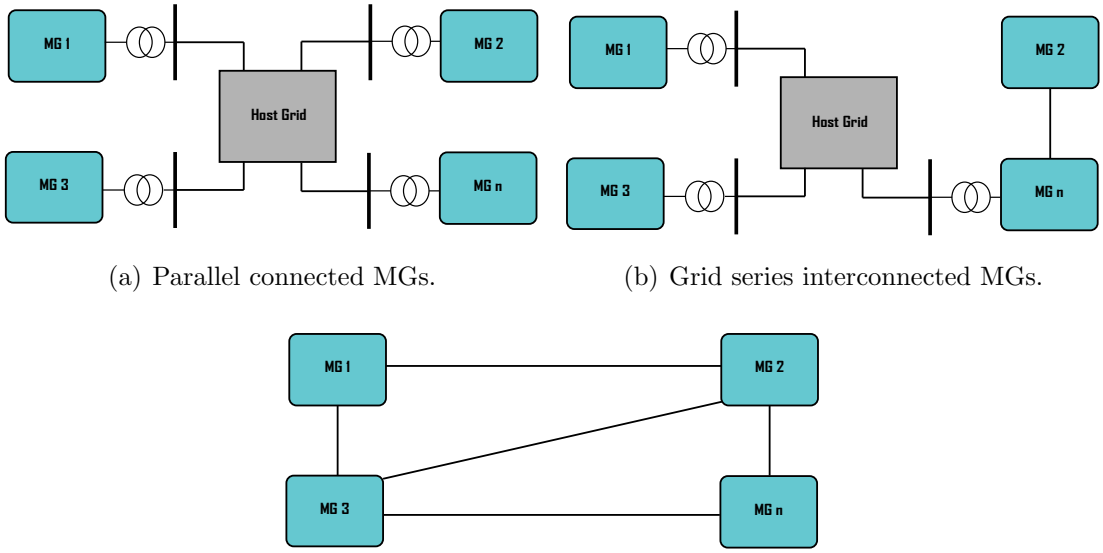

(a) Parallel connected MGs.

(b) Grid series interconnected MGs.

(c) Mixed parallel/series connected MGs.

Figure 2.11: Different MMG architectures [42].

- Mixed parallel/series connection that involves a combination of the aforementioned architectures as shown in Figure 2.11(c).

Each layout has its advantages and disadvantages in terms of protection, reliability, costs, and stability. The MGs in the system could be either ac, dc, or dc-ac systems. To solve synchronization problem among the interconnected MGs, a power exchange unit that consists of VSCs and BESS has been proposed to interface the MGs to enhance and control the energy exchange among the interconnected MGs [14, 41], as previously discussed.

2.3.2 Centralized Control

As already mentioned, an MMG could be controlled and coordinated either through centralized or distributed control schemes. Each one of these schemes has its advantages, disadvantages, and applications.

In a centralized control scheme such as the one depicted in Figure 2.12 , a global central controller obtains data from the system to be used in solving an optimization problem to enhance the stability and energy management of the whole MMG. These data include the

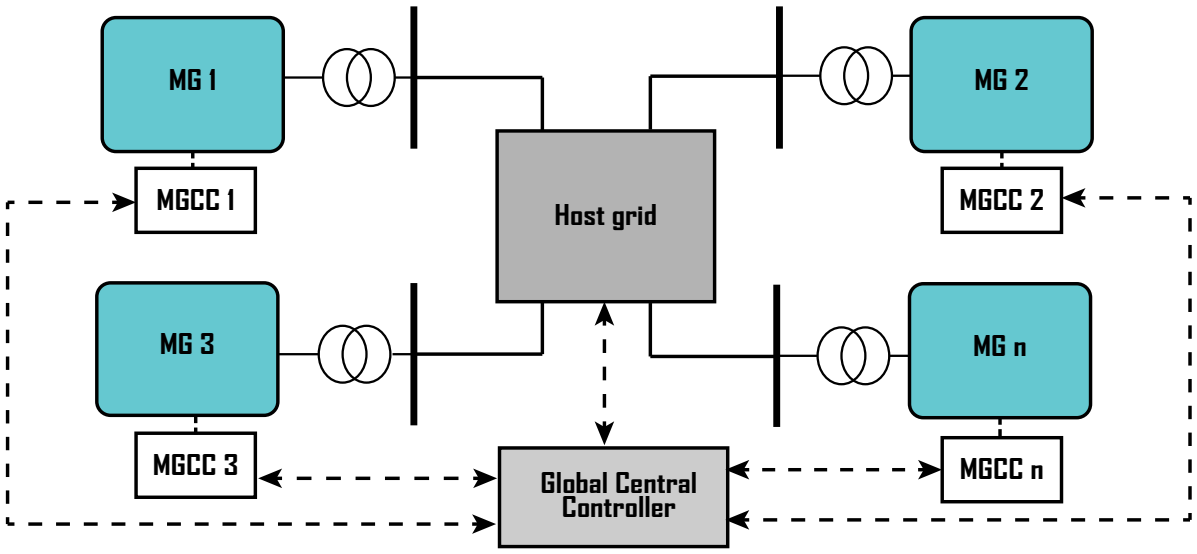

Figure 2.12: Centralized control of an MMG [4].

generation profile of DERs, SOC of BESSs, and load profiles. A centralized control system is effective at controlling an MMG system [4]; however, if there are multiple owners in the system, such a scheme may be difficult to implement.

2.3.3 Distributed Control

A multi-agent control scheme is the most widely used method for a distributed control of an MMG, where each MG becomes an intelligent agent that communicates with neighboring MGs [7]. Such a control method enhances system reliability, since the failure of an agent does not result in a network-wide failure, and it can be readily implemented for large networks, since it could be easily scaled, as there is no need to handle a significant amount of data from the whole system, unlike a centralized control approach.

A multi-agent control system has several drawbacks that could affect its performance. For instance, optimal coordination among the MGs could become an issue, since reaching a consensus among the MGs could be difficult [4]. Hence, these control approaches are typically sub-optimal.

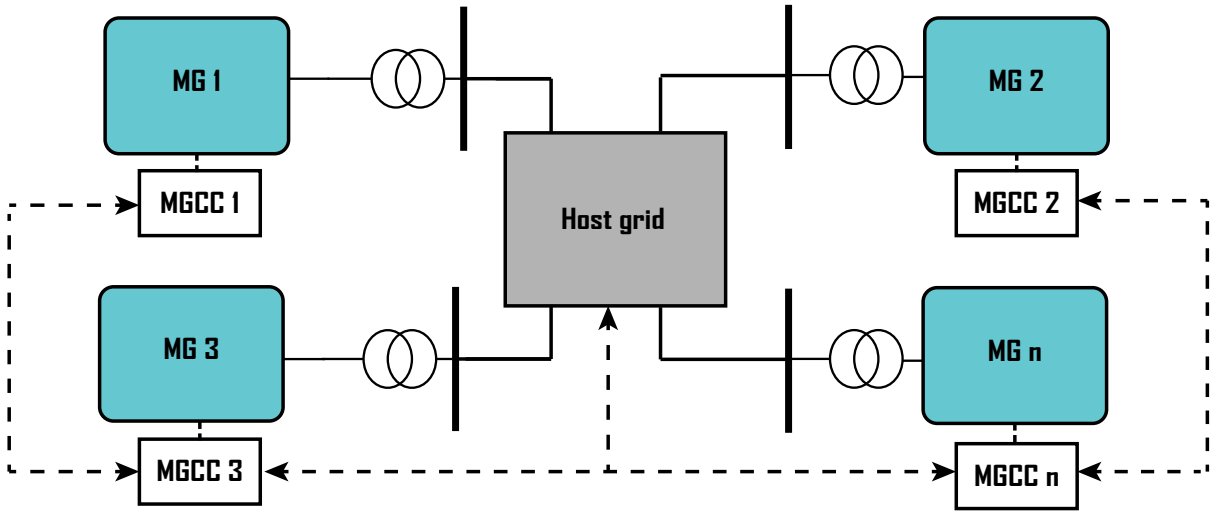

Figure 2.13: Distributed control of an MMG [4].

2.4 Virtual Synchronous Generators

The proposed converters that interface the considered ac and dc MGs in this thesis are assumed to have a control system that behaves like an SG, by emulating its inertia and damping characteristics through the implementation of the SG swing equation in the controllers of the interfacing VSC [62]. Several models have been proposed in the literature to reproduce the dynamics of SGs in VSCs, most of which are voltage controlled, making them susceptible to faults due to the lack of current control loops. Other techniques are based on current control VSGs, which are dependent on a Phase Locked Loop (PLL) for synchronization with the grid. The authors in [63,64] present the control architecture used here, which overcomes the aforementioned issue associated with existing VSG models, and consists of robust cascaded control loops, where a voltage control loop utilizes the virtual rotor angle as a reference, which is generated by the internal swing equation model, cascaded with a current control loop. However, the proposed VSG is not considered in the context of B2B converter interfaces, and the operational constraints on the dc side of the VSC and the AVR of the VSG are not considered, which are all issues addressed in this thesis.

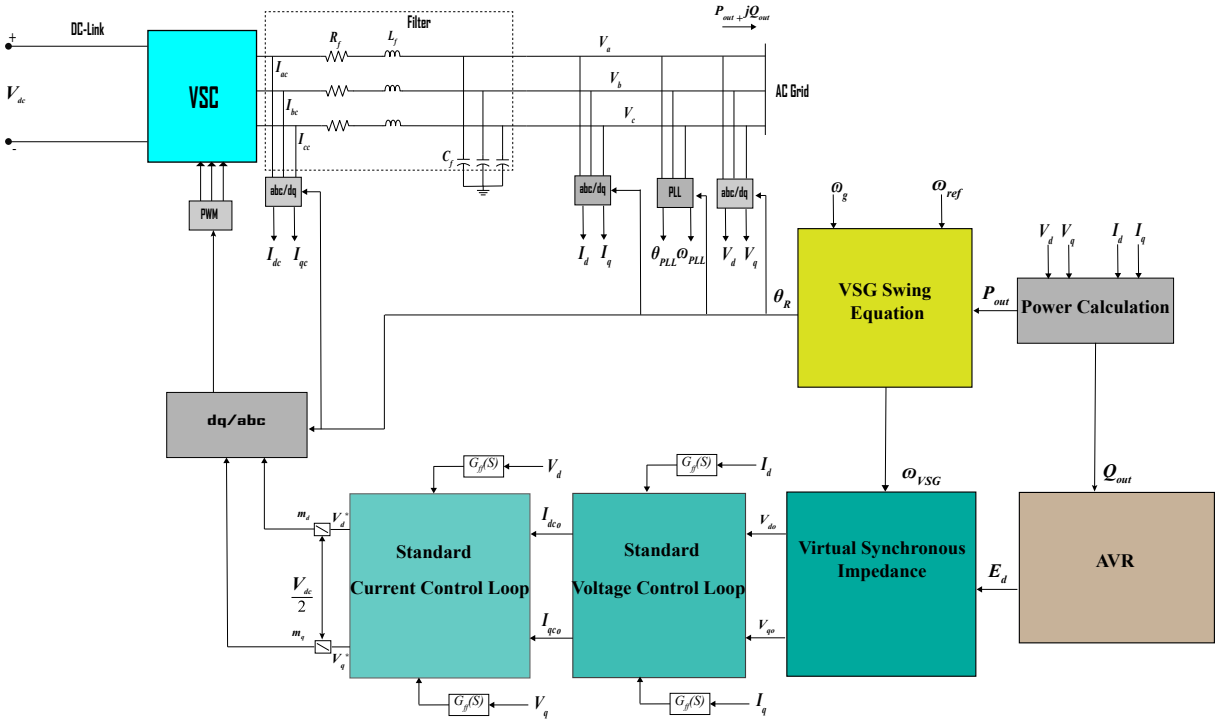

Figure 2.14: Typical current controlled VSG model [64].

2.4.1 VSG Governor and AVR model

The generic architecture of a VSG is shown in Figure 2.14, derived from [64], which consists of several control loops such as an AVR, the VSG swing equation that includes the governor, a virtual synchronous impedance, and standard VSC voltage control and current control loops [65]. A VSG is centered on the virtual implementation of SG swing equation [62]:

$$P_{gov} - P_e = J\ \omega_{VSG}\frac{\mathrm{d}\omega_{VSG}}{\mathrm{d}t} + D(\omega_{VSG} - \omega_{PLL}) \tag{2.9}$$

where P_{gov} is the input power obtained from the virtual governor, P_e is the output power of the VSG, J is the virtual moment of inertia, D is the virtual damping factor, ω_{VSG} is the angular velocity of the VSG, and ω_{PLL} is the angular frequency obtained from the PLL. The angular velocity defines the virtual rotor angle θ_R, which is fed to the dq/abc and abc/dq conversion blocks to synchronize the VSG to the grid, as follows:

$$\frac{\mathrm{d}\theta_R}{dt} = \omega_{VSG} \tag{2.10}$$

The VSG governor includes a droop control to implement the frequency-power relationship in SGs to share the load demand proportionally among the VSGs, which yields the virtual prime-mover power P_{gov} in the swing equation, and is implemented as follows:

$$P_{gov} = \frac{K_P(\omega_{ref} - \omega_{VSG})}{1 + \tau s} + P_o \tag{2.11}$$

where K_P is the VSG droop coefficient, P_o is the VSG reference power, and τ is the virtual turbine time constant.

The AVR generates the virtual internal field voltage E_d, and is used to implement the voltage-reactive power relationship through droop control as follows:

$$E_d = \left[K_Q(Q_o - Q_{out}) + V_o - V_{out}\right]\left(K_{P_Q} + \frac{K_{I_Q}}{s}\right) \tag{2.12}$$

where Q_o is the reference reactive power, Q_{out} is the reactive power output, K_Q is the droop coefficient, V_o is the reference terminal voltage, V_{out} is the VSG output voltage, and K_{P_Q}, and K_{I_Q} are the gains of the AVR PI controller.

2.4.2 Virtual Synchronous Impedance and Voltage Control Loops

The virtual internal field voltage E_d generated by the AVR is behind a virtual synchronous impedance $R_s + jX_s$, and is fed to the voltage control loop to regulate the terminal voltage of the VSG. Thus, the following are the reference input voltages V_{do} and V_{qo} for the voltage control loop:

$$V_{do} = E_d + X_s I_q - R_s I_d \tag{2.13}$$

$$V_{qo} = 0 - X_s I_d - R_s I_q \tag{2.14}$$

These are then utilized in the voltage control loop to generate the dq-axis components of the reference currents for the inner current control loop as follows:

$$I_{dc_o} = (V_{do} - V_d)\left(K_{P_V} + \frac{K_{I_V}}{s}\right) - V_q\ \omega_{VSG}\ C_f + I_d\ G_{ff}(S) \tag{2.15}$$

$$I_{qc_o} = (V_{qo} - V_q)\left(K_{P_V} + \frac{K_{I_V}}{s}\right) + V_d\ \omega_{VSG}\ C_f + I_q\ G_{ff}(S) \tag{2.16}$$

where $G_{ff}(S)$ is a first-order transfer function of a feed-forward filter, I_d and I_q are the dq components of the output current, and K_{P_V} and K_{I_V} are the parameters of the PI controller of the voltage control loop. The reference currents have hard-limits to protect the VSC from overcurrents.

2.4.3 Current Control Loop

The inner current control loop generates the decoupled dq components V_d^* and V_q^*, which are fed to the dq/abc conversion block to be used as a reference for the average modeled VSC, as follows:

$$V_d^* = (I_{dc_o} - I_{dc}) \left(K_{P_I} + \frac{K_{I_I}}{s} \right) - I_{qc}\, \omega_{VSG} L_f + V_d\, G_{ff}(S) \tag{2.17}$$

$$V_q^* = (I_{qc_o} - I_{qc}) \left(K_{P_I} + \frac{K_{I_I}}{s} \right) + I_{dc}\, \omega_{VSG} L_f + V_q\, G_{ff}(S) \tag{2.18}$$

where K_{P_I} and K_{I_I} the parameters of the PI controller of the current control loop.

2.5 Summary

This chapter briefly covered the main relevant background for the proposed research. Thus, a general overview of MG modeling, operation, and control were first presented. Then, a brief review of dc MGs was provided. Different layouts and architectures of an MMG were also discussed, together with associated, coordination, and control issues of a network of MGs. Finally, the VSG principles models, and controls used throughout the thesis were presented.

Chapter 3

Distributed Control of Interconnected MGs

This chapter first presents a distributed, droop-free voltage control of a dc MG in grid-connected and isolated mode. The proposed control technique, based on a distributed consensus approach, addresses reliability issues of centralized controllers that are prone to single point failure, while sharing the loads among DERs more effectively than conventional decentralized droop controllers. The distributed control scheme is implemented, demonstrated, and compared with a conventional droop control using time-domain simulations for a model of an actual dc MG in Xiamen University, China, based on various realistic scenarios.

The second part of the chapter proposes a hierarchical control scheme based on the aforementioned distributed controller to coordinate the MMG system. Thus, a proposed control approach of MG interfaces is presented, based on VSGs to control the power exchange of interconnected ac and dc MGs, and provide frequency support, voltage regulation, and virtual inertia for individual MGs and the host grid as required. A hierarchical distributed control technique is proposed, with primary controls of interfacing VSGs providing adaptive inertia for the ac systems, while a secondary distributed control of the system regulates the frequency and the voltages of the host grid and the interconnected MGs, based on a consensus technique with limited information about the overall system. The proposed controller shares the total system load among the grid and MGs, while minimizing the overall frequency and dc-voltage deviations in all interconnected systems. The presented interface and the controller are implemented, tested, and validated using time-domain simulations for an MMG test system, which is based on a CIGRE benchmark medium voltage system and consists of both ac and dc MGs.

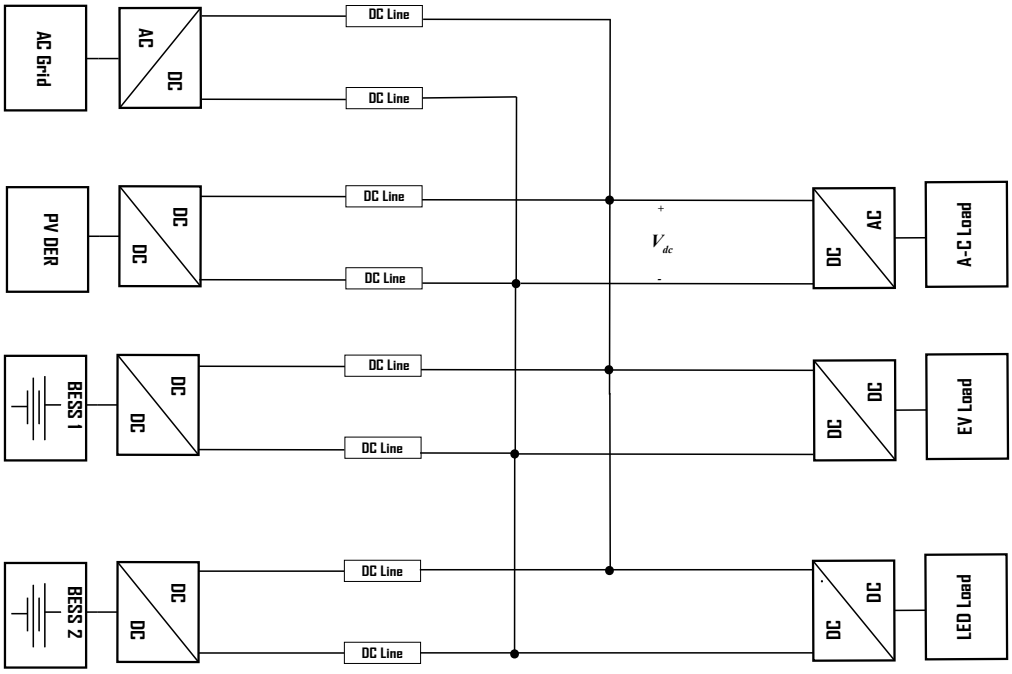

Figure 3.1: Test dc MG based on [66].

3.1 Distributed Droop-Free DC Voltage Controller

The proposed controller described in this section is based on distributed consensus control theory [39], which is first applied to a dc MG, and later for an MMG system.

3.1.1 DC MG Configuration

The test dc MG used here is based on a building at Xiamen University [66], which is a two-wire, unipolar 380 V dc grid as shown in Figure 3.1. The MG contains a set of 150 kW PV panels; a 200 Ah, 336 V lead-acid battery bank, split in two parts to increase the number of DERs for testing purposes; and a 160 kW bidirectional ac-dc converter for grid connection. The loads are 20 kW LED lights, a 40 kW Electrical Vehicle (EV) charging station, and a 30 kW Air-Conditioning (A-C) system. Line resistances are small (5 mΩ), given the small-scale of the dc grid [56]. Average converter models are used to model the interface of all grid components, as described in Chapter 2. The data for the this test system is presented in Appendix A.

3.1.2 Communication Graph Algebraic Theory

To form a bidirectional communication graph, the dispatchable DERs of a dc MG are linked with communication channels. Two sets of vectors are used to represent a graph $G = (\mathcal{V}, \mathcal{E})$, where $\mathcal{E}$ represents the links from node v_i to node v_j, while the set $\mathcal{V}$ contains the vertices or nodes of the graph $[v_1, v_2, .., v_N]$, corresponding only to the systems' dispatchable DERs [39]. A connectivity matrix $A_G = [a_{ij}]$ includes weights $a_{ij} = 0$ if DER i does not exchange information with DER j, or $a_{ij} > 0$ if a link $(v_i, v_j) \in \mathcal{E}$ exists.

The communication topology of an MG, shown in Figure 3.2 for the test dc MG, as per [39], is sparse and includes spanning trees, is robust against communication link failures, and reflects the geographical placement. In this topology, the communication links among the DERs are bidirectional and each DER can communicate only with neighbouring DERs. The connectivity matrix of Figure 3.2 is then:

$$A_G = \begin{bmatrix} 0 & 1 & 0 \\ 1 & 0 & 1 \\ 0 & 1 & 0 \end{bmatrix} \tag{3.1}$$

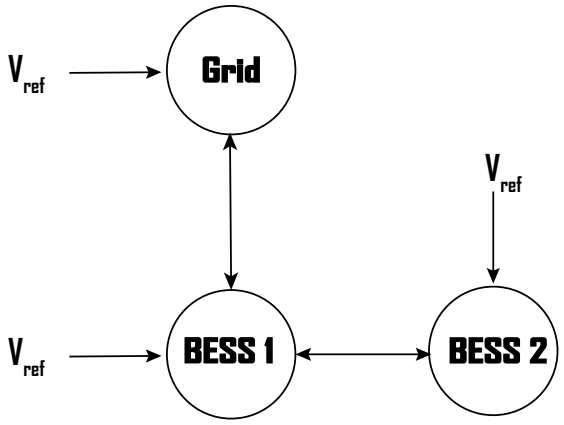

Figure 3.2: Proposed communication graph of the test dc MG.

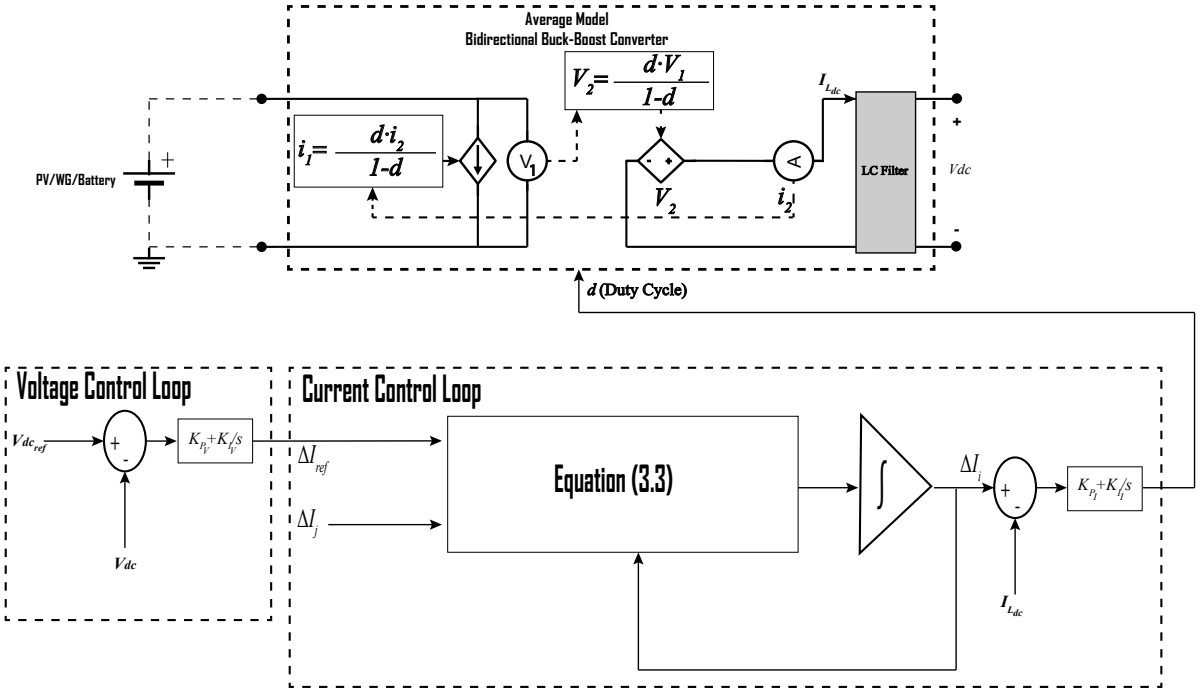

Figure 3.3: Proposed distributed consensus controller for DC interfaces.

3.1.3 Proposed Distributed Controller

The proposed and generic distributed technique to regulate the voltage of a dc MG consists of two parts. The first one is the local voltage control loop for all dispatchable DERs as follows:

$$\Delta I_{ref} = (V_{dc_{ref}} - V_{dc})\left(K_{P_V} + \frac{K_{I_V}}{s}\right) \tag{3.2}$$

where $V_{dc_{ref}}$ is the reference rated voltage of the dc MG, and V_{dc} is the measured voltage of the dc MG, as shown in Figure 3.1; K_{P_V} and K_{I_V} are the parameters of the local PI-controller of the voltage control loop; and ΔI_{ref} is the change in the reference current to be used in the inner current control loop of the distributed controller. Note that non-dispatchable DERs (e.g., solar PV sources) are not controllable since their output power is intermittent, as these are designed to obtain their maximum available active power [27], and hence do not participate in the proposed control approach. Therefore, for the example considered here, the controlled dispatchable DERs are the grid connection, BESS 1, and BESS 2, operating at $V_{dc_{ref}} = 380$ V.

The output current changes of neighbouring DERs ΔI_j are communicated to the local DER i, to be used in the inner current control loop as follows, based on a consensus control principle technique:

$$\frac{\mathrm{d}\Delta I_i}{\mathrm{d}t} = \sum_{j \in N_i} a_{ij} \left(\frac{\Delta I_j}{I_{max_j}} - \frac{\Delta I_i}{I_{max_i}} \right) + b_i \left(\Delta I_{ref} - \frac{\Delta I_i}{I_{max_i}} \right) \forall i \tag{3.3}$$

where ΔI_i is the local control signal tracking ΔI_{ref} for DER i; ΔI_j is the output current variation of a neighbouring DER j; I_{max_j} and I_{max_i} are the maximum current capacities of the neighbouring DER and the local DER respectively; a_{ij} is either 1 or 0, depending on the communication network linking the dispatchable DERs, as explained in the previous section; and b_i is a binary variable set to 1 if the DER has access to the reference current ΔI_{ref} generated from the voltage control loop, otherwise $b_i = 0$. The tracking current error $\frac{\mathrm{d}\Delta I_i}{\mathrm{d}t}$ integration results in the convergence of ΔI_i to ΔI_{ref}. The dispatchable DERs of the system are then integrated with the proposed controller as shown in Figure 3.3 and Figure 3.4.

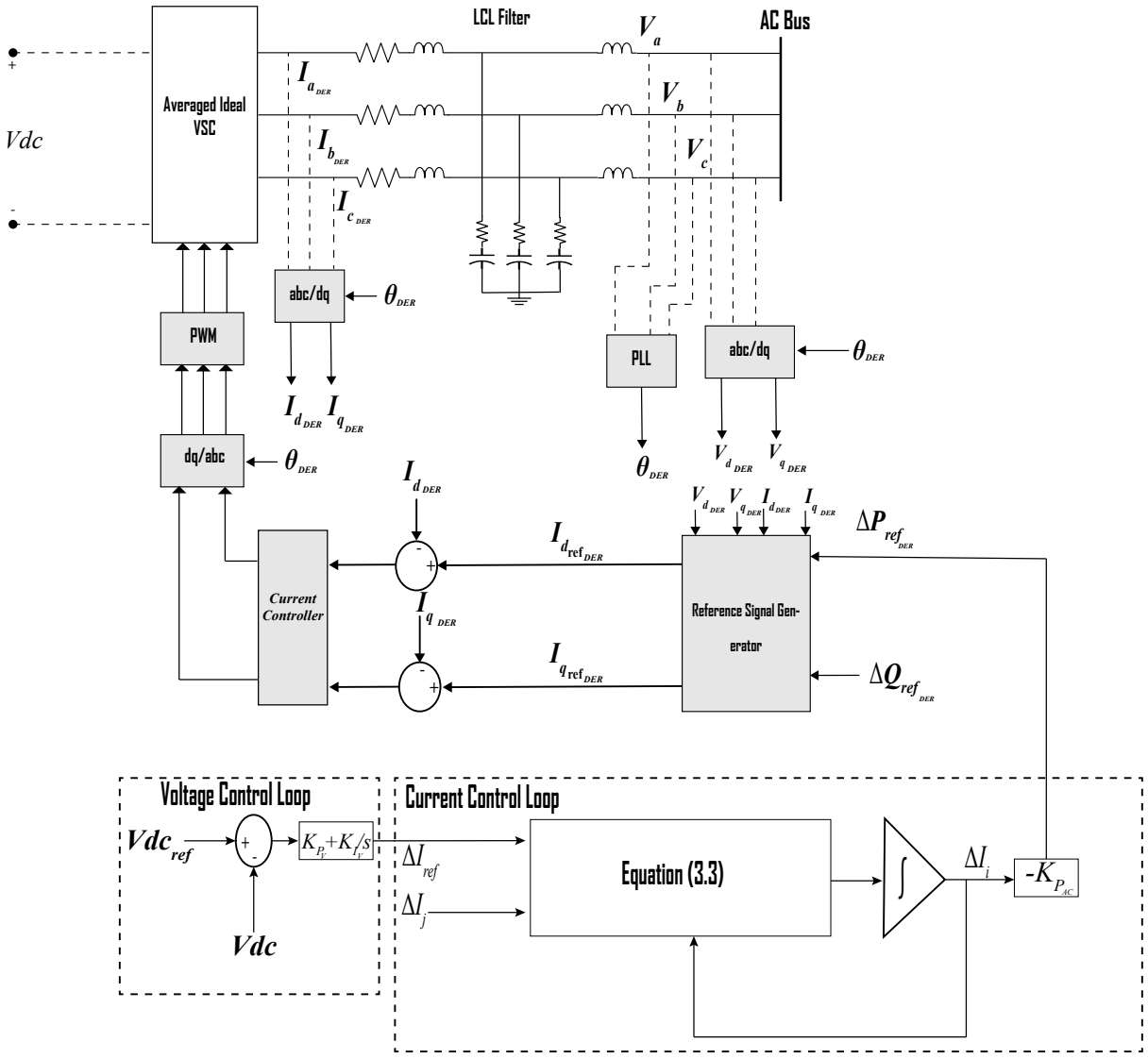

Figure 3.4: Proposed distributed consensus controller for the AC grid interface.

3.1.4 Case Studies and Results

The aforementioned distributed control technique is demonstrated and validated on the test system shown in Figure 3.1. A dynamic model of the system is implemented here, and throughout the thesis, for time-domain simulations in PSCAD [67], based on average

converter models.

The grid connection and BESSs are responsible for regulating the voltage of the system, while the solar PV DER produces an output power obtained from an actual generation profile [68], as shown in Figure 3.5 with its impact on the system voltage for conventional droop control. The initial droop gains of the primary voltage controllers of the grid connection and BESSs are selected by trial-and-error to ensure that the voltage of the dc MG does not deviate by more than 10 % due to the variability of the output power of the PV, and considering load sharing proportional to DER rating.

3.1.4.1 Validation and Comparison

In Figure 3.6, the proposed distributed controller is compared with the conventional primary droop control, as described in Chapter 2, with different droop gains K_D. Observe that as droop gains of the DERs increase, the voltage regulation of the system improves. However, the proposed distributed control technique performs much better than conventional droop control even if a high gain is chosen, with the dc voltage being always maintained close to the rated 380 V.

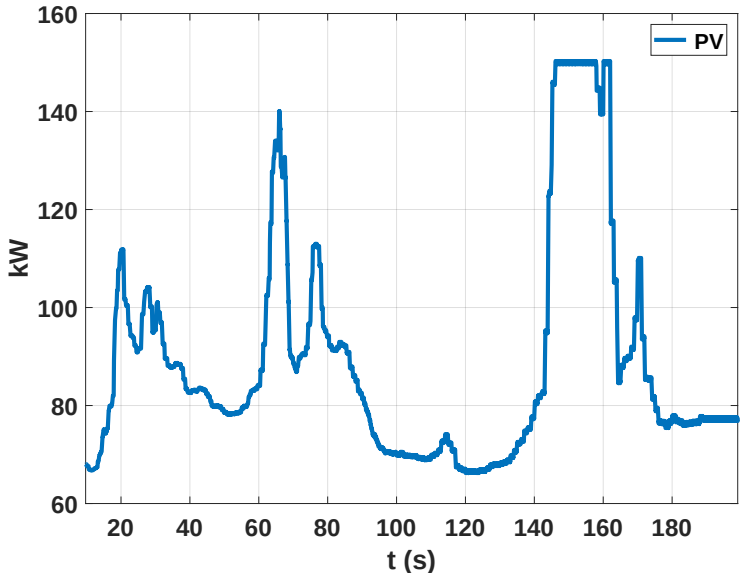

(a)

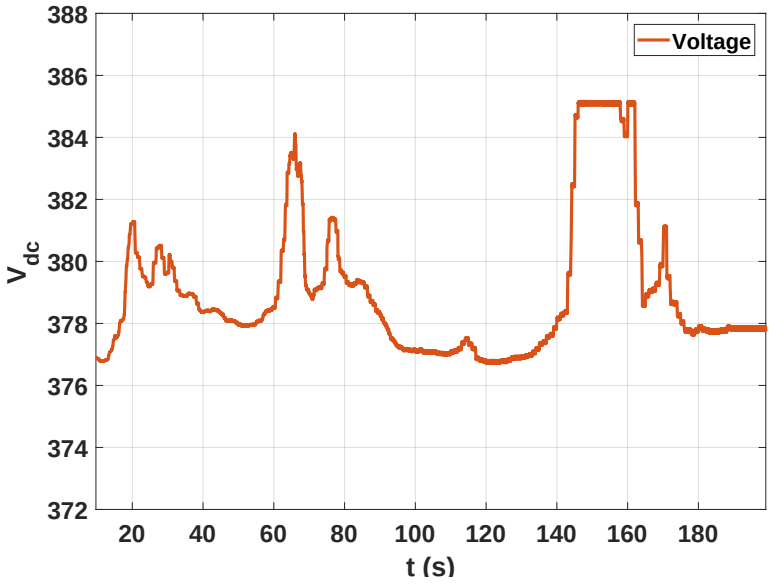

(b)

Figure 3.5: DC MG test system (a) PV power output, and (b) dc voltage for conventional droop control.

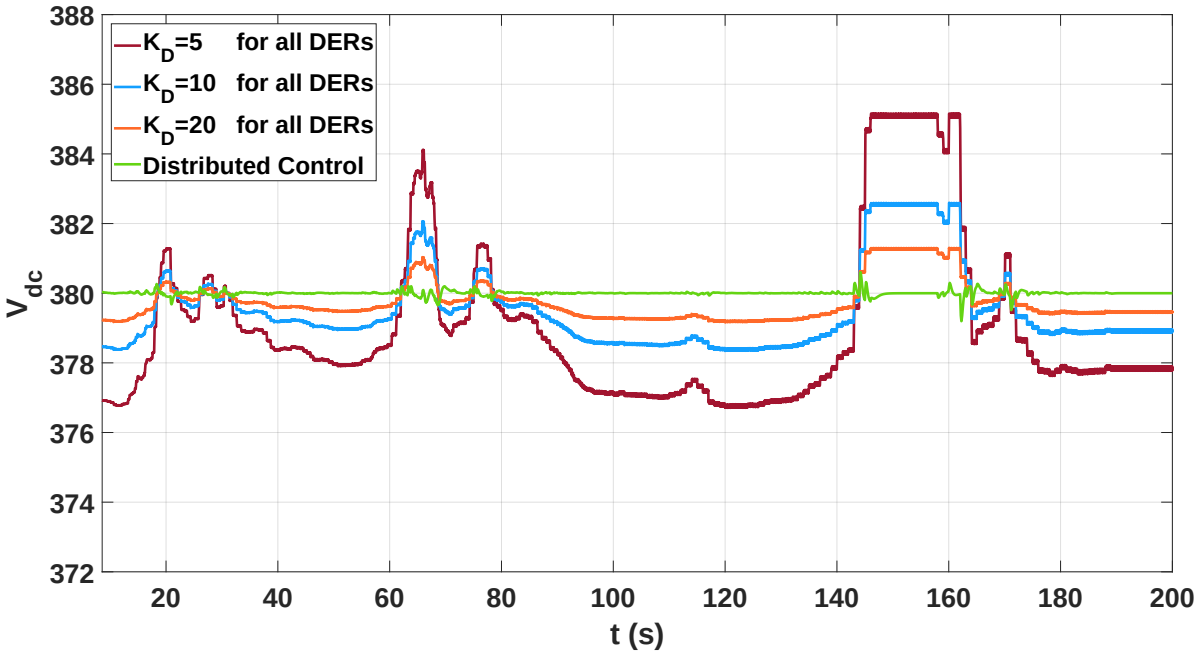

Figure 3.6: DC MG voltage with conventional droop control and the proposed distributed control.

The output powers of the grid connection and the BESSs with the proposed distributed control are shown in Figure 3.7. Note that the proposed distributed technique shares the power proportionally among the DERs according to their maximum current capacity. Observe also that the power exchange with the grid connection is significant compared to the other DERs, since the power capacity of the grid connection is bigger. A centralized integrator-based controller, which is an alternative option to recover the dc voltages in the MG, could be implemented and compared with the proposed decentralized approach; however, this was not pursued here, as this is a well-known solution, and the research was rather focused on the development and implementation of a decentralized approach.

3.1.4.2 Stability Analysis

The impact of the distributed controller on the post disturbance stability of the system is empirically investigated in this section, with the output power of the PV being reduced by 50 % at $t = 100$ s. The simulation results using conventional droop control, with maximum droop gain for all DERs, and the distributed controller are shown in Figure 3.8. Note that

the conventional droop control becomes unstable, while the proposed distributed controller is stable and recovers the system voltage to the nominal value.

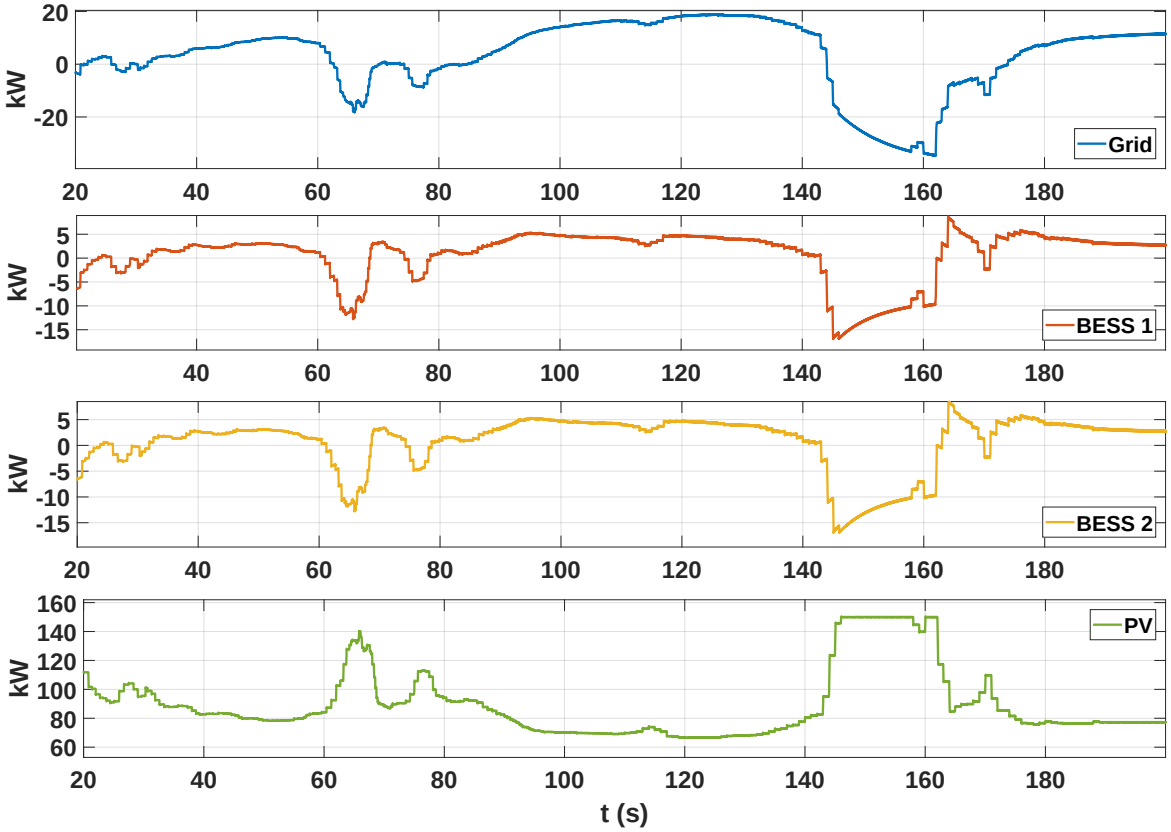

Figure 3.7: Output power of dc MG DERs for the proposed distributed control.

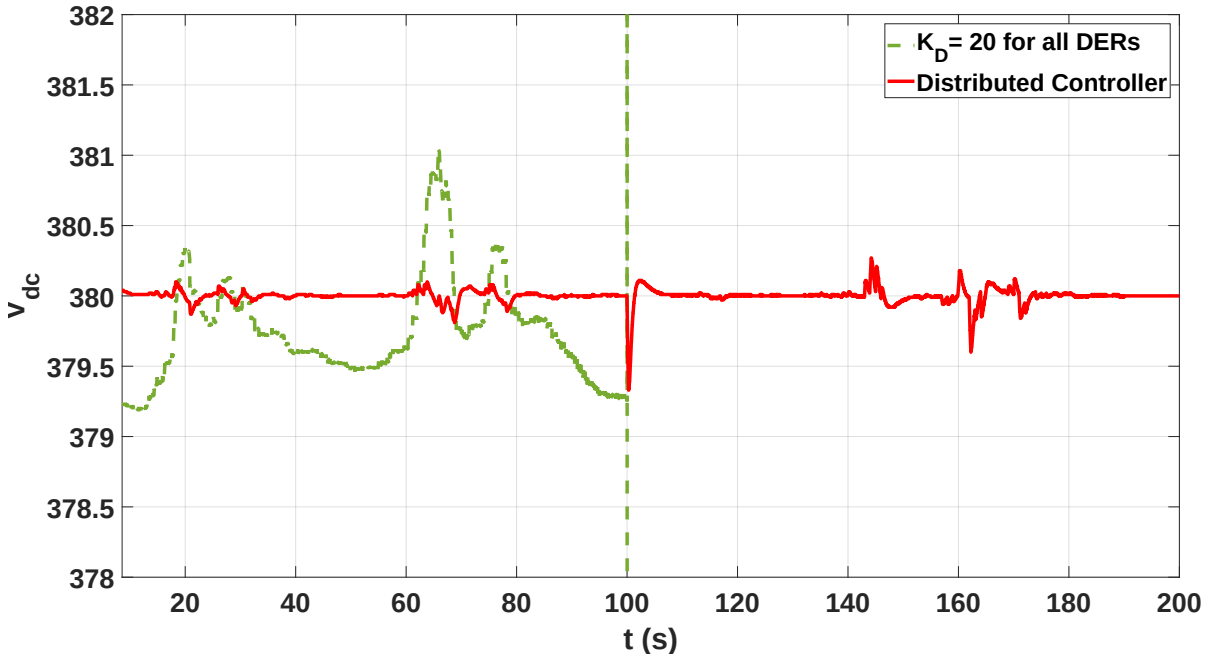

Figure 3.8: DC MG voltage after 50% reduction of PV output power at $t = 100\,\text{s}$.

3.1.4.3 Communication Link Failure and Islanding Mode

This section investigates the impact of islanding the dc MG by disconnecting the grid interface at $t = 100\,\text{s}$, which is the slack DER for this system and thus sized to cover all power demands, to test the robustness of the distributed controller against a communication link failure. The simulation results using conventional droop control and the proposed distributed controller are shown in Figure 3.9. Observe that the distributed controller maintains the voltage of the dc MG close to the rated voltage, even if the communication link to the grid interface is lost and the MG is islanded, demonstrating the robustness of the distributed controller. The conventional droop control, on the other hand, shows significant voltage variations compared to the distributed controller.

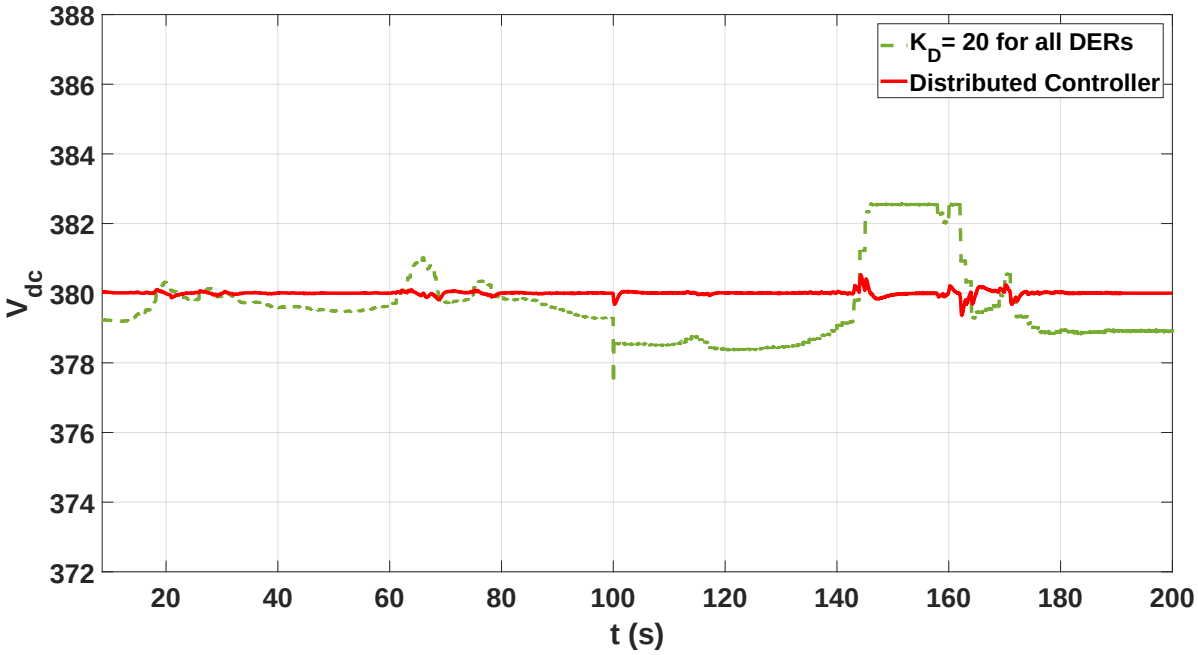

Figure 3.9: DC MG voltage after disconnecting the grid interface and a communication link failure at $t = 100\,\text{s}$.

3.1.4.4 Communication Delay

The impact of communication delay on the distributed control technique is investigated in this section. In this case, the output current measurement of a neighbouring DER ΔI_j received by DER i is subjected to a time delay $G_d(s) = e^{-s\tau}$, where τ is the time delay. Hence, equation (3.3) is modified as follows:

$$\frac{\mathrm{d}\Delta I_i}{\mathrm{d}t} = \sum_{j \in N_i} a_{ij} \left(\frac{\Delta I_j}{I_{max_j}} e^{-s\tau} - \frac{\Delta I_i}{I_{max_i}} \right) + b_i \left(\Delta I_{ref} - \frac{\Delta I_i}{I_{max_i}} \right) \forall i \tag{3.4}$$

The controller was thus tested with the following time delays: $\tau = 20\,\text{ms}$, $\tau = 0.5\,\text{s}$, $\tau = 5\,\text{s}$, and $\tau = 15\,\text{s}$ to emulate various operating conditions.

The simulation results are shown in Figure 3.10, where it can be observed that the performance of the distributed controller is only affected when time delays are longer than $\tau = 5\,\text{s}$, which satisfies 0.1 s to 5 s time delay requirements for smart grid applications [69]. Note that the performance of the proposed distributed controller is superior to droop control for communication delays of up to $\tau = 5\,\text{s}$.

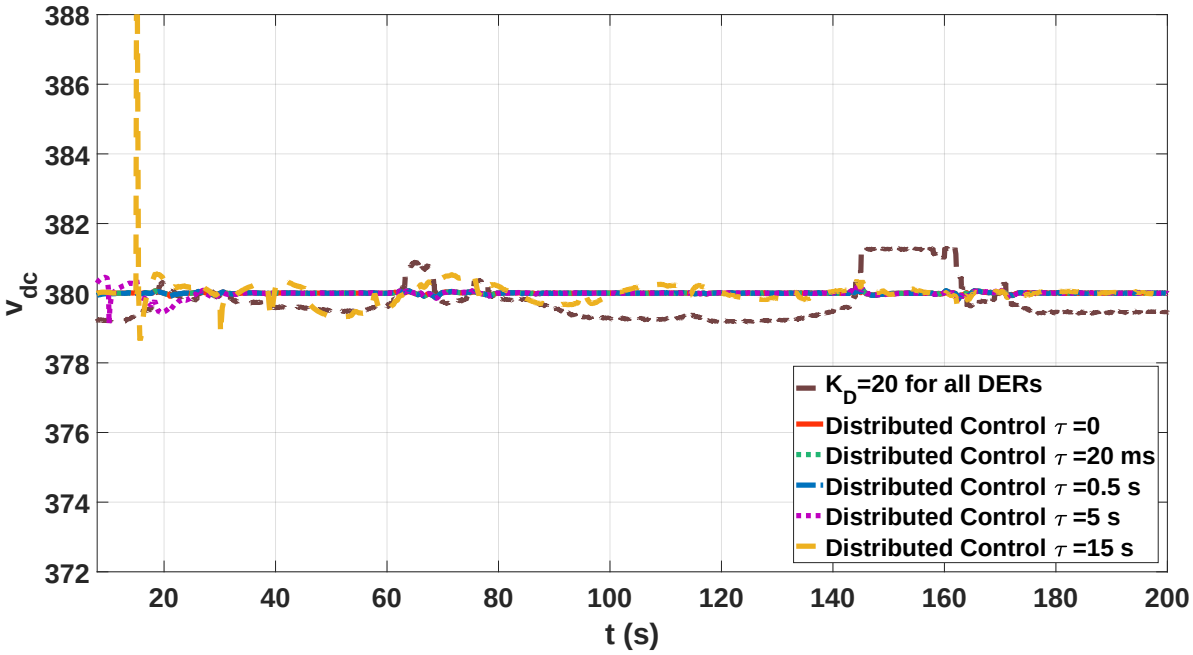

Figure 3.10: DC MG voltage with different distributed control communication latencies.

3.2 Distributed Control of MMG

3.2.1 Proposed AC Micorgrid Interface

The proposed control scheme interfaces the dc and ac MGs with the host ac grid through a VSG controller. This approach offers several advantages, such as full controllability of the power flow among the linked MGs, while decoupling the frequencies of ac MGs and the voltage of dc MGs, thus allowing MGs to operate at different frequencies or dc voltages, hence minimizing the impact of disturbances on the MGs. This also allows providing virtual inertia by implementing the aforementioned VSG control approach in the B2B converters, which modulates the inertia of the interconnected system and thus improves the frequency response of the overall system.

3.2.1.1 B2B VSG Interface

The B2B interface consists of two VSC connected through the DC-Link as depicted in Figure 3.11 [65], where each VSC includes the control loops shown in Figure 3.12. The left-hand side connects to the MG while the right-hand side connects to the main ac grid. Both VSCs are capable of operating in VSG mode and regulate the DC-Link voltage, depending on the coordination technique for the MMG system. Thus, if the ac MG needs frequency regulation, the left-hand side VSC will operate in VSG mode and provide frequency support for the MG, while the right-hand side regulates the DC-Link voltage. If the MG has excess generation capacity from its DERs, it can export power to the rest of the system by operating the right-hand-side in VSG mode, while the left-hand-side VSC regulates V_{dc}.

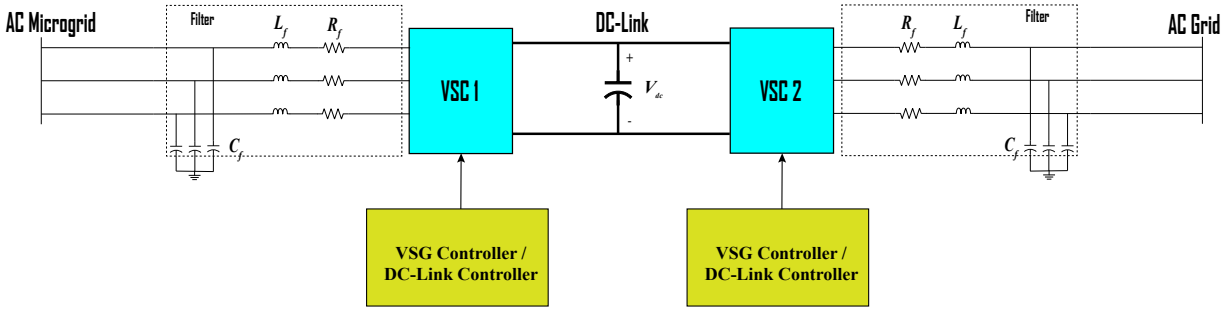

Figure 3.11: B2B VSG Interface.

3.2.1.1.1 DC-Link Voltage Regulation

The VSC that regulates V_{dc} works in current control mode, controlling the active power output of the VSC to satisfy the power balance of the DC-Link and maintain a constant dc voltage. The dq-components of the reference currents in this case are calculated as follows:

$$I_{d_{ref}} = \frac{2}{3} \frac{P_{ref} V_d + Q_{ref} V_q}{V_d^2 + V_q^2} \tag{3.5}$$

$$I_{q_{ref}} = \frac{2}{3} \frac{P_{ref} V_q - Q_{ref} V_d}{V_d^2 + V_q^2} \tag{3.6}$$

where V_d and V_q are the dq-components of the output voltage, and P_{ref} and Q_{ref} are the desired active and reactive power, respectively, with P_{ref} being obtained from the DC-Link voltage regulator loop as follows [65]:

$$P_{ref} = -\left(V_{dc_o}^2 - V_{dc}^2\right)\left(K_{Pdc} + \frac{K_{Idc}}{s}\right) + P_{dc} \tag{3.7}$$

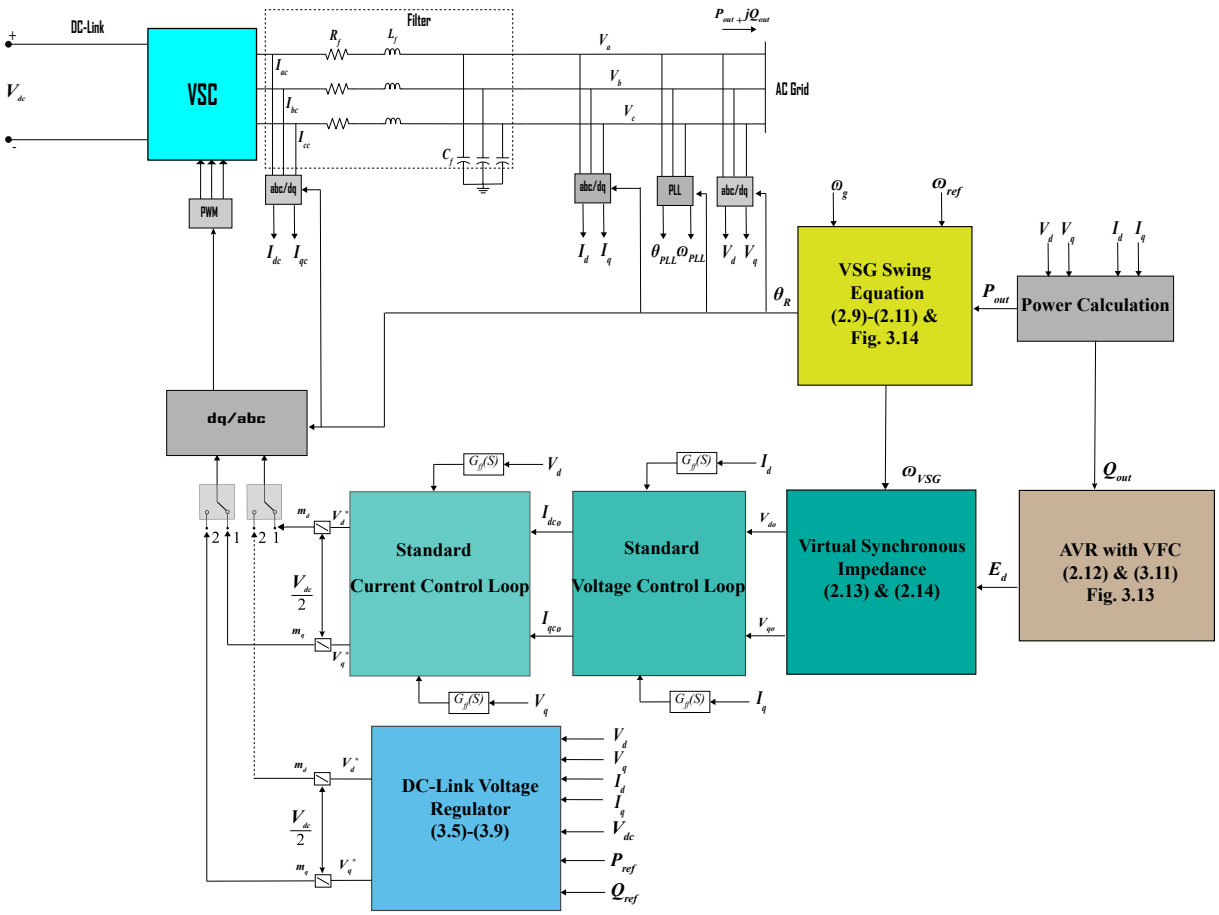

Figure 3.12: VSC with VSG control scheme interface [64].

where V_{dc_o} is the reference DC-Link voltage, V_{dc} is the actual DC-Link voltage, K_{Pdc} and K_{Idc} are the parameters of the PI controller of the dc link regulator loop, and P_{dc} is the feed-forward term that represents the DC-Link power, which is approximately equal to the output power of the other VSC that is operating in VSG mode.

The reference currents $I_{d_{ref}}$ and $I_{q_{ref}}$ are inputs for the current control loop with decoupling feed-forward terms to obtain the dq-axes voltage references, which are fed to the

VSC in Figure 3.12 after transformation to the abc-reference frame, as follows [57]:

$$V_d^* = \left(I_{d_{ref}} - I_d\right)\left(K_{P_I} + \frac{K_{I_I}}{s}\right) - I_q\omega L_f - V_q\ \omega C_f R_f + V_d(1-\omega^2 L_f C_f) + I_d R_f \quad (3.8)$$

$$V_q^* = \left(I_{q_{ref}} - I_q\right)\left(K_{P_V} + \frac{K_{I_I}}{s}\right) + I_d\omega L_f + V_d\ \omega C_f I_d + V_q(1-\omega^2 L_f C_f) + I_q R_f \quad (3.9)$$

The parameters of the PI controllers of the DC-Link voltage regulator and the current control loop are tuned to ensure the control loops are stable when the VSC injects or absorbs its rated power [70, 71].

3.2.1.1.2 VFC

It is usually assumed that reactive power does not impact the DC-Link power balance, since it is produced from the exchanged energy among the phases of the VSC [65]. However, in ac MGs, loads are typically voltage-dependent, and hence, with suitable voltage control, the frequency of the MG could be controlled by controlling the operating voltage of the MG [44], minimizing the impact of disturbances on the system and creating more active power reserves, thus allowing the VSG interface to export more power to the rest of the system. Therefore, the AVR of the VSG is augmented here with a VFC controller based on [44], considering that the loads of the MG are represented by an exponential model per (2.2) and (2.3). Thus, adjusting the voltage setpoints of the DERs and the B2B VSC affects the load demand as follows:

$$\Delta P_D = \sum_{l=1}^{N_L} K_{LP_l}\left[(V+\Delta V)^{\alpha_{P_l}} - V^{\alpha_{P_l}}\right] \quad \forall l \quad (3.10)$$

The frequency of the system could then be controlled by adjusting the change in the operating voltage of the MG as follows:

$$\Delta V = \left(K_{P_{VFC}} + \frac{K_{I_{VFC}}}{s}\right)\frac{1+\tau_{1_Q}s}{1+\tau_{2_Q}s}\,\Delta f \quad (3.11)$$

where $K_{P_{VFC}}$ and $K_{I_{VFC}}$ are the parameters of a PI controller, and τ_{1_Q} and τ_{2_Q} are lead-lag time constants. It is important to note that the VFC does not only provide frequency regulation by adjusting the voltage setpoints, but also enhances the VSG fault ride-through by reducing output voltage during faults. The proposed VFC is integrated into the AVR of the VSG interface.

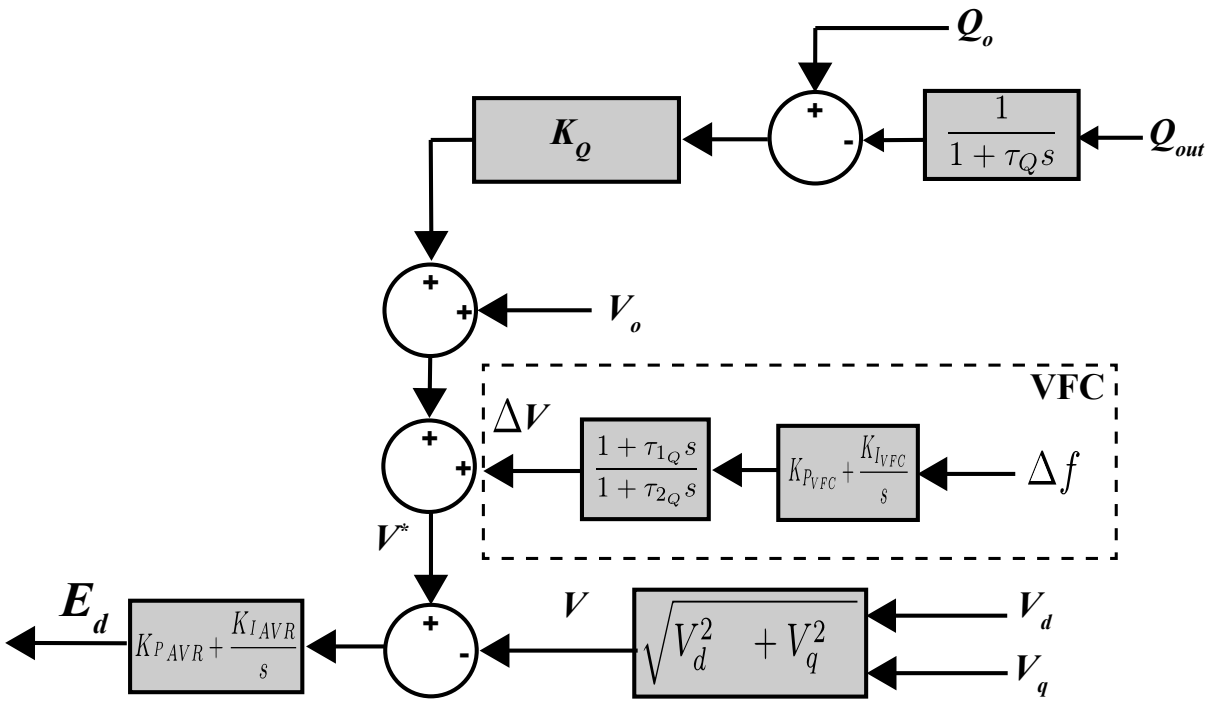

Figure 3.13: AVR with VFC.

The AVR in Figure 3.13 consists of a reactive power droop controller cascaded by a VFC, which generates the reference voltage V^* for the voltage regulator as follows:

$$V^* = V_o + \Delta V + K_Q \left(Q_o - \frac{Q_{out}}{1 + \tau_Q s} \right) \tag{3.12}$$

The regulator then utilizes a PI controller to generate the virtual internal field voltage E_d as follows:

$$E_d = \left(K_{P_{AVR}} + \frac{K_{I_{AVR}}}{s} \right) (V^* - V) \tag{3.13}$$

3.2.1.1.3 Adaptive Inertia

Unlike conventional SGs, the inertia and damping characteristics of the VSG could be adjusted with a suitable controller to obtain an optimal frequency response and enhanced stability. The technique proposed here is based on adjusting the inertia constant of the VSG as discussed in [72]; however, that approach has some limitations, since it alternates

Frequency	$\mathrm{d}\omega_{VSG}/\mathrm{d}t$	Mode	Inertia	Damping
$f \geq f_{min}$	$\lvert a_{LP} \rvert$ $\uparrow$	Accel.	$J_{big} + a_{LP}$	D_o
$f \geq f_{min}$	$\lvert a_{LP} \rvert$ $\downarrow$	Decel.	J_{small}	D_o
$f \leq f_{min}$	$\lvert a_{LP} \rvert$ $\uparrow$	Fault	J_{small}	$D_{big} + a_{LP}$

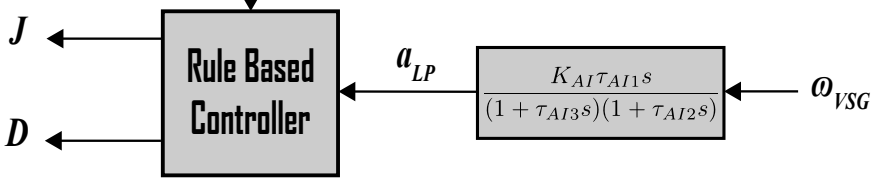

Figure 3.14: Rule-based VSG adaptive inertia.

the inertia constant between a large inertia J_{big} during acceleration of the VSG and a small inertia J_{small} during deceleration of the VSG, independent of the operating condition of the system and the severity of the disturbance. Furthermore, the damping constant of the virtual swing equation is not utilized to further improve the dynamic response of the system.

The control technique proposed here adjusts the values of the inertia and the damping constants using the rule-based approach shown in Figure 3.14, based on a low pass filtering of the measured rate of change of the ω_{VSG}, with parameters K and τ; this is more accurate and requires less measurement than the method presented in [72]. Thus, the proposed controller samples and filters the absolute value of the derivative of the angular velocity of the VSG, yielding a_{LP} in Figure 3.14 to determine if the VSG is accelerating or decelerating and to capture the severity of the disturbance. If the VSG is accelerating, a large inertia constant J_{big} (e.g., $J_{big} = 10J_o$) is chosen, while also adding a_{LP} to reflect the disturbance stress; this slows the VSG and limits further frequency excursions. Otherwise, a small inertia constant J_{small} (e.g., $J_{small} = J_o/50$) is chosen to speed up the recovery of the frequency of the system. However, if the frequency at the converter regulating the dc voltage drops below a minimum frequency (e.g., $f_{min} = 59.8$ Hz), the controller chooses a large value for the damping constant D_{big} (e.g., $D_{big} = 3D_o$), and adds a_{LP} to reflect the disturbance severity, while reducing the inertia constant to its minimum value J_{small}, as illustrated in Figure 3.14, which makes the VSI on the VSG side sluggish, thus reducing its power draw. This will have a stabilizing effect on the system regulating the dc voltage, especially during disturbances, since it would mitigate the possible collapse of the DC-Link voltage of the B2B converter, and prevent frequency or voltage collapse on a system that does not have enough generation capacity to regulate the DC-Link.

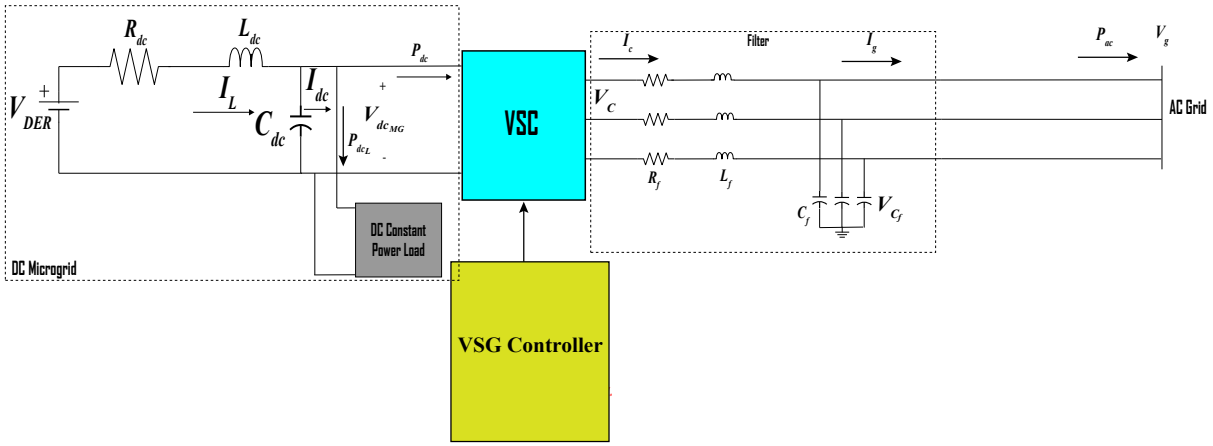

Figure 3.15: DC MG interface.

3.2.1.2 DC MG Interface

A dc MG interface connects these types of MGs to the MMG system, as shown in Figure 3.15. The VSC converter in this case utilizes a different VSG control with VFC than the B2B, as explained next.

The presence of converter interfaced loads in dc MGs have a detrimental impact on the stability of the system, since they act as constant power loads, resulting in a negative incremental impedance that causes significant voltage and power oscillations in these MGs [37, 38]. Thus, the dc converter interface can contribute to reducing voltage oscillations in dc MGs if a proper controller is utilized. In this case, the impact of a VSG dc MG interface on the dynamics of the dc MG can be examined by analyzing the equations that represent the dynamics of the currents and voltages. Thus, the current of the interface from the dc side can be calculated as

$$I_{dc} = \frac{P_{dc}}{V_{dc_{MG}}} \tag{3.14}$$

where $V_{dc_{MG}}$ is the dc MG voltage, and P_{dc} is the converter's dc side power; for an average model of the converter, $P_{dc} = P_{ac}$ neglecting converter losses. The dynamics of an average model dc DER, based on the simplified MG model shown in Figure 3.15, can then be

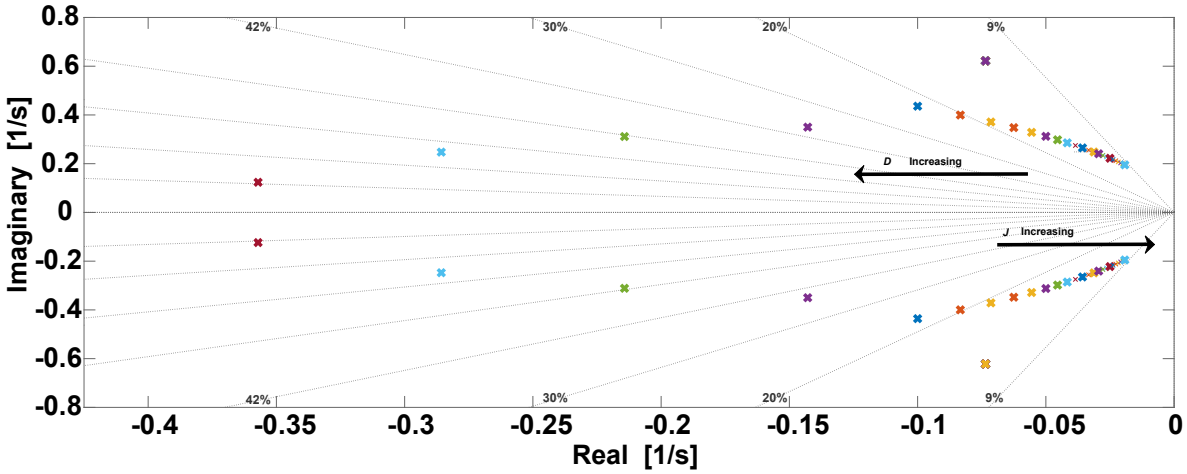

Figure 3.16: Impact of damping and inertia constant on dominant eigenvalues and damping ratios for the VSG dc MG interface.

written as follows:

$$L_{dc}\frac{\mathrm{d}I_L}{\mathrm{d}t} = V_{DER} - R_{dc}I_L - V_{dc_{MG}} \tag{3.15}$$

$$C_{dc}\frac{\mathrm{d}V_{dc_{MG}}}{\mathrm{d}t} = I_L - I_{dc} \tag{3.16}$$

$$I_{dc} = \frac{P_{dc_L} + P_{dc}}{V_{dc_{MG}}} \tag{3.17}$$

$$J\omega_{VSG}\frac{\mathrm{d}\omega_{VSG}}{\mathrm{d}t} = P_{gov} - P_{dc} - D\Delta\omega \tag{3.18}$$

$$C_f\frac{\mathrm{d}V_{C_f}}{\mathrm{d}t} = I_c - I_g \tag{3.19}$$

$$L_f\frac{\mathrm{d}I_c}{\mathrm{d}t} = V_c - R_fI_c - V_{C_f} \tag{3.20}$$

where V_{C_f}, I_c and I_g are the phase a filter voltage and converter output currents respectively. A set of state-space linear time-invariant first order differential equations can be obtained from equations (3.15)-(3.20) as follows:

$$\Delta\dot{x} = \mathcal{A}\Delta x + \mathcal{B}\Delta u \tag{3.21}$$

$$\Delta y = \mathcal{C}\Delta x + \mathcal{D}\Delta u \tag{3.22}$$

Based on this linear model, the impact of damping and inertia constant on the dominant eigenvalues can be obtained. Thus, it can be observed in simulations, as shown in Figure

3.16 that increasing the damping shifts the dominant eigenvalues to the left in the complex plane, leading to a more stable system, while increasing the inertia constant shifts the dominant eigenvalues to the right, resulting in oscillatory modes. Hence, the proposed controller for the dc-ac converter should adaptively adjust the damping constant as a function of the absolute value of the rate of change of the VSG angular velocity, so that the VSG damping through $\Delta\omega_{VSG}$ increases, as follows:

$$D = \frac{1+\tau_{1_{dc}}s}{1+\tau_{2_{dc}}s}\frac{K_{dc}s}{1+\tau_{dc}s}|\Delta\omega_{VSG}| + D_o \tag{3.23}$$

where D_o is a nominal value of the damping constant, and K_{dc} and all τ's are gains and time constants that need to be properly tuned. Hence, this controller ensures that the interface power exchanges with the rest of the system do not result in significant dc-voltage transients. This interface may also include the previously discussed VFC controller for the ac host grid.

3.2.2 Proposed Distributed Control System

A distributed droop-free frequency and dc-voltage control that fulfills the role of secondary control is developed in this section to coordinate the grid of MG system by controlling the output powers of the MG VSG interfaces. The technique is derived from the distributed consensus technique proposed in Section 3.1.2, which is modified to coordinate both ac and dc MGs in the MMG system.

Based on bidirectional communication, the proposed distributed control consists of a control layer that is associated with a communication graph approach discussed in Section 3.1.2. The aim of the controller is to coordinate the output powers of the MGs, and thus, the interfacing VSGs are linked with communication channels to exchange coordination information. Thus, the proposed communication topology to coordinate the MMGs, as for example in the system shown in Figure 3.17, as per [39], the spanning tree communication links among the MGs are bidirectional and each MGs can communicate only with neighbouring MGs, while the host grid communicates bidirectionally with all MGs. Thus, the connectivity matrix is defined as follows:

$$A_G = \begin{bmatrix} 0 & 0 & 1 & 1 & 0 & 0 \\ 0 & 0 & 0 & 1 & 0 & 1 \\ 1 & 0 & 0 & 1 & 1 & 0 \\ 1 & 1 & 0 & 1 & 1 & 0 \\ 0 & 0 & 1 & 1 & 0 & 1 \\ 0 & 1 & 0 & 1 & 1 & 0 \end{bmatrix} \tag{3.24}$$

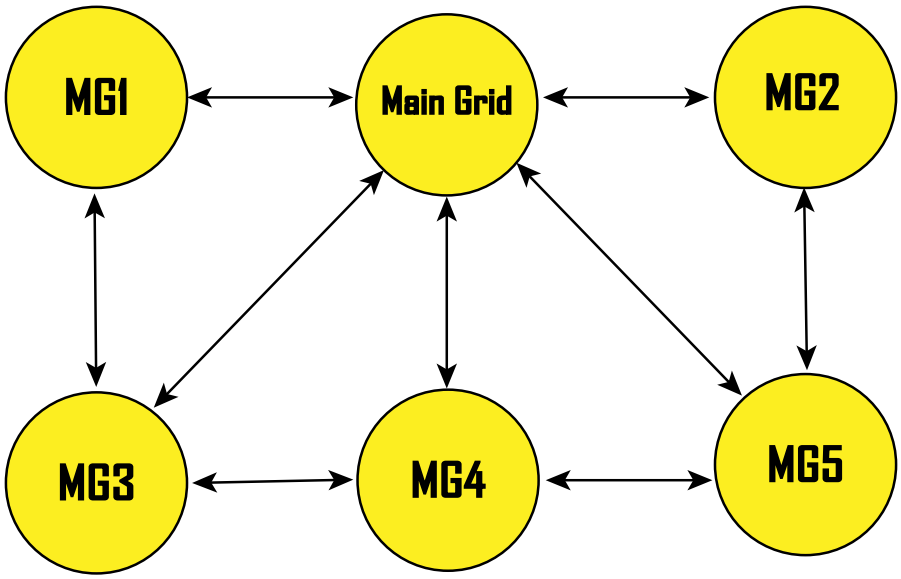

Figure 3.17: Communication topology of the proposed distributed controller.

3.2.2.1 Adaptive Distributed Control

The proposed distributed consensus controller relies on a rule based technique to coordinate the output powers of the MGs, which is based on normalized indices of frequencies for ac MGs and dc voltages for dc MGs, as follows:

$$\gamma^{'} = \frac{\gamma - \gamma_{min}}{\gamma_{max} - \gamma_{min}} \tag{3.25}$$

where $\gamma_i^{'}$ is the normalized ac frequency or dc voltage index; γ is the actual frequency or dc voltage of the MG; γ_{max} and γ_{min} are the maximum and minimum allowable frequency or dc voltage deviations. Thus, if $\gamma_i^{'} > 0$, MG i has available power generation from DERs and VFC, with the MG acting as a source through the VSG interfaces, which is controlled by the distributed consensus controller described below. Note that the MGs are allowed to exchange power with the host grid as long as the frequency or the dc-voltage index is $\gamma_i \geq \gamma_{min}$, to allow a suitable margin for the MGs to act either as a source or a load, since the DERs and VFC regulate the frequency of the MGs to its nominal value. If $\gamma_i^{'} < 0$, MG i has a power imbalance due to not enough generation to supply local demand, with the MG being considered a controllable load in this case. If $\gamma_i^{'} = 0$, then there is no power exchange with the MMG, as either the ac frequency of the MG is at f_{min} (e.g., 59.8 Hz as per [73]), or the dc voltage of the MG is at its minimum steady state value V_{min} (e.g., 675

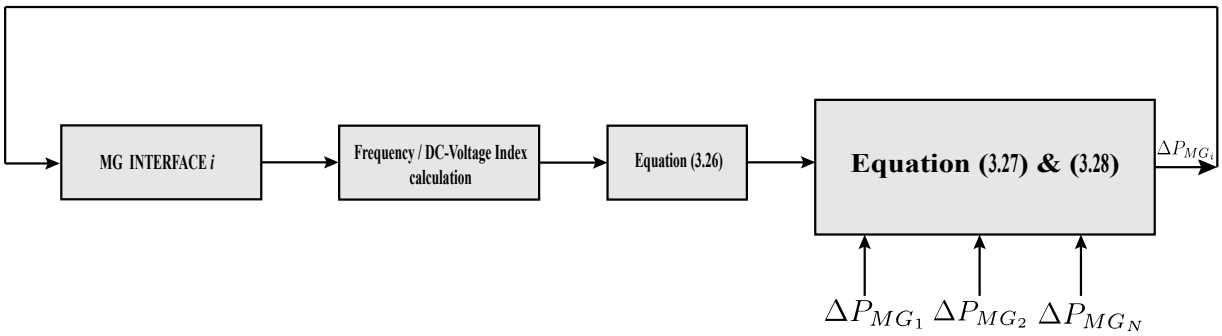

Figure 3.18: Proposed MMG distributed controller.

V), which is a 10% voltage deviation of the nominal value, according to [74] for the test system in Section 3.2.3). If $\gamma_i^{'} = 1$, either the ac frequency of the MG is at its maximum value (e.g., 60.2 Hz as per [73]) or the dc voltage of the MG is at its maximum value at its nominal value (e.g., 825 V or 10% for the test system in Section 3.2.3).

3.2.2.2 Rule Based Controller

Unlike the distributed control technique proposed in [39], which only coordinate the DERs of a single MG. The proposed controller here coordinates the MMG system to regulate both the frequencies of ac MGs and the dc voltages of dc MGs. Thus, the proposed distributed consensus control is activated for an MG when its $\gamma_i^{'} > 0$, in which case:

$$P_{MG_i^{'}} = \gamma_i^{'} \overline{P_{MG_i}} \tag{3.26}$$

where $\overline{P_{MG_i}}$ is the maximum output power of the interfacing VSG, and $P_{MG_i^{'}}$ is used in the distributed consensus controller to share the power proportionally among the MGs. In this case, the MGs coordinate their output power through the distributed consensus controller as follows:

$$\Delta P_{MG_{ref}} = \left(\gamma_o^{'} - \gamma^{'}\right)\left(K_P + \frac{K_I}{s}\right) \ \forall i \tag{3.27}$$

$$\frac{\mathrm{d}\Delta P_{MG_i}}{\mathrm{d}t} = \sum_{j \in N_i} a_{ij}\left(\frac{\Delta P_{MG_j}}{P_{MG_j^{'}}} - \frac{\Delta P_{MG_i}}{P_{MG_i^{'}}}\right) + b_i\left(\Delta P_{MG_{ref}} - \frac{\Delta P_{MG_i}}{P_{MG_i^{'}}}\right) \ \forall i \tag{3.28}$$

where equation (3.27) is the local frequency control loop; $\gamma_o^{'}$ is the index value corresponding to the nominal frequency γ_o of the main grid; $\gamma^{'}$ is the measured frequency index of the main grid; K_P and K_I are the parameters of the local PI-controller of the frequency control loop; and $\Delta P_{MG_{ref}}$ is the reference power to be used in the inner power control loop of the distributed consensus controller.

Equation (3.28) is the inner power control loop, where output powers of neighbouring interfacing VSGs are communicated to the local VSG interface i, to be used in the inner power control loop. In this equation, ΔP_{MG_i} represents the local control signal tracking $\Delta P_{MG_{ref}}$ for MG i; ΔP_{MG_j} is the output power variation of a neighbouring MG j; $P_{MG_i^{'}}$ and $P_{MG_j^{'}}$ are the maximum power capacities of the local MG and neighbouring MG, respectively, which are modulated by the frequency or dc-voltage index of the corresponding MG as shown in (3.26); a_{ij} is either 1 or 0, depending on the communication network linking the interfacing VSGs, as explained in the previous section; and b_i is a binary variable set to 1 if the VSG has access to the reference frequency index $\Delta P_{MG_{ref}}$ generated from the frequency control loop, otherwise $b_i = 0$. This equation results in the convergence of ΔP_{MG_i} to $\Delta P_{MG_{ref}}$. The proposed distributed controller is implemented as shown in Figure (3.18).

If the MGs have a frequency index $\gamma_i^{'} < 0$, the MG acts as a controllable load. In this case, the interfacing VSG regulates the frequency or the dc voltages as a function of the frequency index of the main grid, such that if the main grid frequency decreases, the power exchange from the main grid to the MG that acts as a load decreases as follows:

$$\Delta P_{MG_{ref_i}} = \left(\gamma^{'} - \gamma_i^{'}\right)\left(K_P + \frac{K_I}{s}\right) \quad \forall i \tag{3.29}$$

The proposed controllers is integrated into the VSG shown in Figure 3.12 to control the VSG reference power P_o (2.11), inside the VSG governor block. Note that the DERs within the MGs utilize droop control and VFC to regulate the frequency of ac MGs and the dc voltages in dc MGs.

3.2.3 Case Studies and Results

The proposed VSG-based interface and the aforementioned controllers are tested, validated, and compared on an MMG system derived from a CIGRE benchmark MG test system, which has been used for several studies [44, 57]. The topology of the MMG is depicted in Figure 3.19, which has been implemented for time-domain simulations in PSCAD [67], and consist of five MGs, two of which are dc MGs while the rest are ac MGs. DC MG

1 consist of a 1151 kW converter-interfaced load with power controls, two BESSs rated at 431 kW each, and a solar PV DER rated at 520 kW; dc MG 2 consist of a 1391 kW converter-interfaced load with power controls, two BESSs rated at 481 kW each, and a solar PV DER rated at 600 kW; ac MG 1 consist of a 1266 kW voltage dependent load, a 1040 kVA Diesel Generator (DG), a 212 kW BESS, and a 485 kW Wind Generator (WG); ac MG 2 consist of a 1091 kW voltage dependent load, a 978 kVA DG, a 212 kW BESS, and a 485 kW WG; and ac MG 3 consist of a 1260 kW voltage dependent load, a 1040 kVA DG, a 212 kW BESS, and a 485 kW WG. The data for this test system is provided in Appendix B.

The WGs in all MGs are assumed to be type 4, modeled as explained in Section 2.1.2.3, and are operated at unity power factor. The ac loads are assumed to be unbalanced as in the original CIGRE MG system, modeled as explained in Section 2.1.2.4, and consist of 60% constant impedance load, 30% constant current load, and 10% constant power load. The dynamic models of the DERs in ac MGs are the same as the ones used in the original CIGRE MG system [44,57], as discussed in Section 2.1.2 while the dc MG DERs are based on averaged models [75]. The rating of the VSG-based MG interfaces is 1.5 MW, and modeled as discussed in Sections 2.4 and 3.2.1.

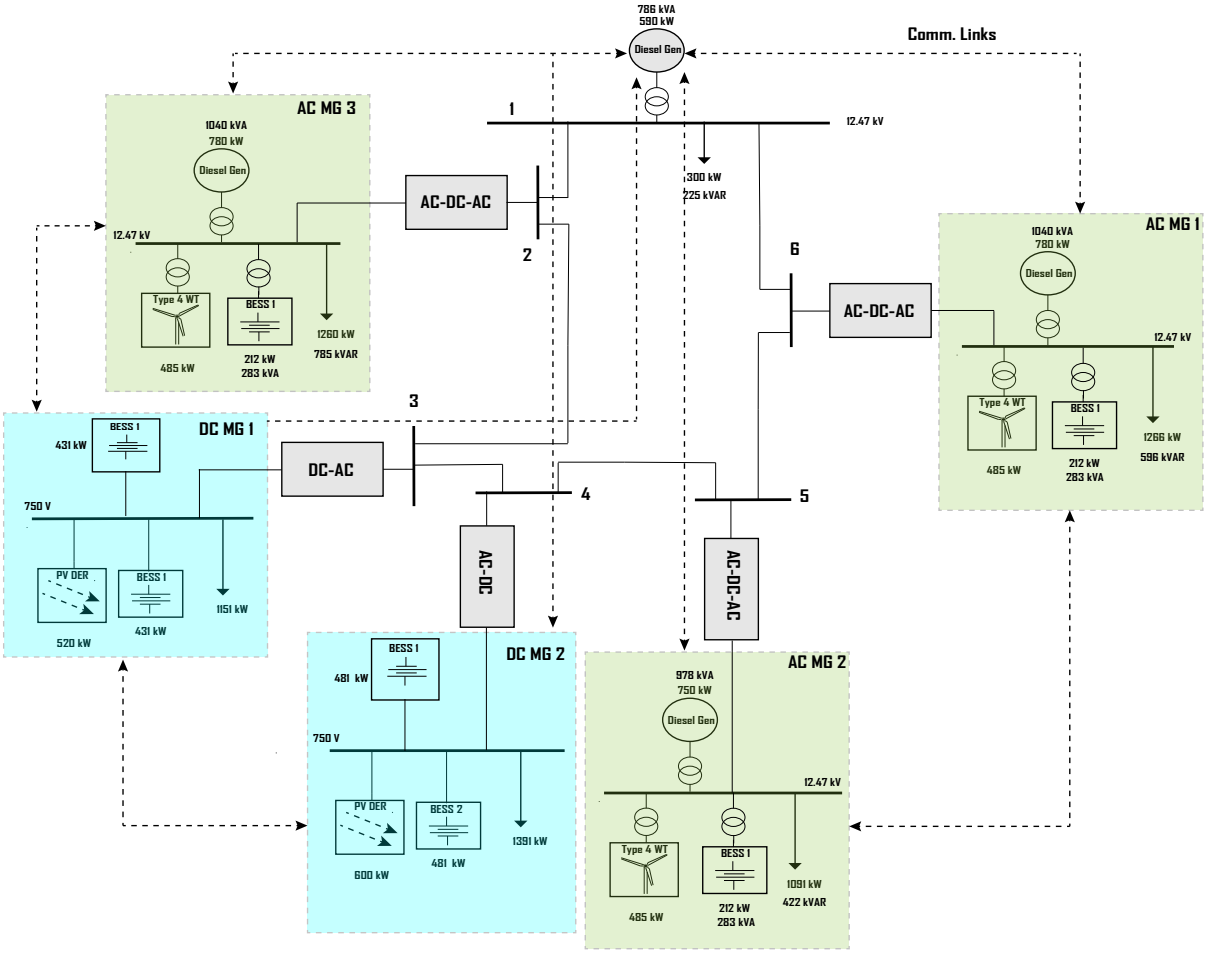

Figure 3.19: MMG test system.

The proposed VSG-based interface's performance along with the proposed controllers, are compared through the following study cases:

- Case 1 corresponds to the MG interfaces integrated into the host grid using frequency and voltage droop controllers, which is the existing approach.

- Case 2 corresponds to the MG interfaces operating as VSGs with fixed inertia.

- Case 3 is similar to Case 2 but with the proposed VSG adaptive inertia controllers.

- Case 4 corresponds to Case 3 but with a distributed controller and VFC controllers.

These cases are tested through multiple sequential disturbances. Thus, first, the BESS and WG of ac MG 1 are disconnected at t=25 s, followed by a 15% load shedding in ac MG 3 at t=35 s, and a 50% reduction of solar PV power and a 25% reduction in BESS output power in dc MG 2 at t=50 s; finally, a three phase fault is applied at t=70 s at Bus 5 with a duration of 150 ms.

The simulation results in Figure 3.20 depict the frequencies of the ac MGs for the aforementioned cases and disturbances. Note in Figure 3.20(a) that the MG 1 frequency successfully and rapidly recovers to its nominal value in Case 4 for the first disturbance, with Cases 3 and 4 showing better frequency response than the rest of the cases. Observe for the other cases that the frequency falls below its nominal value, which could trigger system protections. Notice as well that the proposed controllers do not result in significant frequency deviations in the other ac MGs despite the increased power sharing, as shown in Figures 3.20(b) and 3.20(c); this is due to the VFC, which provides power reserves in the ac MGs by modulating the load voltages. Figure 3.20(c) shows the frequency of ac MG3, with the sudden load interruption at 35 s resulting in an increase in the MG frequency for Cases 1, 2, and 3; however, in Case 4, the proposed distributed controller increases the power exchanged with the main grid at 50 s, since the exchanged power is a function of the frequency index as defined in (3.26).

Figure 3.21 shows the voltages of the dc MGs. Observe that the disturbances result in dc voltage oscillations for Case 1 and 2. Note also in Figure 3.21(b) that the dc voltage of the dc MG 2 successfully recovers to its nominal value for Case 4, while for the other cases, the dc voltage deviates from its nominal value. It can also be observed that since the exchanged power of the MG with the main grid is dependent on the dc voltage index (3.26), the proposed distributed controller reduces its exchanged power with the rest of the system, since the disturbances result in a reduction of the dc voltage index for the MG. Finally, note that, in general, Case 4 shows better dc-voltage regulation and dynamics than the other cases.

Observe in Figures 3.20 and 3.21 that the Bus 5 three-phase fault at t=70 s results in instabilities for Cases 1 and 2. However, for Case 3 and 4, the system recovers and is stable due to the proposed adaptive inertia. Table 3.1 shows the global average frequency and dc voltage deviations for all test cases, demonstrating that the proposed distributed controller has a superior performance compared to the other three cases.

Figure 3.22 depicts the interfacing VSGs' active output powers with the proposed coordination technique. Figure 3.23 illustrates the impact of the VFC on the voltages of the ac

MGs and the host grid. Figures 3.24 and 3.25 show the changes in the moment of inertia and the damping coefficient of the VSG interfaces due to the proposed adaptive inertia controller, illustrating the expected variations on these controller parameters as the MMG system condition change.

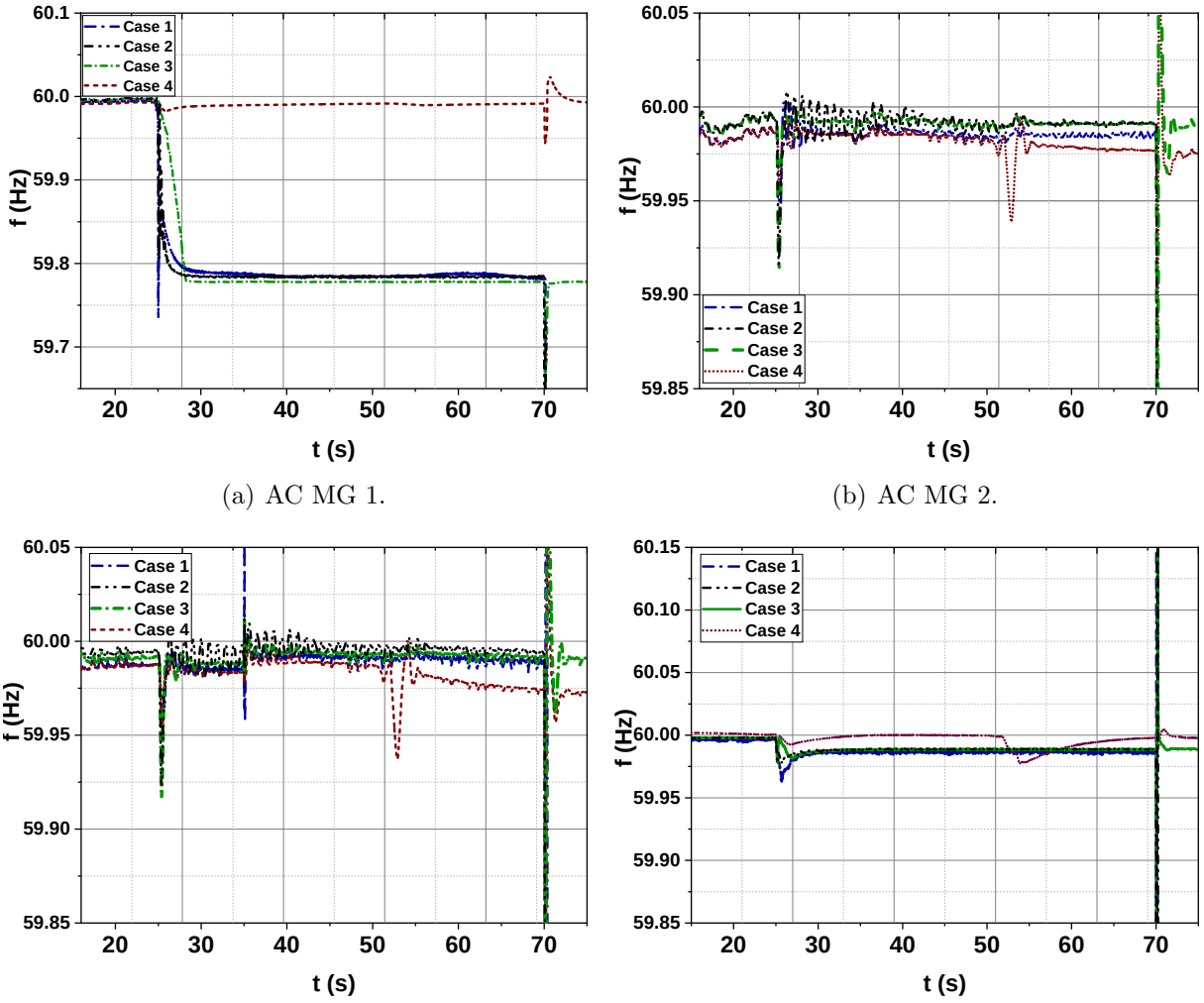

(a) AC MG 1.

(b) AC MG 2.

(c) AC MG 3.

(d) Main grid.

Figure 3.20: AC MMG system frequencies for different disturbances.

Table 3.1: Global average frequency and dc voltage deviations.

Control scheme	Δf_{AVE}		$\Delta V_{dc_{AVE}}$	
	Hz	%	**V**	%
Case 1	0.173623	0.289372	143.5068	19.13424
Case 2	0.182531	0.304218	148.708	19.82773
Case 3	0.045508	0.075846	26.0635	3.475133
Case 4	0.011235	0.018725	14.66873	1.955831

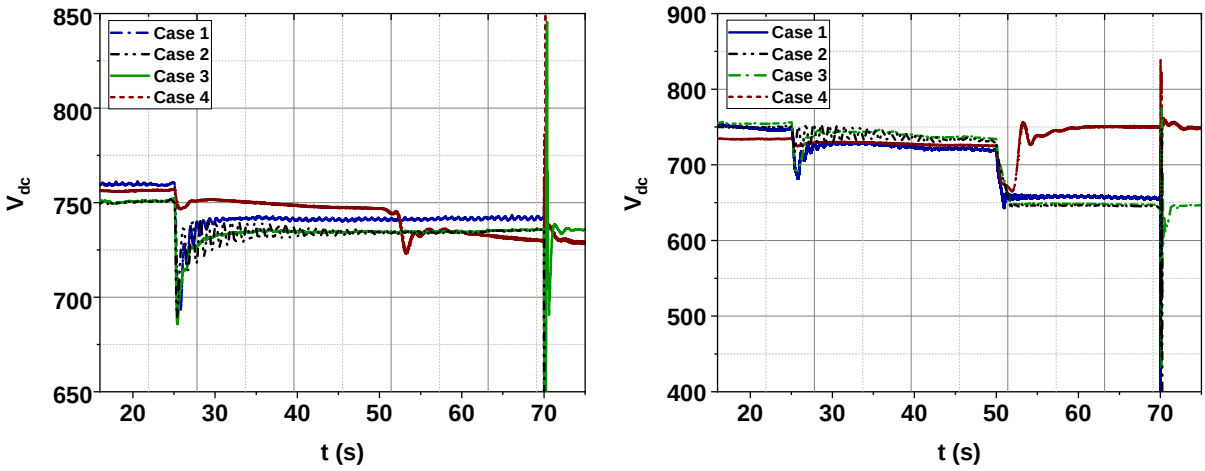

(a) DC MG 1.

(b) DC MG 2.

Figure 3.21: DC MG voltages for different disturbances.

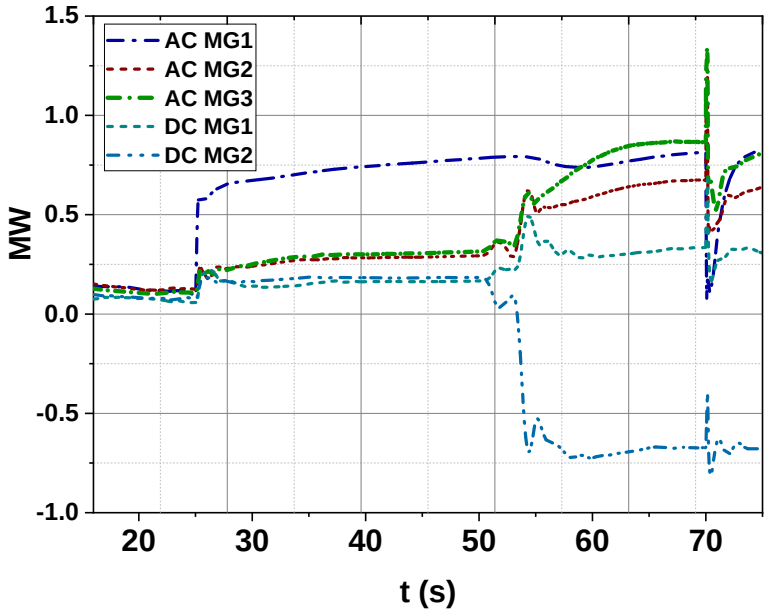

Figure 3.22: Output powers of the VSG interfaces with proposed controllers for Case 4.

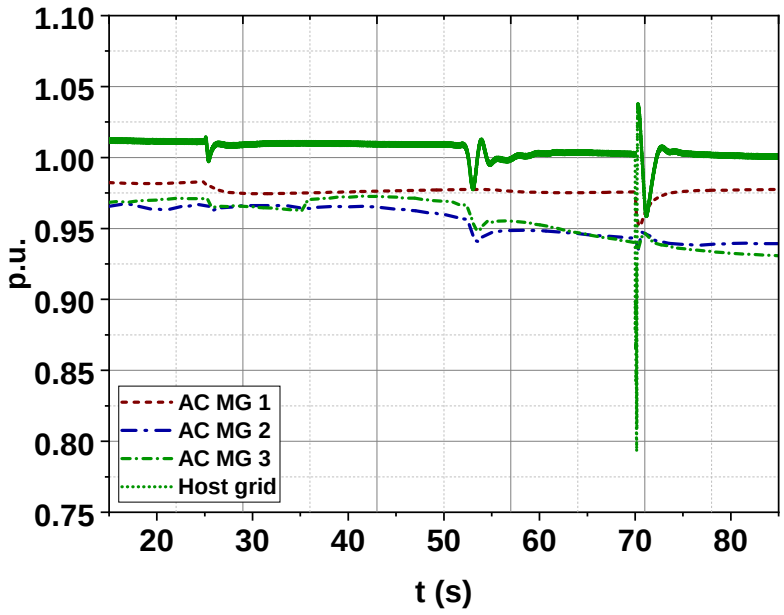

Figure 3.23: Voltages of the ac MGs and the host grid for Case 4.

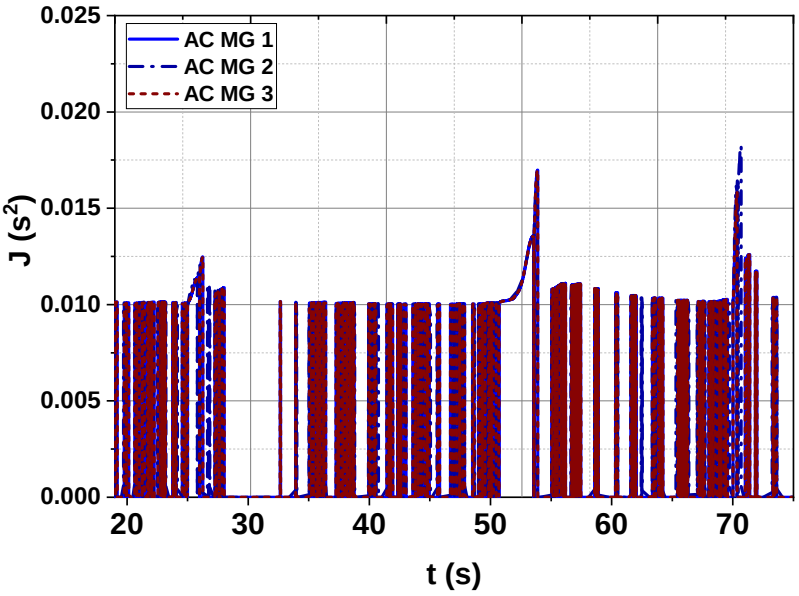

Figure 3.24: Inertia of B2B VSG interfaces for Case 4.

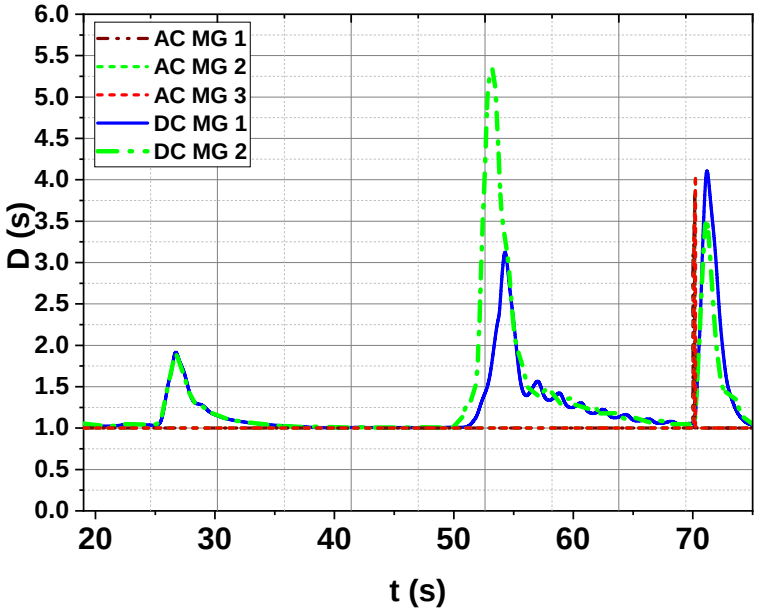

Figure 3.25: Damping coefficient of dc-ac VSG interfaces for Case 4.

3.3 Summary

A distributed control scheme was first proposed and discussed in this chapter for voltage regulation of a dc MG, while proportionally sharing the loads among the DERs and acting as a primary and secondary control at the same time. Simulation results demonstrate the superiority of the distributed controller compared to conventional droop controls, which present several technical challenges, such as the need for careful selection and tuning of droop gains, and stability and voltage regulation issues. The proposed controller is shown to be robust against system disturbances in a realistic test dc MG, and communication link latencies, and could be readily implemented in dc MGs with minimal communication infrastructure and thus costs.

In the second part of this chapter, a hierarchical distributed control system to regulate the frequencies and voltages of an MMG system was proposed and developed here. The controller was integrated into a network architecture based on interfacing the MGs with VSG-based MG interfaces, which provide virtual inertia through the realization of the SG swing equation, providing frequency support for an MMG system. A hierarchical controller was also proposed based on an adaptive inertia technique that enhances the system's frequency and dc-voltage responses by adjusting the inertia and damping constants. Furthermore, a distributed controller based on an adaptive consensus technique was presented, which aims to coordinate the output power of both ac and dc MGs to regulate the frequencies and the dc voltages of all MGs based on local MG measurements. This controller can be readily scaled up for larger MMG systems, with minimum communication bandwidth and infrastructure, compared to existing centralized controllers that are prone to single point failures. The results obtained for a test ac/dc MMG demonstrate the advantages of the proposed VSG-based adaptive inertia and damping controllers for the MG interfaces, coordinated by the presented distributed control approach.

Most of the contents of this chapter have been published in [75] and [76].

Chapter 4

Frequency Regulation Through Optimal Droop Gain and Voltage Control

This chapter first presents an adaptive active power droop controller and voltage setpoint control in isolated MGs for optimal frequency response and stability after disturbances. The control scheme involves an optimal and model predictive control approach that continuously adjusts the active power droop gains and the voltage setpoints of DERs to maintain the frequency of the system within acceptable limits and enhance the primary frequency response of the system, while taking into account the active power sensitivity of the MG loads to the system's operating voltage. The proposed control scheme is tested, validated, and compared with previously proposed techniques using time-domain simulations for a test system based on a CIGRE medium voltage benchmark MG under different realistic conditions, demonstrating the advantages of the proposed approach.

The second part of the chapter proposes an adaptive droop controller for the coordination of an MMG system, based on the aforementioned optimization-based controller. The proposed controller is based on centralized control technique that adaptively adjusts the droop gains of the interfacing VSGs based on an optimization problem, which also integrates the adaptive inertia controller proposed in the previous chapter. The proposed controller shares the total system load among the grid and MGs, while minimizing the overall frequency and dc-voltage deviations. The controllers are implemented, tested, and validated using time-domain simulations for an MMG test system of Chapter 3 that consists of both ac and dc MGs.

4.1 Droop and Voltage Control for Optimal Frequency Regulation

As previously discussed, both DER primary frequency and voltage control in isolated ac MGs play a significant role in frequency regulation. Since the droop parameters of DER primary frequency controllers significantly affect the system's frequency regulation, choosing suitable droop gains for the DER is important, with low values resulting in a poorly regulated system frequency, while high values could make some DERs unstable [25]. In addition, the operating voltage of the MG can significantly affect the load demand and thus, the frequency of the system.

4.1.1 Optimization Model

An approach to overcome the aforementioned issues with primary control in isolated MGs would be to formulate a control scheme that dynamically and optimally adjusts both the active power droop constant and the voltage setpoints of the DERs, as per Figure 2.6, using an optimization approach to minimize the difference between generation and voltage-dependent loads. Therefore, a nonlinear optimization, discrete approach is proposed here as explained next.

4.1.1.1 Objective Function

The main objective would be to minimize the power changes at time t every Δt in generators and voltage-dependent loads as follows:

$$\min_{K_{DER},V} \Delta P_t = \sum_{i=1}^{N_{DG}} \Delta P_{DU_{i,t}} + \sum_{j=1}^{N_{BESS}} \Delta P_{BESS_{j,t}} - \sum_{l=1}^{N_L} K_{LP_l}(V_t^{\alpha_{Pl}} - V_{t-1}^{\alpha_{Pl}}) \quad (4.1)$$

where P_{DU} is the output power of the N_{DU} Diesel Generators (DGs); P_{BESS} is the output power of the N_{BESS} BESSs; $K_{DER} = (K_{DG}, K_{BESS})$ are the DER droop gains; the parameter K_{LP_l} and α_{Pl} correspond to the load model in (2.2); and V is the DERs' voltage setpoints and load voltages, as the grid is neglected here as explained below, which should be constrained within limits, i.e., $\underline{V} \leq V \leq \overline{V}$. It is assumed in this case that the BESSs are fully charged and thus act as sources; charging BESS could be simply treated as constant current loads in this approach.

4.1.1.2 Droop Constraints

The droop constraints for DUs, BESSs, and their associated limits can be defined as follows:

$$K_{DU_{i,t}} = \beta_{DU_i} P_{DU_{i,t}} \qquad \forall i \tag{4.2}$$

$$0 \leq K_{DU_{i,t}} \leq \overline{K_{DU_i}} \qquad \forall i \tag{4.3}$$

$$K_{BESS_{j,t}} = \beta_{BESS_j} P_{BESS_{j,t}} \qquad \forall j \tag{4.4}$$

$$0 \leq K_{BESS_{j,t}} \leq \overline{K_{BESS_j}} \qquad \forall j \tag{4.5}$$

where β_{DU_i} and β_{BESS_j} are parameters chosen based on a linear relation between the maximum power of DERs and maximum values of droop constants, as proposed in [41].

4.1.1.3 Power Constraints

The output powers of DUs and BESSs are constrained as follows:

$$P_{DU_{i,t}} = P_{DU_{o_{i,t}}} + \Delta P_{DU_{i,t}} \qquad \forall i \tag{4.6}$$

$$\underline{P_{DU_i}} \leq P_{DU_{i,t}} \leq \overline{P_{DU_i}} \ \forall i \tag{4.7}$$

$$P_{BESS_{j,t}} = P_{BESS_{o_{j,t}}} + \Delta P_{BESS_{j,t}} \qquad \forall j \tag{4.8}$$

$$\underline{P_{BESS_j}} \leq P_{BESS_{j,t}} \leq \overline{P_{BESS_j}} \ \forall j \tag{4.9}$$

And the power balance between generators and loads should be maintained, considering system loss changes, albeit small, as follows:

$$\sum_{i=1}^{N_{DU}} \Delta P_{DU_{i,t}} + \sum_{j=1}^{N_{BESS}} \Delta P_{BESS_{j,t}} \geq \sum_{l=1}^{N_L} K_{LP_l} (V_t^{\alpha_{pl}} - V_{t-1}^{\alpha_{pl}}) \tag{4.10}$$

4.1.1.4 BESS Constraints

The BESS SOC and its limits can be defined as follows [77]:

$$SOC_{j,t} = SOC_{j,t-1} + (P^C_{BESS_{j,t}} \eta_{C_j} - P^D_{BESS_{j,t}} / \eta_{D_j}) \Delta t \qquad \forall j \tag{4.11}$$

$$P_{BESS_{j,t}} = P^C_{BESS_{j,t}} - P^D_{BESS_{j,t}} \qquad \forall j \tag{4.12}$$

$$P^C_{BESS_{j,t}} P^D_{BESS_{j,t}} = 0 \qquad \forall j \tag{4.13}$$

$$\underline{SOC_j} \leq SOC_{j,t} \leq \overline{SOC_j} \qquad \forall j \tag{4.14}$$

where SOC is the BESS SOC; P^{C}_{BESS} and P^{D}_{BESS} are the BESS charge and discharge powers, respectively, with (4.13) reflecting the fact that the BESS cannot charge and discharge at the same time; and η_C and η_D are the charge and discharge efficiencies, respectively.

4.1.1.5 Discussion

Note that the full optimization problem (4.1)-(4.14) ignores power flow equations, since previous studies on isolated MGs have demonstrated that the grid and its losses are not significant [58, 78]. A detailed justification for this assumption is shown in [58], where the authors show that the losses of a relatively large benchmark MG system are very small; thus, the system may be represented with a single bus for the purposes of frequency regulation. Similar optimization problems for time-domain simulations of large distribution networks that also ignore the power flow equations are presented in [11, 12]. Furthermore, note that even in large power systems, where transmission lines have a significant impact on the system, power flow equations are usually not considered for frequency regulation, control, studies, and applications [79].

This optimization problem is solved continuously in time t every Δt, which may be defined to be fractions of a second, depending on the system and its frequency response, as illustrated in Section 4.1.4. The proposed model is a Nonlinear Programming Problem (NLP), which can be solved using standard NLP solvers, since the number of optimization variables for a typical MG is low, as demonstrated in Section 4.1.4.

An MGCC would perform the proposed optimization-based control scheme once the frequency of the MG deviates by $\overline{\Delta f}$, which is the maximum acceptable frequency deviation. For example, in [80], $\overline{\Delta f}$ is set as low as 0.2 Hz for tripping distributed generators at medium voltage networks within 300 s, and as high as 3 Hz to trip distributed generators within 0.16 s; therefore, the lowest value of 0.2 Hz is used here to force the frequency deviations to be within an acceptable narrow range to avoid generator tripping. The MGCC will then update the droop parameters and the voltage setpoints of the DERs with the ones obtained from the proposed model every Δt, to enhance the performance of primary frequency controllers.

The implementation of the proposed optimization is illustrated in Figure 4.1, where OPT refers to the proposed frequency control optimization method (4.1)-(4.14). Observe that if the optimization problem fails to converge, the droop and voltage setpoints will remain fixed at their last value.

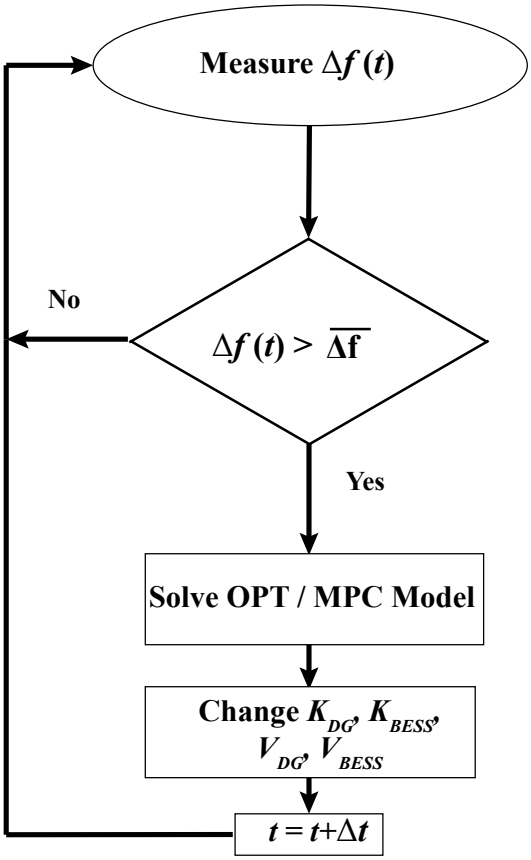

Figure 4.1: Implementation of the proposed optimal frequency control approach.

4.1.2 MPC Approach

An MPC version of (4.1)-(4.14) is proposed here to improve the optimal frequency control performance, considering the relation between active power deviation and frequency deviation of the MG, which can be modeled as a first-order transfer function as follows [26, 56, 79, 81]:

$$G(S) = \frac{Output}{Input} = \frac{\Delta f(S)}{\Delta P(S)} = \frac{1}{M_{MG} + D_{MG}} \tag{4.15}$$

where M_{MG} and D_{MG} correspond to the MG equivalent inertia and damping, estimated with appropriate system identification techniques from the frequency response of the sys-

tem. This transfer function can then be discretized through a Z transform as follows:

$$Z\left(\mathcal{L}^{-1}\left(\frac{1}{M_{MG}+D_{MG}}\right)\right)=\frac{1}{D_{MG}}\,\frac{1-e^{\frac{-D_{MG}\Delta t}{M_{MG}}}}{z-e^{\frac{-D_{MG}\Delta t}{M_{MG}}}} \tag{4.16}$$

Hence, the predicted frequency deviation per unit power deviation in the time domain can be represented as follows:

$$\Delta f_{t+k+1}=\Delta f_{t+k}e^{\frac{-D_{MG}\Delta t}{M_{MG}}}+\frac{\Delta P_{t+k}}{D_{MG}}\left(1-e^{\frac{-D_{MG}\Delta t}{M_{MG}}}\right) \tag{4.17}$$

Therefore, the objective function (4.1) of the proposed optimization approach can be replaced by the following function:

$$\min_{K_{DER},V}\quad\sum_{k=0}^{N_P}|\Delta f_{t+k+1}|=\sum_{k=0}^{N_P}\left|\Delta f_{t+k}e^{\frac{-D_{MG}\Delta t}{M_{MG}}}+\frac{\Delta P_{t+k}}{D_{MG}}(1-e^{\frac{-D_{MG}\Delta t}{M_{MG}}})\right| \tag{4.18}$$

where Δf_{t+k+1} is the predicted frequency deviation of the MG, and

$$\Delta P_{t+k}\;=\;\sum_{i=1}^{N_{DU}}\Delta P_{DU_{i,t+k}}+\sum_{j=1}^{N_{BESS}}\Delta P_{BESS_{j,t+k}}-\sum_{l=1}^{N_L}K_{LP_l}(V_{t+k}^{\alpha_{pl}}-V_{t+k-1}^{\alpha_{pl}}) \tag{4.19}$$

plus constraints (4.2)-(4.14) for each MPC iteration k.

The MPC problem is solved at each control interval k at time t for N_P samples into the future, and defines the droop gains K_{DER} and the voltage setpoints V for only the first control sample. The parameter N_P defines the prediction horizon and should be selected carefully to keep the computational burden reasonable, so that the proposed approach can be applied online, as discussed in the next section. This procedure is implemented as illustrated in Figure 4.1.

4.1.3 Discussion

The proposed control techniques solve optimization problems with the objective of minimizing the power balance of the system, and thus recover the nominal frequency by adjusting the droop gains and the voltage setpoints, hence fulfilling the typically integrated role of frequency regulation controls in MGs. Note that the proposed frequency controllers do

not interact with the MG's secondary controls associated with the EMS, which optimally defines the DER setpoints in longer time frames (e.g., every 5 minutes), as is typically the case in MGs [27], given the significant different time frames of the proposed controllers (seconds) and the EMS (minutes). Tertiary control is not applicable here, since being an isolated system, secondary control is the highest control level, as per [27].

The objective of the proposed optimization-based controllers is to ensure an optimal compromise between load sharing and frequency regulation, which cannot be achieved by a traditional droop frequency control approach, since increasing the droop gain of a specific DER increases its frequency regulation, resulting in less load sharing with the rest of the DERs. On the other hand, the proposed optimization-based techniques allow an optimal trade off between frequency regulation and load sharing.

4.1.4 Case Studies and Results

The proposed optimization-based control schemes using the OPT model described in Section 4.1.1, and its MPC variation explained in Section 4.1.2 are tested, validated, and compared here based on a modified version of the CIGRE benchmark MG used in several studies [44, 57, 58, 82]. The topology of the MG is shown in Figure 4.2, which has been implemented for time-domain simulations in PSCAD, using MATLAB to solve both OPT and MPC models.

To test the presented approaches using a larger number of DERs than typically found in MGs, the test system is modified to include: 5 DUs, with DUs 1-4 having a total rating of 5.5 MVA, and DU 5 being rated at 2.25 MVA to be used for frequency disturbances; one aggregated Type 4 WG rated at 4 MW; four BESSs rated at 2.2 MVA combined; and a total load of 9.55 MVA. The composition of the loads is assumed to be a realistic combination, for MGs, of 10% constant power, 30% constant current, and 60% constant impedance, with the same unbalancing as in [83]. For these operating conditions, the losses are determined to be only 1% of the total power generated, thus confirming their small impact of the grid in typical MGs. The data for this test system is provided in Appendix C.

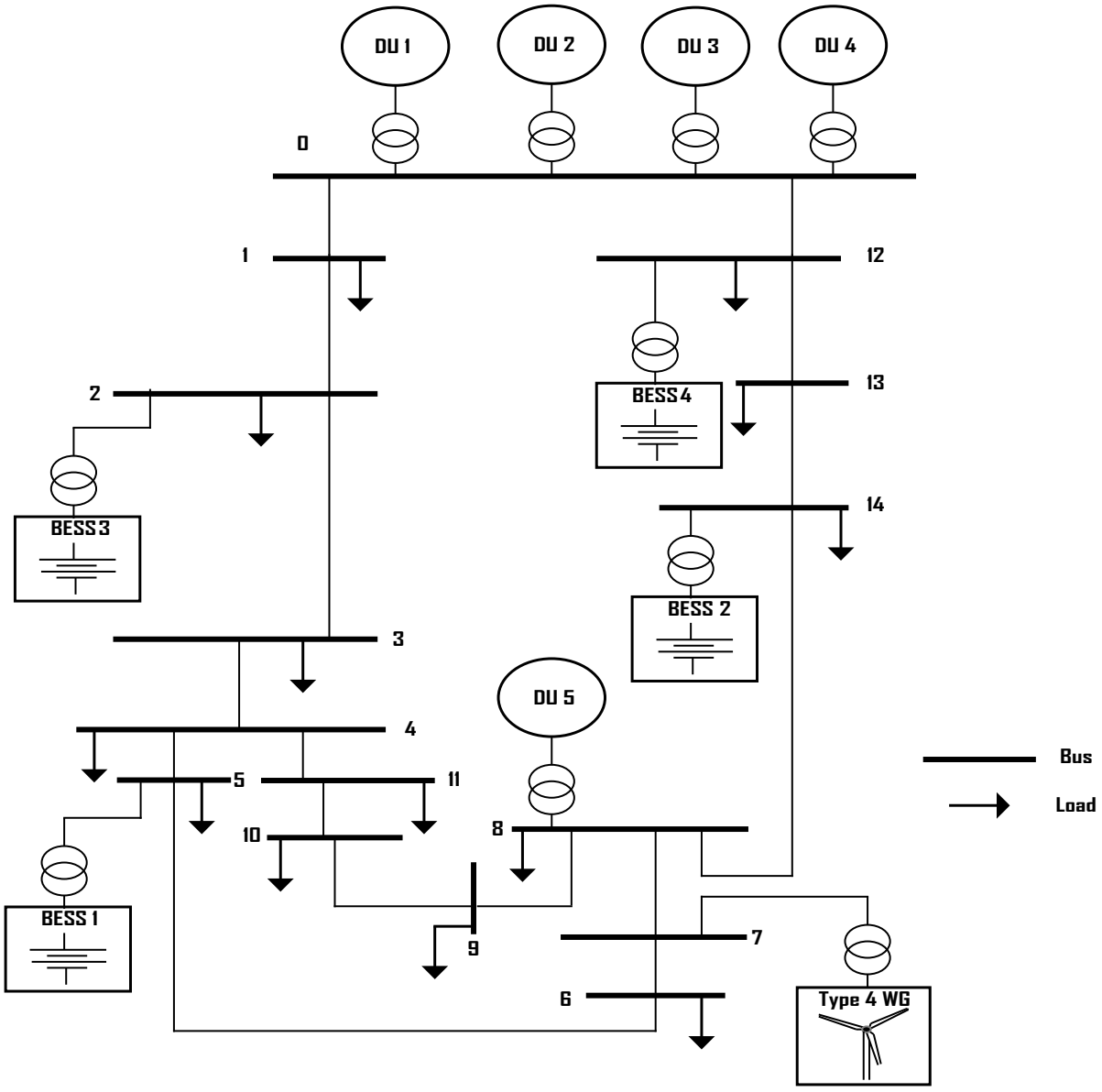

Figure 4.2: Modified CIGRE benchmark test MG [44].

The DUs and BESSs are responsible for regulating the frequency of the MG and providing primary frequency and voltage control, while the aggregated WG is operated in unity power factor mode [44, 83]. The WG output power variation and its impact on the system frequency are illustrated in Figure 4.3, considering that WGs do not regulate the

frequency through deloading or virtual inertia techniques, as such controls techniques are not common in MGs [27], thus presenting a more challenging condition for frequency regulation and control; the generation profile of the wind turbines is based on actual data from [44]. The initial droop gains of the primary frequency controllers of the DUs and BESSs are selected to ensure that the frequency of the MG does not deviate beyond $\overline{\Delta f} = 0.2$ Hz for the base system, due to the variability of the output power of the wind turbines observed in Figure 4.3.

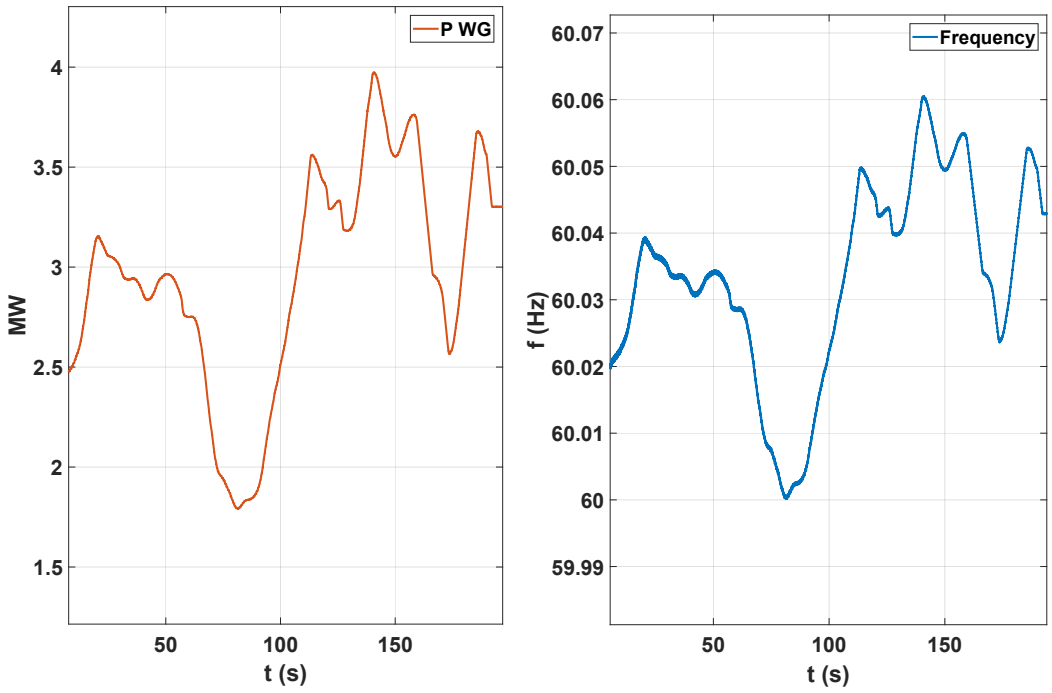

(a) (b)

Figure 4.3: (a) WG power variations and (b) frequency of the test MG for the base case.

4.1.4.1 Validation and Comparisons

The proposed control OPT and MPC schemes are compared here with respect to the VFC controller presented in [44], for sudden trips of BESS 2-4, which are manageable contingencies from the frequency stability point of view, and for a trip of DU 5. The contingencies occur at $t = 80$ s, which is the worst possible frequency stability scenario, since the reserves of the system are at its lowest at this time. Thus, in Figure 4.1, the

sample time is defined as $\Delta t = 0.5$ s, with an acceptable maximum frequency deviation range of $\overline{\Delta f} = 0.2$ Hz, as previously explained, so that the proposed control schemes are activated when the frequency of the MG is below 59.8 Hz, and continues until the frequency of the system stabilizes within ± 0.2 Hz.

In this scenario, the disconnection of DU 5 results in a reduction of the estimated values of M_{MG} from 1.96 to 0.78 s^2, and for D_{MG} from 36 to 30.21 s, using the Steiglitz-McBride system identification technique [57]; all BESSs are fully charged in this case. The choice of the prediction horizon for the MPC approach depends on the dynamics of the system; hence, a low value of $N_P = 2$ proves to be sufficient to obtain optimal results due to the fast dynamics of the MG, thus minimizing computation times. This simulation allows evaluating the effect of the proposed control scheme on the frequency of the system during disturbances.

Figure 4.4 shows the MG frequency response for the trips of BESS 2-4. Observe that the fixed droop control is able to regulate the frequency, albeit slowly and remaining below its nominal value, as an integral frequency controller was not implemented in this case to highlight the fact that the proposed methods do not need such a controller to recover the nominal frequency. On the other hand, both proposed techniques quickly recover the frequency to its nominal value, without the need for additional integral controls.

The simulation results for the DU 5 trip are shown in Figure 4.5. Observe that the frequency of the system with fixed droops is unstable after the generator trip, which results in a system blackout [80]; on the other hand, with the proposed optimization approaches, the frequency recovers quickly to the required range. Furthermore, note that both OPT and MPC approaches recover to the same frequency, showing better frequency recovery than the VFC technique proposed in [44].

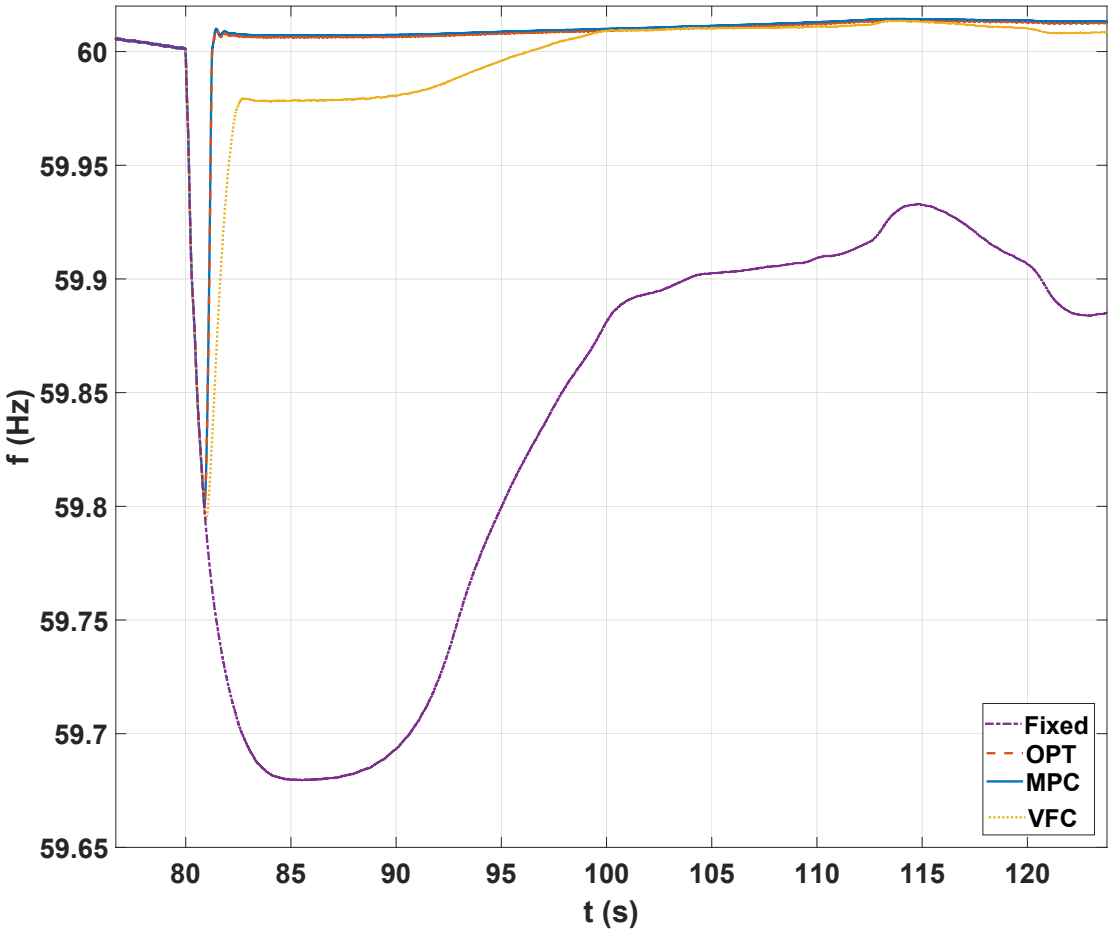

Figure 4.4: MG frequency for various control schemes for BESS 2-4 trips.

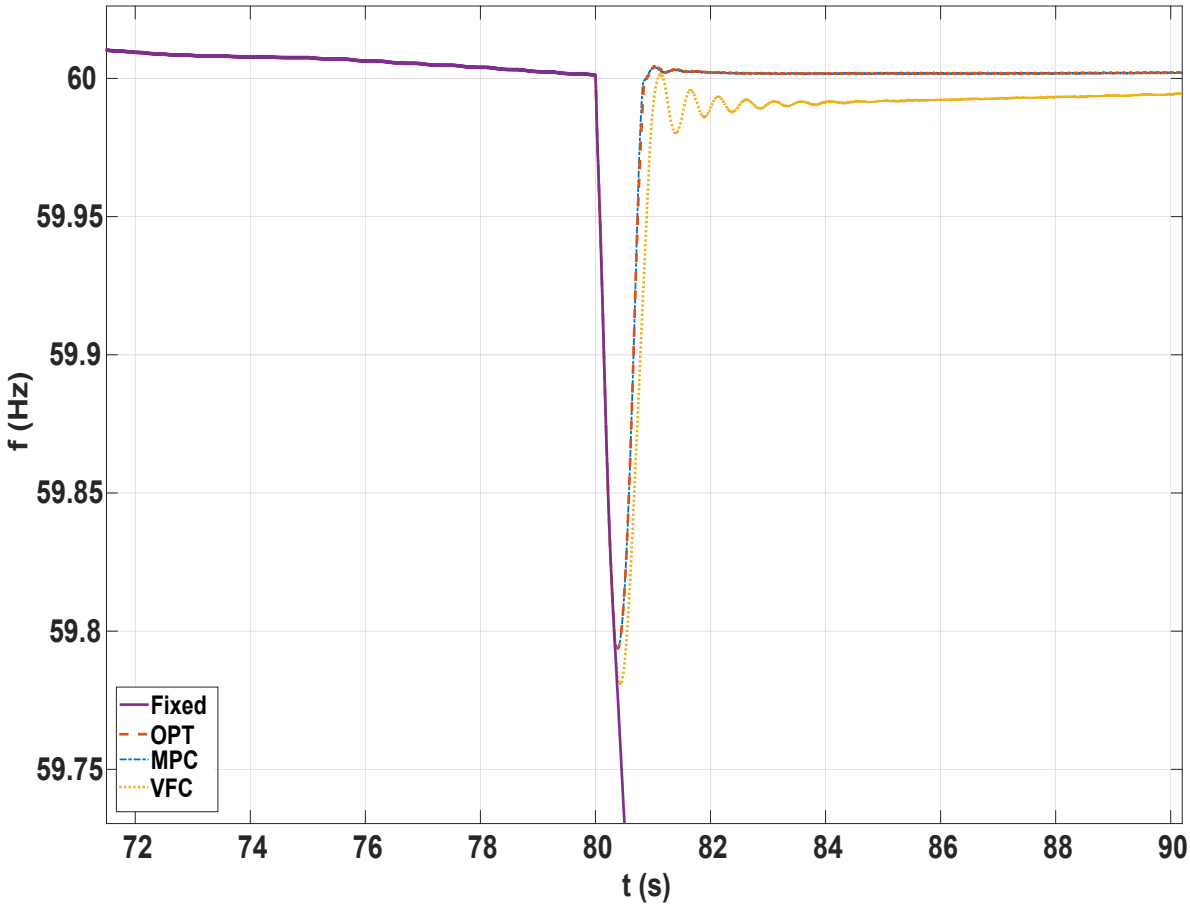

Figure 4.5: MG frequency for various control schemes for a DU 5 trip.

The droop gains and voltage setpoints obtained from the optimization are shown in Figure 4.6. Observe that the proposed optimization approach dynamically adjusts the droop gains and the voltage setpoints of the DERs to stabilize the frequency of the system. Figure 4.7 depicts the DERs' active output powers during the optimization period. Figure 4.8 illustrates the voltages at two of the farthest load buses in the test MG, showing the little impact of the grid, as the load voltages follow closely the reference voltage setpoint from the controller and are practically the same, despite the significant voltage variations allowed in this case.

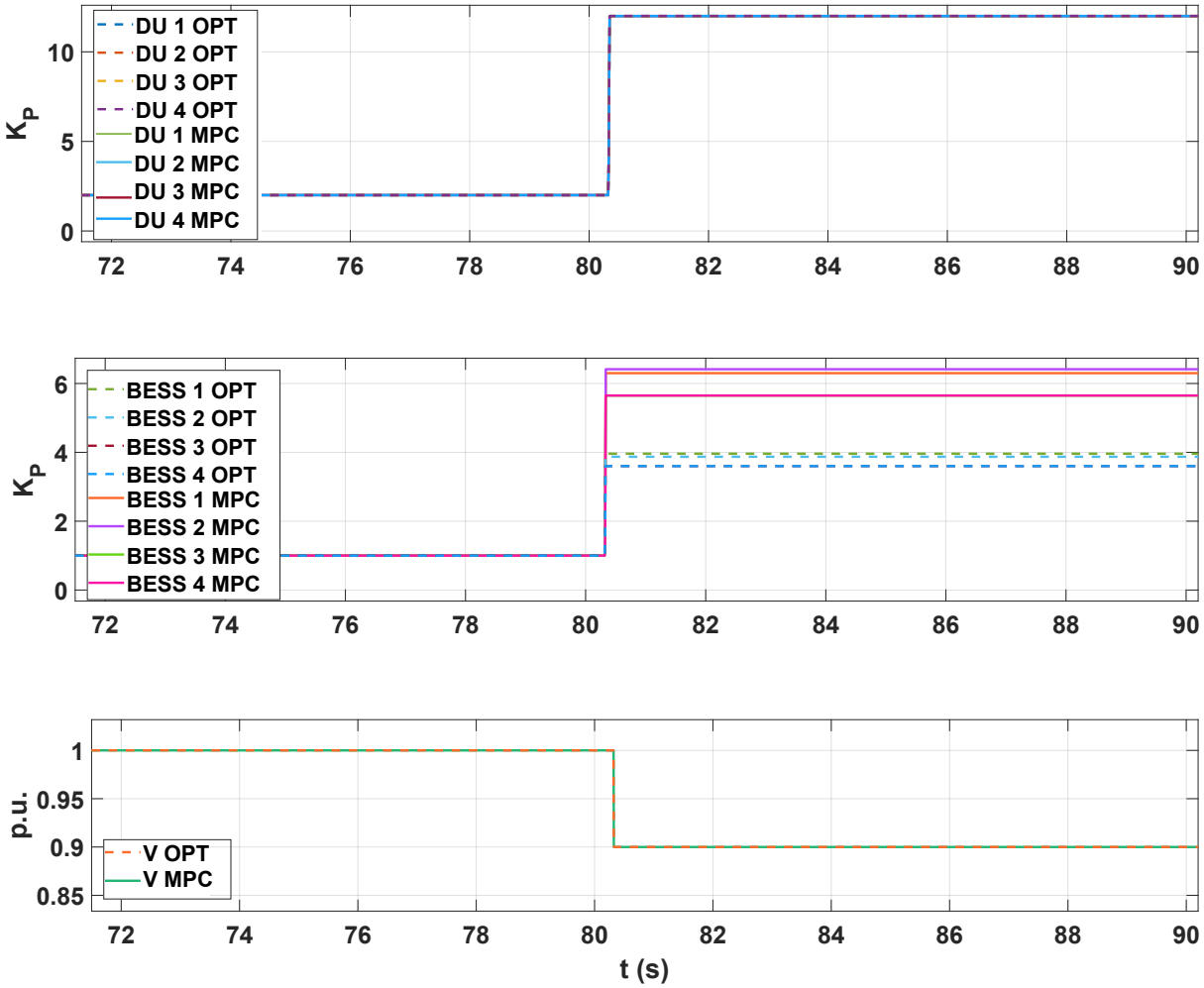

Figure 4.6: Droop gains from the proposed methods for a DU 5 trip.

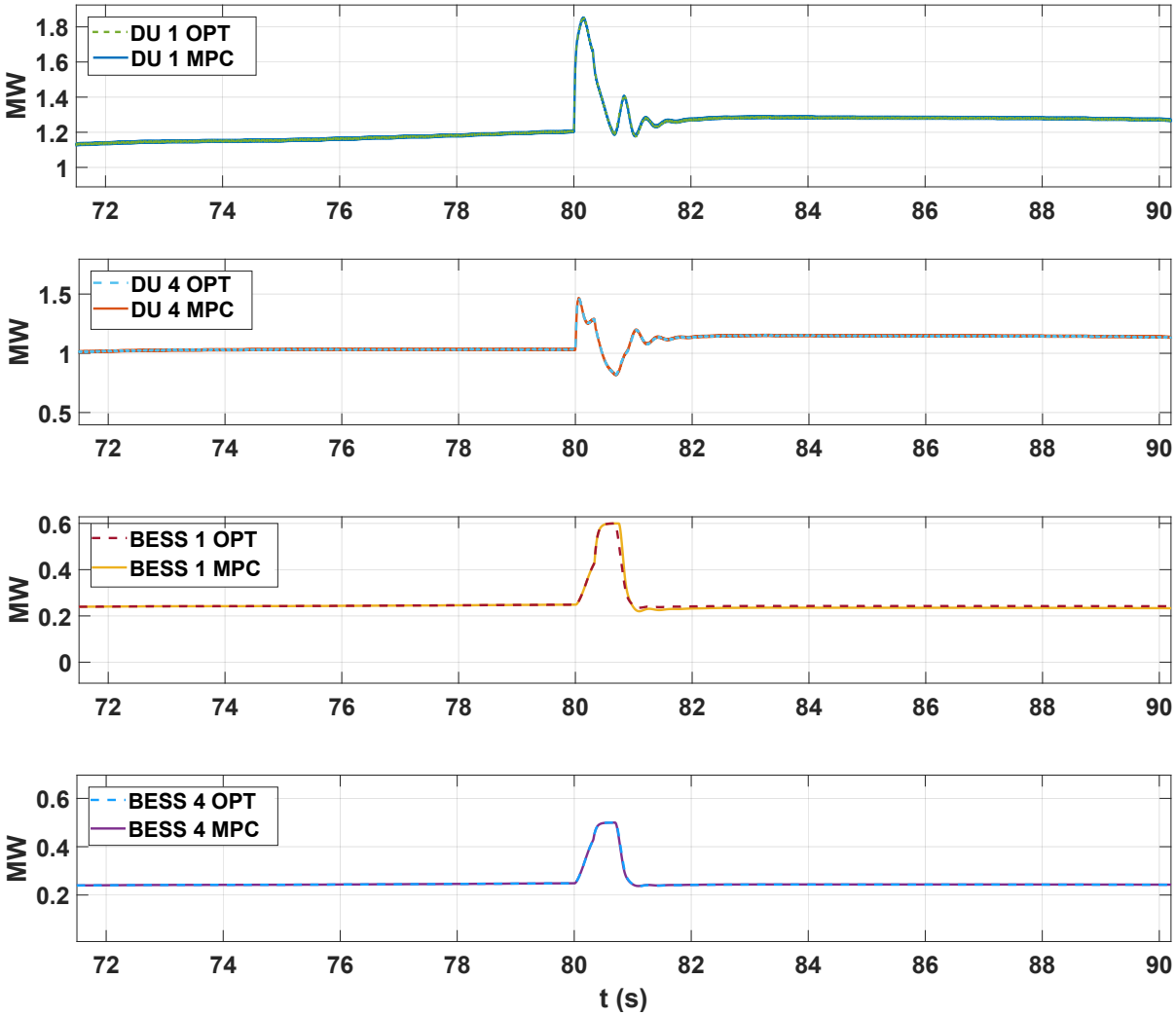

Figure 4.7: Active power outputs of DERs for a DU 5 trip; note that the smaller droop gains of the BESSs with respect to the DUs, due to their smaller ratings, limit their response to frequency variations.

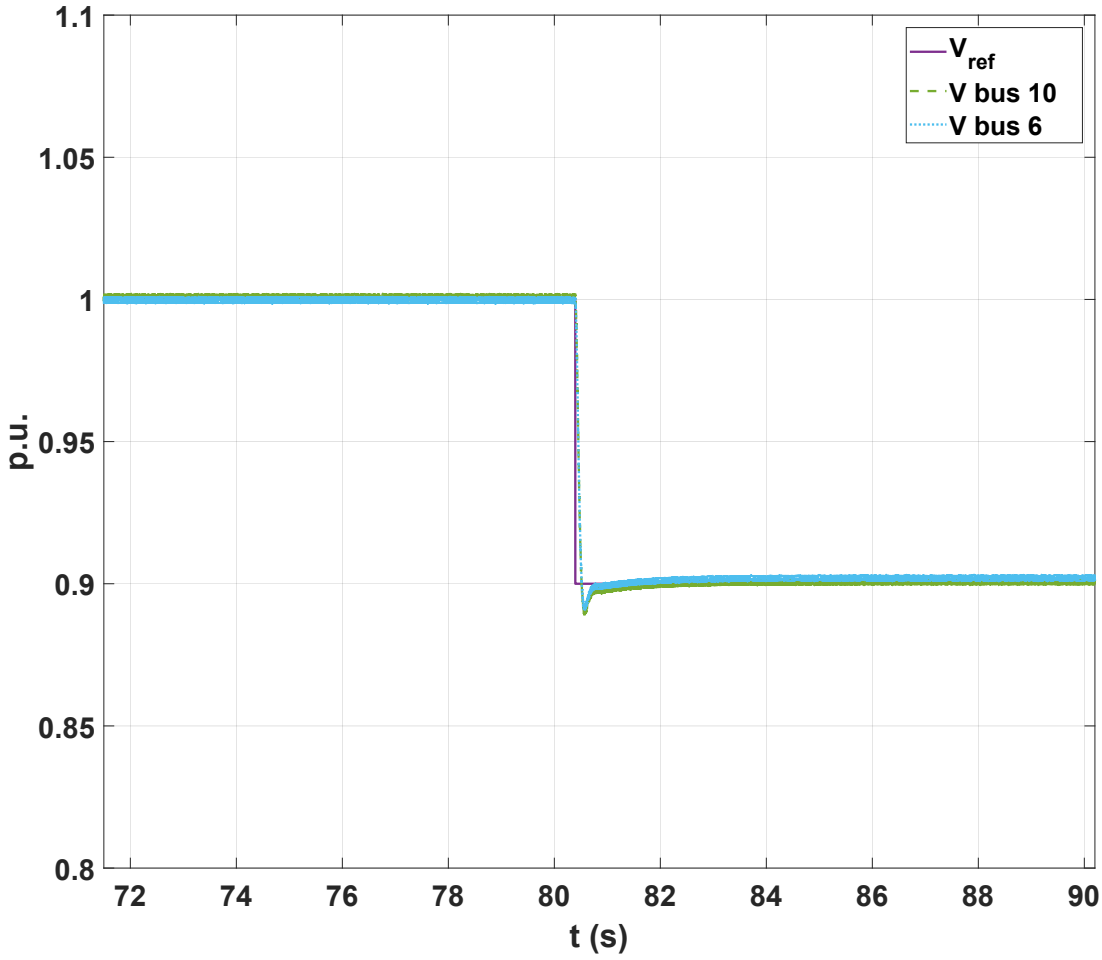

Figure 4.8: DER voltage setpoints and voltages at two of the farthest load buses for both OPT and MPC models.

4.1.4.2 Sensitivity Analysis of Optimization Parameter

The following parameters need to be carefully selected to obtain adequate results: the sample time, i.e., Δt, the maximum limit of the DER droop gains, and the limits of the voltage setpoints. For the results depicted in Figures 4.4 to 4.8, the optimization problem is solved every $\Delta t = 0.5$ s. The maximum limits of the droop gains were determined through

Table 4.1: MG frequency for different Δt and N_P values for DU 5 and BESS 4 trips.

Control	**f [Hz]**	**Δt**				
		1 s	**0.5 s**	**0.2 s**	**0.015 s**	**0.015 s $N_P = 5$**
MPC	59.79	80.46 s	80.46 s	80.46 s	80.46 s	80.46 s
	60	80.96 s	80.93 s	80.93 s	80.92 s	80.92 s
OPT	59.79	80.46 s	80.46 s	80.46 s	Unstable	–
	60	81 s	80.93 s	80.93 s	Unstable	

small-signal stability of the system, by increasing the droop gains until the maximum droop gain is found for the worst operating condition with the system remaining stable, thus resulting in $\overline{K_{DU}} = 12$, and $\overline{K_{BESS}} = 8$ for all DUs and BESSs, respectively.

To investigate the impact of the sample time and the voltage limits on the proposed control techniques, trips for DU 5 and BESS 4 at $t = 80$ s and $t = 80.4$ s, respectively, are simulated. The sample time Δt needs to be selected carefully, because if the OPT model is solved too often, the rapid changes in the droop gains and the voltage setpoints, especially for DUs, would cause the system to become unstable, as illustrated in Table 4.1. On the other hand, the MPC method is not significantly affected by faster sample times, as shown in Table 4.1, due to the fact that this technique estimates the frequency response of the system and reacts accordingly. Furthermore, observe that the faster the sample time, the faster frequency recovers; however, the computational burden is an issue in this case, since if the sample time is too short, the model will not be solvable online. Also, increasing the prediction horizon N_P does not result in a noticeable improvement in the frequency response of the system, mainly due to the fast dynamics of the system associated with the diesel generator trip, which resulted in a significant decrease in the equivalent values of M_{MG} and D_{MG}, as mentioned earlier.

In the previous studies, the limits on the DER voltage setpoints are 0.9 and 1.1. Simulation results for more restrictive voltage limits are shown in Figure 4.9, observing that the MG frequency recovery decreases as the limits become more restrictive, as expected; however, the proposed control technique seems robust against restrictive voltage limits. Note that the proposed MPC performs better than the VFC as the voltage setpoint limits decreases.

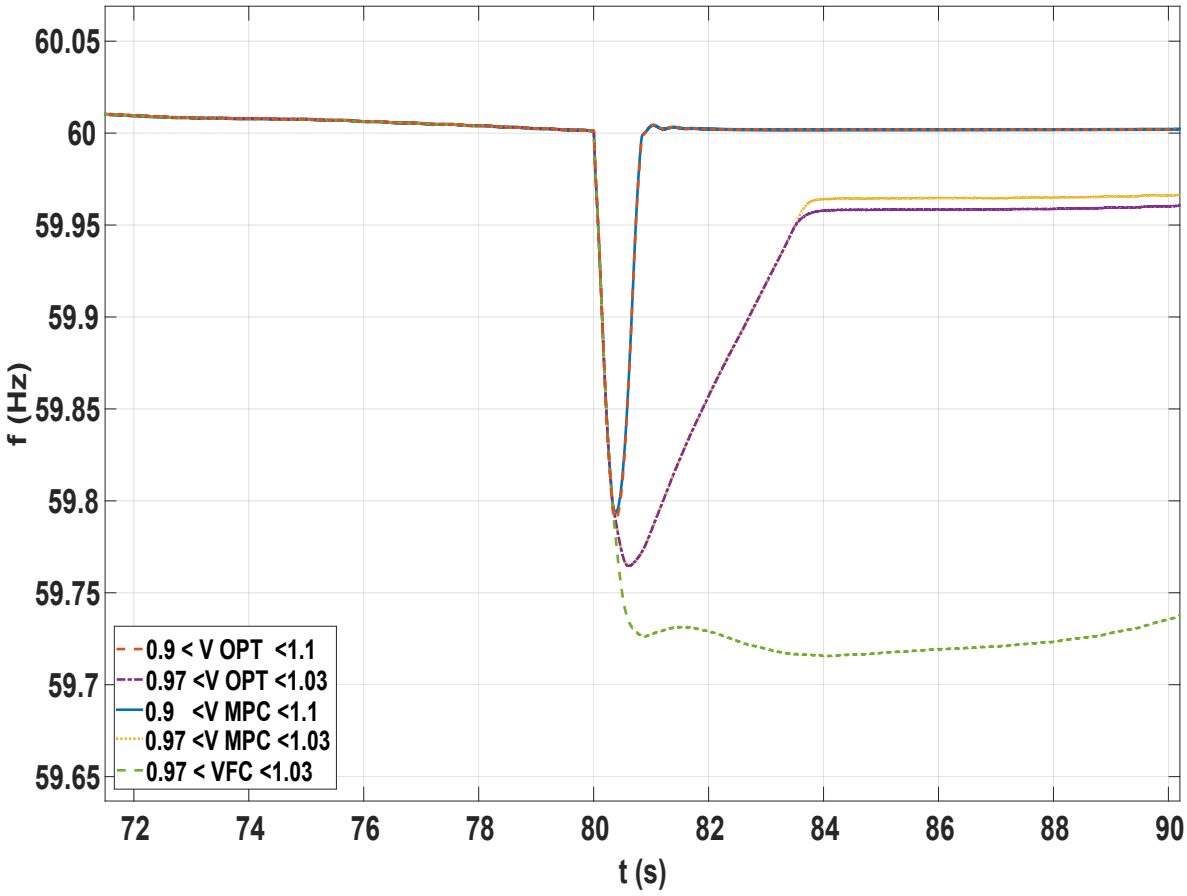

Figure 4.9: MG frequency for different limits on DER voltage setpoints for a DU 5 trip and $\Delta t = 0.5$ s.

4.1.4.3 Severe Disturbance

The proposed controls are tested here for an even larger disturbance in the system; thus, DU 5 and BESS 2-4 are tripped at $t = 80$ s. The results are shown in Figure 4.10, where it can be observed that the proposed control schemes OPT and MPC successfully maintain the frequency stable and within the 0.2 Hz steady-state limit compared to the system without these controls, which is unstable, and to the VFC. Note also that proposed control techniques show better frequency recovery compared to the VFC, with the latter exceeding the frequency range limits of 0.2 Hz, which could trigger DU protections as per [80]. The

instability of the frequency for the fixed control in Figures 4.5 and 4.10 can be associated with a system eigenvalue crossing onto the right-half plane due to the severe disturbance.

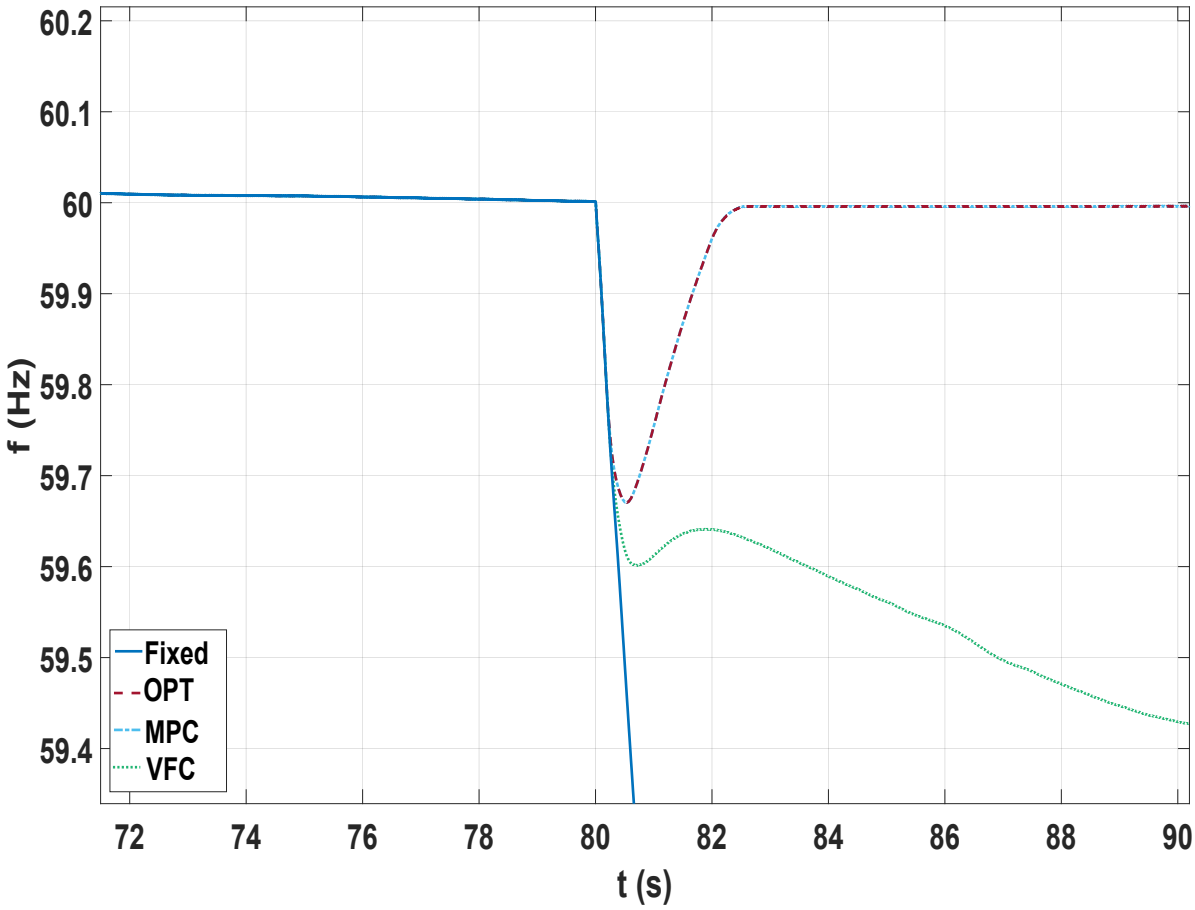

Figure 4.10: MG frequency for DU 5 and BESS 2-4 trips and $\Delta t = 0.5$ s.

4.1.4.4 Parameter Uncertainty

The impact of uncertainty of the load parameters, as well as the estimated system's M_{MG} and D_{MG} values, are studied in this section to test the robustness of the proposed techniques. Thus, note that the significant reduction in the M_{MG} and D_{MG} values due to the DU 5 trip does not have a noticeable impact on the proposed MPC technique, as seen in

Figure 4.5; hence, the MPC is shown to be not very sensitive to variations in the dynamics of the system due to disturbances.

Figure 4.11 depicts the results of assuming load exponents $\alpha_P = 0.5$ for all voltage dependent loads, which are significantly different from the α_P values used in the previous simulations, thus introducing a significant error in the estimated load model used in the proposed control approach. Observe that the frequency still recovers to a reasonable value within the allowable range, demonstrating that both OPT and MPC approaches are robust against uncertainties in the load models.

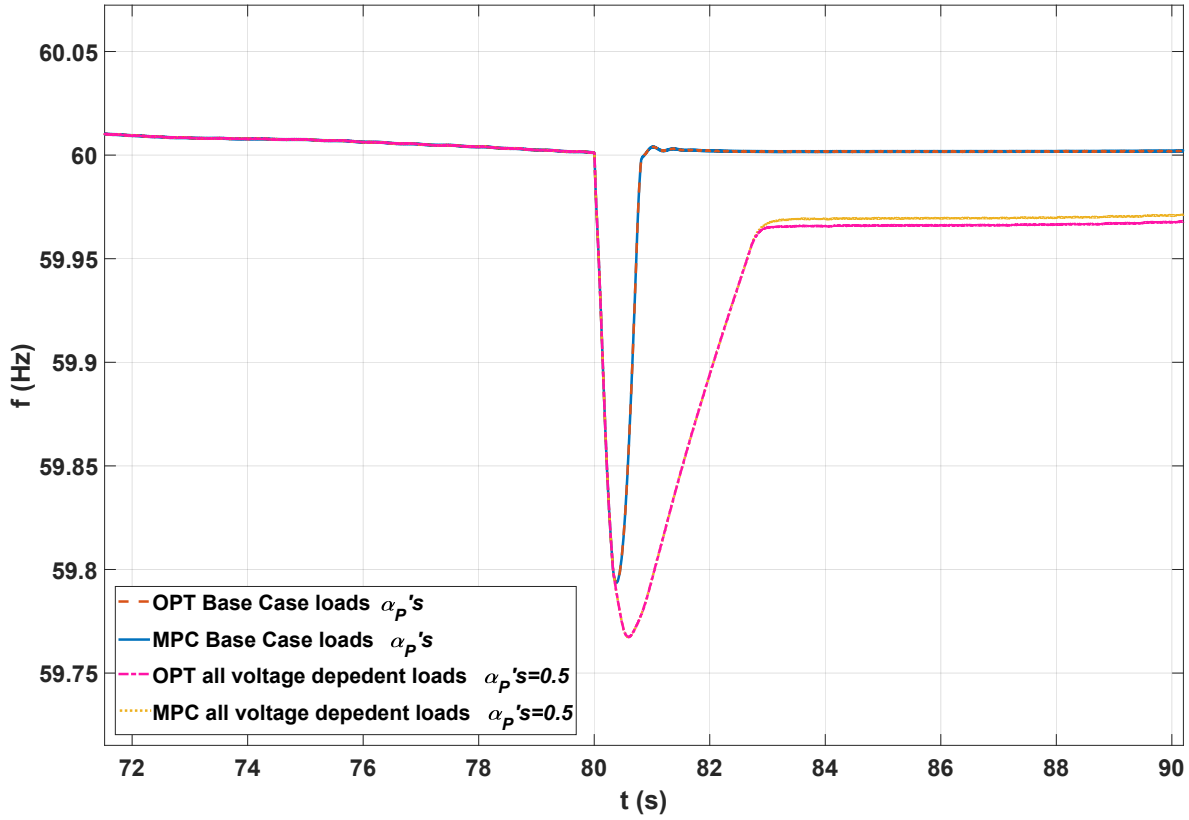

Figure 4.11: Impact of uncertainty on the load parameters for the proposed control techniques for a DU 5 trip.

4.1.4.5 Impact of Communication Delay

The impact of communication delay on the performance of the proposed controllers is studied in this section. Thus, a time delay transfer function $G_d(s) = e^{-s\tau}$, where τ is the time delay, is added between the proposed optimal controls' outputs and the corresponding system setpoints. The following time delays were then studied: 100 ms, 250 ms, 500 ms, which are typical time delays used in [84], for which instabilities were observed. The simulation results are shown in Figure 4.12, for a DU 5 trip where it can be observed that longer time delays result in lower frequency nadirs. However, in all cases, the system frequency properly recovers, thus demonstrating the robustness of the proposed controllers against time delays.

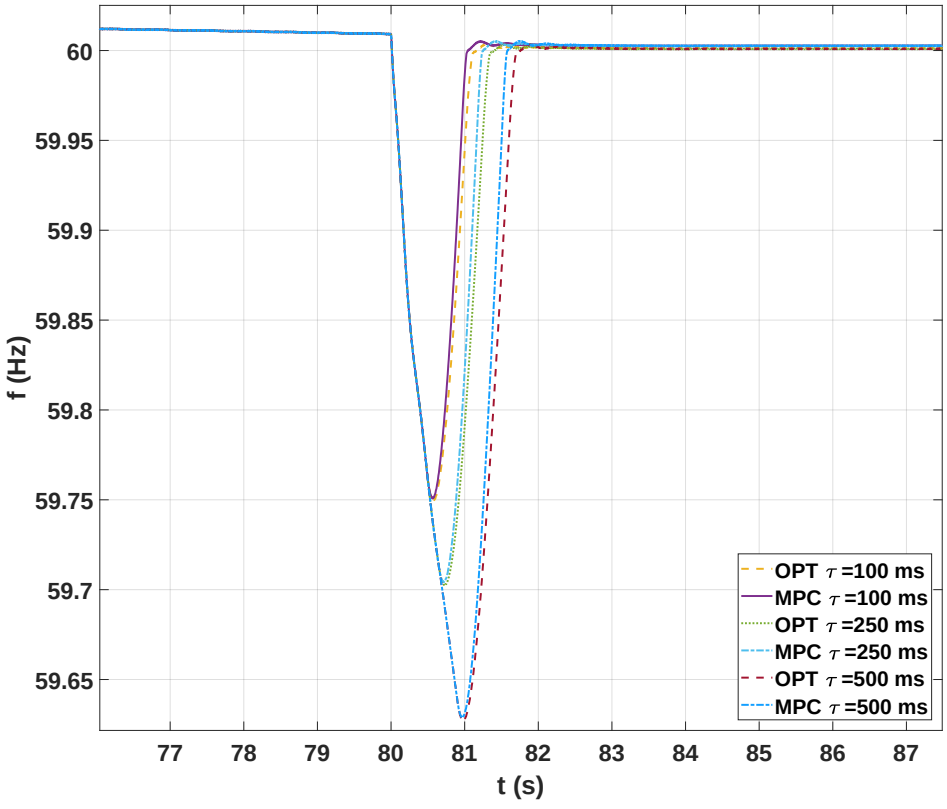

Figure 4.12: Impact of communication delays on the proposed controllers for DU 5 trip for DU 5 trip

Table 4.2: Computational performance comparison

Technique	**MPC**	**OPT**	**Ref** [31]	**Ref** [11]
CPU Time (ms)	11	8	5	4

4.1.4.6 Discussion

The proposed approaches are compared with previously presented MPC and optimal techniques for frequency regulation described in [11] and [31], respectively, for the first (BESS 2-4 trips) and second (DU 5 trip) contingencies. The obtained results are illustrated in Figure 4.13, where it can be observed that for the first contingency in Figure 4.13(a), the dynamic response of the proposed techniques is better than the one obtained with the existing methods, whereas for the second contingency in Figure 4.13(b), the system becomes unstable with the existing techniques. The computational performance of the techniques is illustrated and compared in Table 4.2, observe that even though the proposed techniques are slower compared to existing ones, the computational cost is such that their application to real-time frequency regulation is feasible, as per [69].

It is important to highlight the fact that the OPT and MPC models are non-convex, nonlinear mathematical models, i.e., Nonlinear Programming (NLP) problems. However, the constraints are at most quadratic, and hence do not present a significant challenge for existing NLP solvers, especially considering the reasonable size of the problem. Thus, for example, for the complex CIGRE benchmark MG system used here, which includes a significant number of DERs, both OPT and MPC models can be solved in less than 0.02 seconds at most, using the CONOPT solver in MATLAB for all cases.

The main factors that could adversely affect the performance of the proposed techniques are the droop gain and voltage setpoint limits of DERs, which should be carefully selected to avoid large system voltage variations. The sample time should also be appropriately chosen so that the proposed models are not solved too often, while still properly regulating frequency; furthermore, since the developed control methods would be implemented in an MGCC with an existing MG communication infrastructure, communication delays should be taken into consideration when defining the sample time.

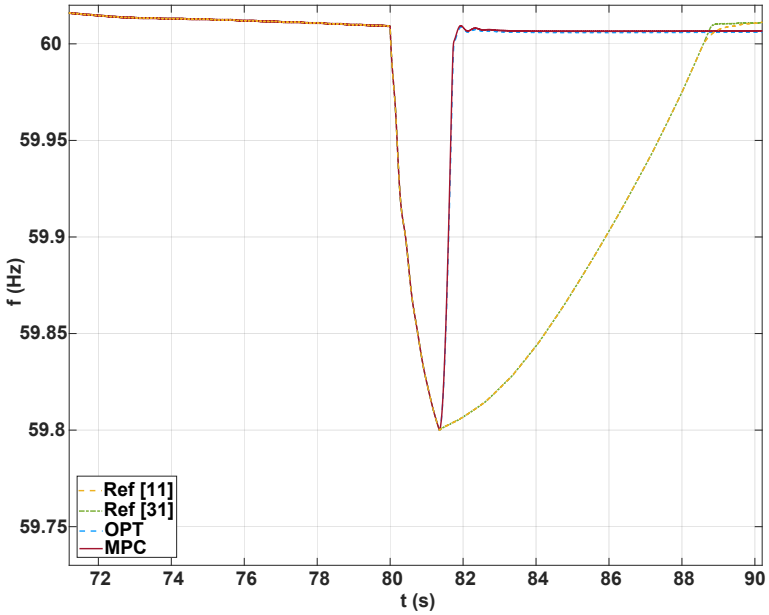

(a) BESS 2-4 Disturbance.

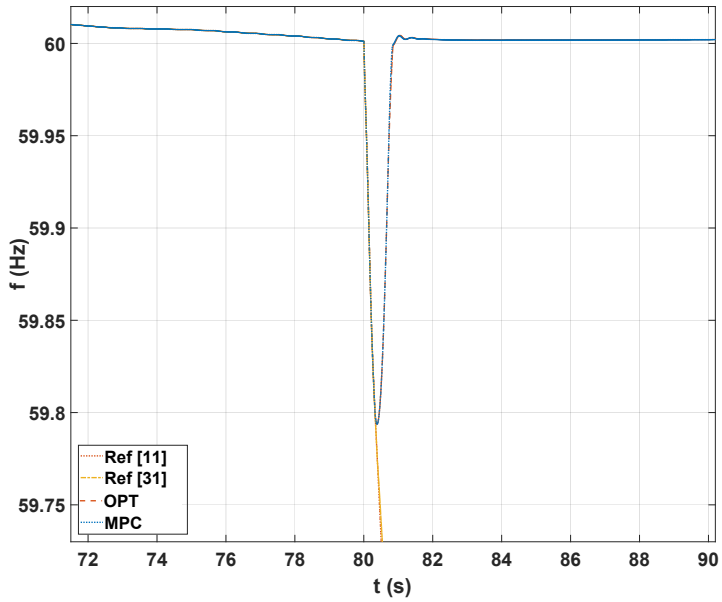

(b) DU 5 Disturbance.

Figure 4.13: Comparison with respect to existing techniques.

4.2 MMG Adaptive Droop Control

The aforementioned optimal droop controller for MGs is extended here for an MMG system, and compared with the proposed distributed consensus control coordination technique discussed in Chapter 3. Thus, to coordinate the grid and MGs of an MMG system, a centralized technique that optimally adjusts the droop gains of the interfacing VSGs is proposed in this section, since frequency regulation is directly proportional to the interfacing VSG droop gain but inversely proportional to the interfacing VSG load-sharing capability. Thus, increasing the droop gain of the interfacing VSG results in more frequency regulation, but that results in a decrease in the VSG load sharing. Hence, to achieve an optimal compromise between load sharing and frequency regulation, an optimization problem based on the model described in Section 4.1 is proposed here to adjust the droop gains of the interfacing converters as discussed next.

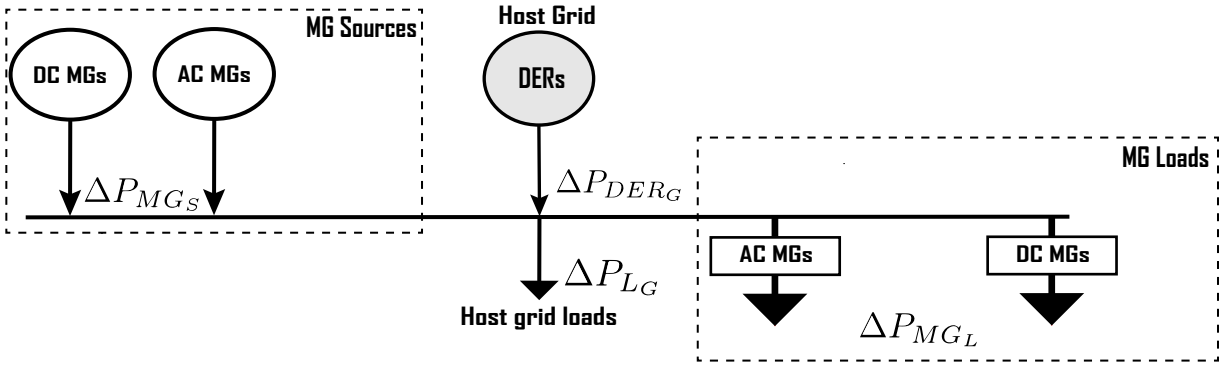

Figure 4.14: Representation of the MMG system for the proposed control optimization problem.

4.2.1 Objective Function

Considering the MMG system depicted in Figure 4.14, the objective would be to minimize at time t the power changes of the MMG as follows, as per (4.1):

$$\min_{K_{MG_S}, K_{DER_G}} \quad \Delta P_{MMG_t} = \sum_{ms=1}^{N_{MG_S}} \Delta P_{MG_{S_{ms,t}}} + \sum_{i=1}^{N_{DER_G}} \Delta P_{DER_{G_{i,t}}} - \sum_{ml=1}^{N_{MG_L}} \Delta P_{MG_{L_{ml,t}}} - \sum_{l=1}^{N_{L_G}} \Delta P_{L_{G_{l,t}}} \tag{4.20}$$

where $P_{MG_{S_{ms,t}}}$ is the output power of the ms^{th} ac/dc MG acting as a source; $P_{DER_{G_{i,t}}}$ is the output power of the i^{th} DER of the host grid; $P_{MG_{L_{ml,t}}}$ is the demand power of the ml^{th} ac/dc MG acting as a load; and $P_{L_{G_{l,t}}}$ is the l^{th} host grid load. ΔP_{MG_L} can be obtained from the corresponding ac/dc MGs acting as loads when the optimization problem is triggered at time t, as follows:

$$\Delta P_{MG_{L_{ml,t}}} = \sum_{l=1}^{N_{L_{MG}}} \Delta P_{L_{ml_{l,t}}} - \sum_{i=1}^{N_{DER_{MG}}} \Delta P_{DER_{ml_{i,t}}} \tag{4.21}$$

where $P_{L_{ml_{l,t}}}$ is the l^{th} load of the ml^{th} MG, and $P_{DER_{ml_{i,t}}}$ is the i^{th} DER power of the ml^{th} MG.

4.2.2 Power Constraints

The output powers of the microgrid interfaces and host grid DERs are constrained as follows:

$$0 \leq P_{MG_{S_{ms,t}}} \leq \overline{P_{MG_{S_{ms,t}}}} \quad \forall ms \tag{4.22}$$

$$P_{MG_{S_{ms,t}}} = P_{MG_{So_{ms,t}}} + \Delta P_{MG_{S}ms,t} \forall ms \tag{4.23}$$

$$P_{DER_{G_{i,t}}} = P_{DER_{G_{o_{i,t}}}} + \Delta P_{DER_{G_{i,t}}} \forall i \tag{4.24}$$

$$\underline{P_{DER_{G_i}}} \leq P_{DER_{G_{i,t}}} \leq \overline{P_{DER_{G_i}}} \quad \forall i \tag{4.25}$$

where $\overline{P_{MG_{S_{ms,t}}}}$ is the available power reserve of the ms^{th} microgrid, which is obtained from the corresponding MG as follows, depending on whether it is an ac MG with voltage dependent loads as per (2.2) or a dc MG:

$$\overline{P_{MG_{S}ms,t}} = \begin{cases} \sum_{l=1}^{N_{L_{MG}}} K_{LP_l} \left[V_{MG_{ms,t}}^{\alpha_{P_l}} - V_{MG_{min}}^{\alpha_{P_l}} \right] + \sum_{i=1}^{N_{DER_{MG}}} \Delta P_{DER_{ms_{i,t}}} & \forall\ ms\ \in\ \mathcal{M}_{MG_{ac}} \\ \sum_{i=1}^{N_{DER_{MG}}} \Delta P_{DER_{ms_{i,t}}} & \forall\ ms\ \in\ \mathcal{M}_{MG_{dc}} \end{cases} \tag{4.26}$$

where $V_{MG_{ms,t}}$ is the ac voltage of the ms^{th} ac MG, and $\Delta P_{DER_{ms_{i,t}}}$ is the available power in the i^{th} DER of the ms^{th} MG. Note that BESSs are not explicitly considered in this model, but can be readily included by adding similar BESS associated constraints such as those presented in Section 4.1.1.4.

The power balance between generators and loads should be maintained, considering system loss changes, albeit small, as follows:

$$\sum_{ms=1}^{N_{MG_S}} \Delta P_{MG_{S_{ms,t}}} + \sum_{i=1}^{N_{DER_G}} \Delta P_{DER_{G_{i,t}}} \geq \sum_{ml=1}^{N_{MG_L}} \Delta P_{MG_{L_{ml,t}}} + \sum_{l=1}^{N_{L_G}} \Delta P_{L_{G_{l,t}}} \tag{4.27}$$

4.2.3 Droop Constraints

The constraints for the droops K_{MGs} of MG interfaces acting as sources and K_{DER_G} of the host grid DERs, and their associated limits can be defined as follows:

$$K_{MG_{S_{ms,t}}} = \beta_{MG_{ms}} P_{MG_{S_{ms,t}}} \qquad \forall ms \tag{4.28}$$

$$0 \leq K_{MG_{S_{ms,t}}} \leq \overline{K_{MG_{S_{ms}}}} \quad \forall ms \tag{4.29}$$

$$K_{DER_{G_{i,t}}} = \beta_{DER_{G_i}} P_{DER_{G_{i,t}}} \quad \forall i \tag{4.30}$$

$$0 \leq K_{DER_{G_{i,t}}} \leq \overline{K_{DER_{G_i}}} \quad \forall i \tag{4.31}$$

where β_{DER} and β_{MG} are parameters chosen based on a linear relation between the maximum power of DERs and MG interfaces, respectively and maximum values of droop constants, as proposed in Section 4.1.1.2.

4.2.4 Implementation

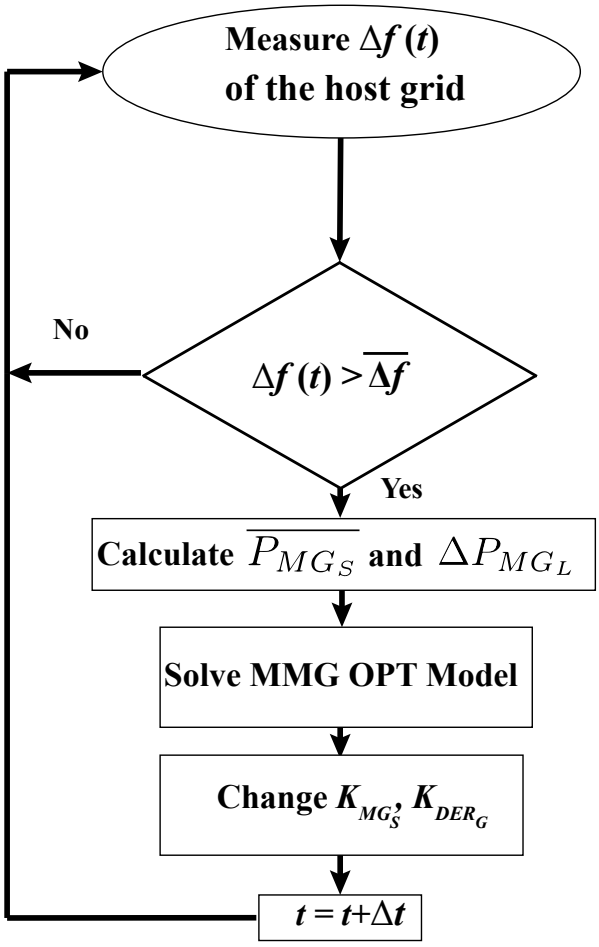

Figure 4.15: Implementation of the proposed optimization control approach.

The implementation of the proposed optimization control approach is illustrated in Figure 4.15, with the optimization problem being solved at time t, every Δt, (e.g., fractions of a second), depending on host grid and its frequency response, as in the case of Figure 4.1. Thus, the optimization problem is solved in a Centralized Controller (CC) when the change in the frequency of the host grid exceeds $\overline{\Delta f}$, which is the maximum acceptable frequency deviation (e.g., 0.2 Hz as per [73]). The CC will accordingly adjust the droop gains of the interfacing VSGs of the MGs acting as sources every Δt, to resolve frequency deviations in

the host grid, which maybe triggered by voltage and/or frequency imbalances within the MMG system and dc MGs, as discussed next.

4.2.5 Case Studies and Results

The proposed controller is compared based on the following case studies, so that direct comparisons of the proposed centralized control can be made, with respect to the distributed controller discussed in Section 3.2.2:

- Case 1 corresponds to the distributed consensus controller for the VSG adaptive inertia and VFC controllers presented in Section 3.2.

- Case 2 corresponds to the proposed adaptive droop controller for the same VSG converters.

The test system, the simulation scenarios, and disturbances are the same as the ones presented in Section 3.2.3.

The simulation results in Figure 4.16 show the frequencies of the ac MGs for the aforementioned cases and disturbances. Note in Figures 4.16(d) and 4.16(a) that the host grid and ac MG 1 frequencies are restored to nominal value after the CC in Case 2 adjusts the droop gains of the interfaces of ac MGs 2 and 3, increasing their frequency regulation, as shown in Figure 4.18 depicting the output powers of the corresponding VSG interfaces. However, the distributed controller in Case 1 shows better overall frequency regulation than Case 2, due to, in part, that it acts continuously as system conditions change, whereas the CC waits until the host grid frequency deviation exceeds a threshold.

Figure 4.17 shows the voltages of the dc MGs. Note in Figure 4.17(b) that the dc voltage of the dc MG 2 recovers to its nominal value for Case 2 after the disturbance at t=50 s, by drawing power from the host grid, as shown in Figure 4.18, which does not affect significantly the host grid frequency due to the frequency regulation provided by the VSGs of ac MGs 2 and 3. Observe that, in general, Case 1 shows better dc-voltage regulation than Case 2 for the aforementioned reasons.

Note in Figures 4.16 and 4.17 that the Bus 5 three-phase fault at t=70 s does not destabilize the system due to the proposed adaptive inertia control in the VSG interfaces for both cases. Table 4.3 shows the global average frequency and dc voltage deviations for all MMG system components, demonstrating that the distributed controller has a superior overall performance compared to the optimization-based adaptive droop controller.

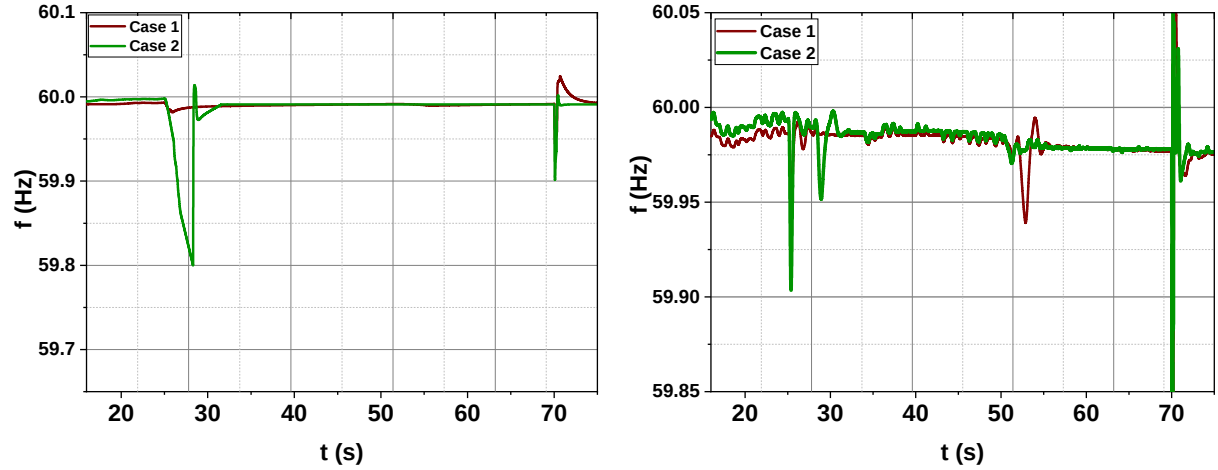

(a) AC MG 1.

(b) AC MG 2.

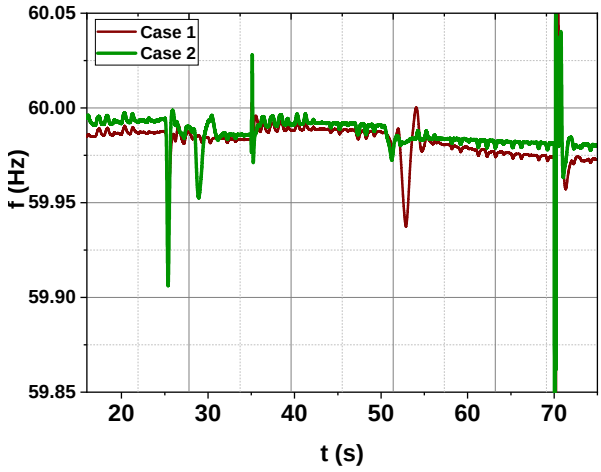

(c) AC MG 3.

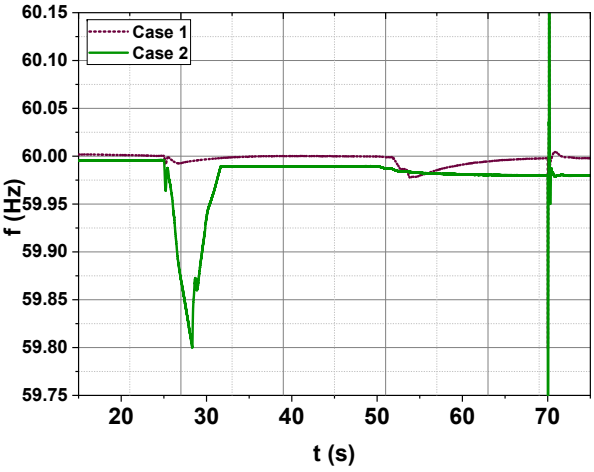

(d) Main grid.

Figure 4.16: AC MG frequencies for different disturbances.

Table 4.3: Global average frequency and dc voltage deviations.

Control scheme	Δf_{AVE}		$\Delta V_{dc_{AVE}}$	
	Hz	%	**V**	%
Case 1	0.011235	0.018725	14.66873	1.955831
Case 2	0.0337675	0.0563	15.59352	2.0791

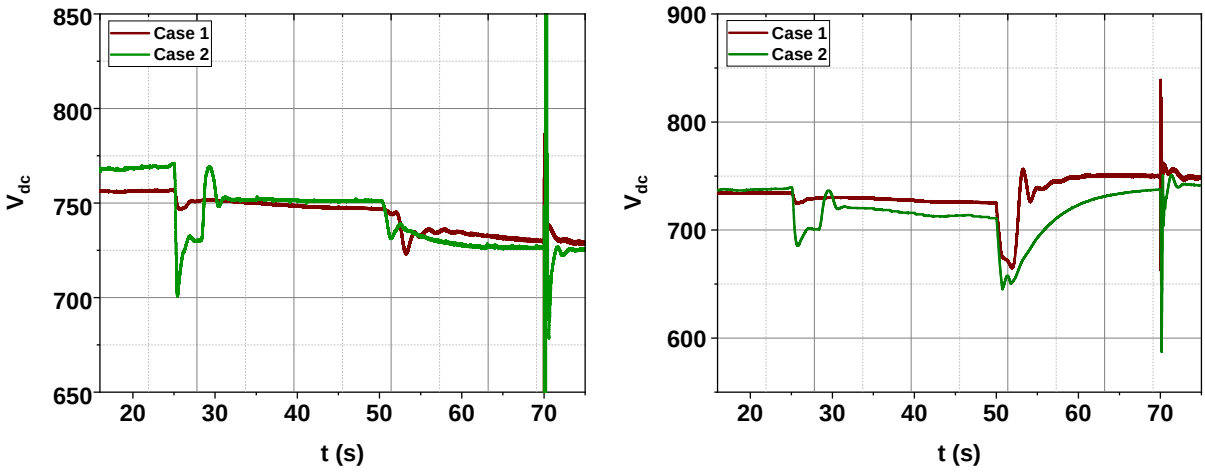

(a) DC MG 1.

(b) DC MG 2.

Figure 4.17: DC MG voltages for different disturbances.

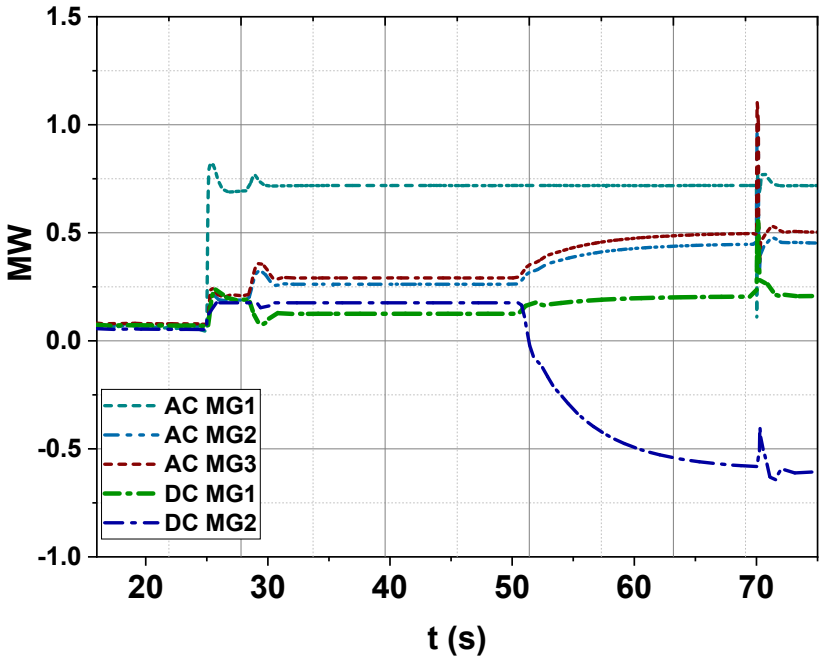

Figure 4.18: Output powers of the VSG interfaces with proposed controllers for Case 2.

4.3 Summary

Two adaptive optimization-based frequency controllers through droop and voltage control for isolated ac MGs have been developed and discussed in this chapter first, to improve the frequency response of the MG and enhance the system's stability and robustness against severe disturbances. The proposed control schemes have been designed to optimally and dynamically change active power droop gains and voltage setpoints of DERs, adjusting their values based on optimization approaches that take into account several factors, such as generation-demand balance, BESS SOC, and the voltage sensitivity of the MG loads. The proposed methodologies were tested on a benchmark MG with multiple DERs, showing that both maintain the frequency stability of the system during severe disturbances, even in the presence of uncertainties and communication delays, performing better than the state-of-art VFC. Overall, the second technique performed slightly better compared to the first proposed method, being more appropriate if faster sample times are required.

In the second part of this chapter, a centralized adaptive droop control technique for the coordination of MMG system is developed, which aims to coordinate the output power

of both ac and dc MGs acting as sources in the overall grid to regulate the host grid frequency based on an optimization approach. The performance of the proposed controller is compared against the distributed consensus controller developed in Chapter 3, observing that the distributed consensus controller shows a superior frequency and dc-voltage regulation compared to the centralized adaptive droop controller.

Some of the content of this chapter has been published in [85].

Chapter 5

Conclusions, Contributions, and Future Work

5.1 Summary

This thesis focuses on control of MGs and MMG systems. Several techniques are proposed in this thesis to control ac and dc MGs and MMG systems, interconnecting the MGs with VSG-Based converter interfaces to control the output powers of the MGs and provide inertia and damping to the system. The output powers of these proposed interfaces are coordinated through both distributed and centralized control schemes. The primary control of the interfacing VSGs adaptively adjusts the inertia and the damping constants to improve both the frequency and dc-voltage responses of the ac/dc interconnected system. Two secondary controllers are proposed to coordinate the MMG system. The first approach is based on a distributed consensus technique that coordinates the system with limited information about the overall grid. The second control approach is based on centralized control technique that adaptively adjusts the droop gains of interfacing VSGs based on an optimization technique. The proposed MG and MMG controllers share the total system load among the host grid and MGs, while minimizing the overall frequency and dc-voltage deviations.

In Chapter 2, the main relevant background for the proposed research was covered. Thus, a general overview of MG modeling, operation, and control were first presented. Then, a brief review of dc MGs was provided. Different layouts and architectures of an MMG were also discussed, together with associated, coordination, and control issues of a

network of MGs. Finally, the VSG principles models, and controls used throughout the thesis were presented.

In Chapter 3, a distributed control scheme was first proposed and discussed for voltage regulation of a dc MG, while proportionally sharing the loads among the DERs and acting as a primary and secondary control at the same time. Simulation results demonstrate the superiority of the distributed controller compared to conventional droop controls, which present several technical challenges, such as the need for careful selection and tuning of droop gains, and stability and voltage regulation issues. The proposed controller is shown to be robust against system disturbances in a realistic test dc MG, and communication link latencies, and could be readily implemented in dc MGs with minimal communication infrastructure and thus costs.

In the second part of Chapter 3, a hierarchical distributed control system to regulate the frequencies and voltages of an MMG system was proposed and developed here. The controller was integrated into a network architecture based on interfacing the MGs with VSG-based MG interfaces, which provide virtual inertia through the realization of the SG swing equation, providing frequency support for an MMG system. A hierarchical controller was also proposed based on an adaptive inertia technique that enhances the system's frequency and dc-voltage responses by adjusting the inertia and damping constants. Furthermore, a distributed controller based on an adaptive consensus technique was presented, which aims to coordinate the output power of both ac and dc MGs to regulate the frequencies and the dc voltages of all MGs based on local MG measurements. This controller can be readily scaled up for larger MMG systems, with minimum communication bandwidth and infrastructure, compared to existing centralized controllers that are prone to single point failures. The results obtained for a test ac/dc MMG demonstrate the advantages of the proposed VSG-based adaptive inertia and damping controllers for the MG interfaces, coordinated by the presented distributed control approach.

In Chapter 4, two adaptive optimization-based frequency controllers through droop and voltage control for isolated ac MGs have been developed and discussed first, to improve the frequency response of the MG and enhance the system's stability and robustness against severe disturbances. The proposed control schemes have been designed to optimally and dynamically change active power droop gains and voltage setpoints of DERs, adjusting their values based on optimization approaches that take into account several factors, such as generation-demand balance, BESS SOC, and the voltage sensitivity of the MG loads. The proposed methodologies were tested on a benchmark MG with multiple DERs, showing that both maintain the frequency stability of the system during severe disturbances, even in the presence of uncertainties and communication delays, performing better than the state-of-art VFC. Overall, the second technique performed slightly better compared to the

first proposed method, being more appropriate if faster sample times are required.

In the second part of Chapter 4, a centralized adaptive droop control technique for the coordination of MMG system is developed, which aims to coordinate the output power of both ac and dc MGs acting as sources in the overall grid to regulate the host grid frequency based on an optimization approach. The performance of the proposed controller is compared against the distributed consensus controller developed in Chapter 3, observing that the distributed consensus controller shows a superior frequency and dc-voltage regulation compared to the centralized adaptive droop controller.

5.2 Contributions

The main contributions of this thesis are the following:

- A VSG based interface for ac MGs with a new adaptive inertia and damping control with VFC has been proposed. The control scheme enhances the frequency response of ac MGs and the host grid in an MMG system, limiting major frequency excursions, especially during severe disturbances, and allowing proper power sharing among the MGs without causing significant power transients, compared to existing control approaches.

- A new control technique has been proposed for VSG-based dc-ac interfaces that improves the voltage dynamics in dc MGs by adjusting the damping constants of the VSG interface, compared to existing control approaches.

- A new distributed consensus controller for dc MGs and MMG systems has been proposed. The proposed controller coordinates the power exchanges among the converter interfaces in dc MGs and the interconnected ac and dc MGs in a MMG systems, maintaining the power balance of the overall system. The developed controller coordinates the system based on limited information about the overall system, which improves its scalability to larger systems and it is robust to single point failures of the communication network.

- Adaptive droop controllers that ensure an optimal compromise between load sharing and frequency regulation for both ac MGs and MMG systems have been presented. The proposed optimization-based techniques continuously adjust the active power droop gains and the voltage setpoints of DERs to maintain the frequency of the system within acceptable limits and enhance the primary frequency response of the

system, while taking into account the active power sensitivity of the loads to the system's operating voltage. The proposed techniques also mitigate stability issues associated with improper selection of DER droop gains.

The contents of this thesis have been published by the time of writing [75], [76], and [85].

5.3 Future Work

Further research may be carried out to address the following issues:

- Develop a distributed OPF for frequency and voltage coordination of the MMG system, and compare its performance against the proposed distributed consensus controller.
- Develop a detailed linearized mathematical models of the VSG interfaces for eigenvalue analyses and study the impact of the synchronous impedance on the eigenvalues of the system.
- Develop an Adaptive Neuro-Fuzzy Inference System (ANFIS) versions of the presented VSG adaptive inertia controllers.

References

[1] M. S. Mahmoud, ed., *Microgrid: Advanced Control Methods and Renewable Energy System Integration*. Butterworth-Heinemann, 1 ed., Nov. 2016.

[2] "IEEE standard for interconnecting distributed resources with electric power systems," *IEEE Std 1547-2003*, pp. 1–28, July 2003.

[3] A. G. Anastasiadis, A. G. Tsikalakis, and N. D. Hatziargyriou, "Operational and environmental benefits due to significant penetration of microgrids and topology sensitivity," in *IEEE PES General Meeting*, pp. 1–8, July 2010.

[4] A. Ouammi, H. Dagdougui, L. Dessaint, and R. Sacile, "Coordinated model predictive-based power flows control in a cooperative network of smart microgrids," *IEEE Transactions on Smart Grid*, vol. 6, pp. 2233–2244, Sept 2015.

[5] H. Dagdougui, A. Ouammi, and R. Sacile, "Optimal control of a network of power microgrids using the Pontryagin's minimum principle," *IEEE Transactions on Control Systems Technology*, vol. 22, pp. 1942–1948, Sept 2014.

[6] A. Ouammi, H. Dagdougui, and R. Sacile, "Optimal control of power flows and energy local storages in a network of microgrids modeled as a system of systems," *IEEE Transactions on Control Systems Technology*, vol. 23, pp. 128–138, Jan 2015.

[7] H. Dagdougui and R. Sacile, "Decentralized control of the power flows in a network of smart microgrids modeled as a team of cooperative agents," *IEEE Transactions on Control Systems Technology*, vol. 22, pp. 510–519, March 2014.

[8] D. Wang, X. Guan, J. Wu, P. Li, P. Zan, and H. Xu, "Integrated energy exchange scheduling for multimicrogrid system with electric vehicles," *IEEE Transactions on Smart Grid*, vol. 7, pp. 1762–1774, July 2016.

[9] Y. Wang, S. Mao, and R. M. Nelms, "On hierarchical power scheduling for the macrogrid and cooperative microgrids," *IEEE Transactions on Industrial Informatics*, vol. 11, pp. 1574–1584, Dec 2015.

[10] C. Bersani, H. Dagdougui, A. Ouammi, and R. Sacile, "Distributed robust control of the power flows in a team of cooperating microgrids," *IEEE Transactions on Control Systems Technology*, vol. 25, pp. 1473–1479, July 2017.

[11] Gil, Nuno, Lopes, and J. Abel, "Exploiting automated demand response, generation and storage capabilities for hierarchical frequency control in islanded multi-microgrids." in *16th PSCC*, Glasgow, Scotland, 2008.

[12] M. Ding, K. Ma, R. Bi, M. Mao, and L. Chang, "A hierarchical control scheme based on multi-agent system for islanded multi-microgrids," in *2013 4th IEEE International Symposium on Power Electronics for Distributed Generation Systems (PEDG)*, pp. 1–5, July 2013.

[13] A. Ghafouri, J. Milimonfared, and G. B. Gharehpetian, "Coordinated control of distributed energy resources and conventional power plants for frequency control of power systems," *IEEE Transactions on Smart Grid*, vol. 6, pp. 104–114, Jan 2015.

[14] P. Wu, W. Huang, N. Tai, and S. Liang, "A novel design of architecture and control for multiple microgrids with hybrid ac/dc connection," *Applied Energy*, vol. 210, pp. 1002 – 1016, 2018.

[15] O. Alarfaj, "Modeling and control of low-voltage dc microgrid with photovoltaic energy resources," Master's thesis, University of Waterloo, 2014.

[16] Y. Nie, M. Dong, W. Yuan, J. Yang, and Z. Liu, "Delay-dependent stability analysis of dc microgrid with distributed control considering communication delay," in *2017 Chinese Automation Congress (CAC)*, pp. 7646–7651, Oct 2017.

[17] S. Moayedi and A. Davoudi, "Distributed tertiary control of dc microgrid clusters," *IEEE Transactions on Power Electronics*, vol. 31, pp. 1717–1733, Feb 2016.

[18] Z. Wang, F. Liu, Y. Chen, S. H. Low, and S. Mei, "Unified distributed control of stand-alone dc microgrids," *IEEE Transactions on Smart Grid*, vol. 10, pp. 1013–1024, Jan 2019.

[19] D. Nguyen and L. Le, "Optimal energy management for cooperative microgrids with renewable energy resources," in *2013 IEEE International Conference on Smart Grid Communications (SmartGridComm)*, pp. 678–683, Oct 2013.

[20] P. Kou, D. Liang, and L. Gao, "Distributed MPC of multiple microgrids for coordinated stochastic energy management," *Applied Energy*, vol. 185, pp. 939 – 952, 2017.

[21] T. Liu, X. Tan, B. Sun, Y. Wu, and D. H. Tsang, "Energy management of cooperative microgrids: A distributed optimization approach," *International Journal of Electrical Power Energy Systems*, vol. 96, pp. 335 – 346, 2018.

[22] P. Srivastava, C. Chang, and J. Cortés, "Participation of microgrids in frequency regulation markets," in *2018 Annual American Control Conference (ACC)*, pp. 3834–3839, June 2018.

[23] C. Chang, S. Martínez, and J. Cortés, "Grid-connected microgrid participation in frequency-regulation markets via hierarchical coordination," in *2017 IEEE 56th Annual Conference on Decision and Control (CDC)*, pp. 3501–3506, Dec 2017.

[24] D. Lu, "Design and Control of a PV Active Generator with Integrated Energy Storages: Application to The Aggregation of Producers and Consumers in an Urban Micro Smart Grid." Ph.D. dissertation, Ecole Centrale de Lille, France, 2010.

[25] K. V. Vidyanandan and N. Senroy, "Primary frequency regulation by deloaded wind turbines using variable droop," *IEEE Transactions on Power Systems*, vol. 28, pp. 837–846, May 2013.

[26] A. Ghafouri, J. Milimonfared, and G. B. Gharehpetian, "Coordinated control of distributed energy resources and conventional power plants for frequency control of power systems," *IEEE Transactions on Smart Grid*, vol. 6, pp. 104–114, Jan 2015.

[27] D. E. Olivares, A. Mehrizi-Sani, A. H. Etemadi, C. A. Cañizares, R. Iravani, M. Kazerani, A. H. Hajimiragha, O. Gomis-Bellmunt, M. Saeedifard, R. Palma-Behnke, G. A. Jiménez-Estévez, and N. D. Hatziargyriou, "Trends in microgrid control," *IEEE Transactions on Smart Grid*, vol. 5, pp. 1905–1919, July 2014.

[28] J. C. Vasquez, J. M. Guerrero, A. Luna, P. Rodriguez, and R. Teodorescu, "Adaptive droop control applied to voltage-source inverters operating in grid-connected and islanded modes," *IEEE Transactions on Industrial Electronics*, vol. 56, no. 10, pp. 4088–4096, 2009.

[29] J. Pan, S. Yu, and M. Ma, "Model predictive load frequency control of isolated micro-grid with electrical vehicles," in *2018 37th Chinese Control Conference (CCC)*, pp. 3588–3593, July 2018.

[30] P. S. V. Sagar and K. S. Swarup, "Load frequency control in isolated micro-grids using centralized model predictive control," in *IEEE International Conference on Power Electronics, Drives and Energy Systems (PEDES)*, pp. 1–6, 2016.

[31] H. Jafari, M. Mahmodi, and H. Rastegar, "Frequency control of a micro-grid in autonomous mode using model predictive control," in *Iranian Conference on Smart Grids*, pp. 1–5, 2012.

[32] X. Dou, P. Xu, Q. Hu, W. Sheng, X. Quan, Z. Wu, and B. Xu, "A distributed voltage control strategy for multi-microgrid active distribution networks considering economy and response speed," *IEEE Access*, vol. 6, pp. 31259–31268, 2018.

[33] S. Bayhan and H. Abu-Rub, "Model predictive droop control of distributed generation inverters in islanded AC microgrid," in *11th IEEE International Conference on Compatibility, Power Electronics and Power Engineering (CPE-POWERENG)*, pp. 247–252, 2017.

[34] A. Saleh, A. Deihimi, and R. Iravani, "Model predictive control of distributed generations with feed-forward output currents," *IEEE Transactions on Smart Grid*, vol. 10, no. 2, pp. 1488–1500, 2019.

[35] J. Mírez, "A modeling and simulation of optimized interconnection between dc microgrids with novel strategies of voltage, power and control," in *2017 IEEE Second International Conference on DC Microgrids (ICDCM)*, pp. 536–541, June 2017.

[36] S. Konar and A. Ghosh, "Interconnection of islanded dc microgrids," in *2015 IEEE PES Asia-Pacific Power and Energy Engineering Conference (APPEEC)*, pp. 1–5, Nov 2015.

[37] M. Hamzeh, M. Ghafouri, H. Karimi, K. Sheshyekani, and J. M. Guerrero, "Power oscillations damping in dc microgrids," *IEEE Transactions on Energy Conversion*, vol. 31, no. 3, pp. 970–980, 2016.

[38] X. Chang, Y. Li, X. Li, and X. Chen, "An active damping method based on a supercapacitor energy storage system to overcome the destabilizing effect of instantaneous constant power loads in dc microgrids," *IEEE Trans. Energy Conversion*, vol. 32, no. 1, pp. 36–47, 2017.

[39] V. Nasirian, Q. Shafiee, J. M. Guerrero, F. L. Lewis, and A. Davoudi, "Droop-free distributed control for ac microgrids," *IEEE Transactions on Power Electronics*, vol. 31, pp. 1600–1617, Feb 2016.

[40] V. Toro and E. Mojica-Nava, "Droop-free control for networked microgrids," in *2016 IEEE Conference on Control Applications (CCA)*, pp. 374–379, Sept 2016.

[41] X. Zhou, L. Zhou, Y. Chen, J. M. Guerrero, A. Luo, W. Wu, and L. Yang, "A microgrid cluster structure and its autonomous coordination control strategy," *International Journal of Electrical Power Energy Systems*, vol. 100, pp. 69 – 80, 2018.

[42] E. Bullich-Massagué, F. Díaz-González, M. Aragüés-Peñalba, F. Girbau-Llistuella, P. Olivella-Rosell, and A. Sumper, "Microgrid clustering architectures," *Applied Energy*, vol. 212, pp. 340 – 361, 2018.

[43] M. Farrokhabadi, C. Cañizares, and K. Bhattacharya, "A voltage-based frequency controller for inverter-based systems in microgrids," in *2016 IEEE Power and Energy Society General Meeting (PESGM)*, pp. 1–5, July 2016.

[44] M. Farrokhabadi, C. A. Cañizares, and K. Bhattacharya, "Frequency control in isolated/islanded microgrids through voltage regulation," *IEEE Transactions on Smart Grid*, vol. 8, pp. 1185–1194, May 2017.

[45] R. Al-Abri, "Voltage stability analysis with high distributed generation (DG) penetration." Ph.D. dissertation, University of Waterloo, Waterloo, Canada, 2012.

[46] E. Nasr-Azadani, "Modeling, stability analysis, and control of distributed generation in the context of microgrids." Ph.D. dissertation, University of Waterloo, Waterloo, Canada, 2014.

[47] F. Guo, C. Wen, J. Mao, and Y. Song, "Distributed secondary voltage and frequency restoration control of droop-controlled inverter-based microgrids," *IEEE Transactions on Industrial Electronics*, vol. 62, pp. 4355–4364, July 2015.

[48] J. Schiffer, T. Seel, J. Raisch, and T. Sezi, "Voltage stability and reactive power sharing in inverter-based microgrids with consensus-based distributed voltage control," *IEEE Transactions on Control Systems Technology*, vol. 24, pp. 96–109, Jan 2016.

[49] A. G. Madureira and J. A. P. Lopes, "Coordinated voltage support in distribution networks with distributed generation and microgrids," *IET Renewable Power Generation*, vol. 3, pp. 439–454, December 2009.

[50] X. Chen, W. Pei, and X. Tang, "Transient stability analyses of micro-grids with multiple distributed generations," in *2010 International Conference on Power System Technology*, pp. 1–8, Oct 2010.

[51] M. Reza, "Stability analysis of transmission systems with high penetration of distributed generation." Ph.D. dissertation, Delft University of Technology, Delft, Netherlands, 2006.

[52] J. G. Slootweg and W. L. Kling, "Impacts of distributed generation on power system transient stability," in *IEEE Power Engineering Society Summer Meeting,*, vol. 2, pp. 862–867 vol.2, July 2002.

[53] C. Dong, Q. Gao, Q. Xiao, X. Yu, L. Pekař, and H. Jia, "Time-delay stability switching boundary determination for dc microgrid clusters with the distributed control framework," *Applied Energy*, vol. 228, pp. 189 – 204, 2018.

[54] D. E. Olivares, A. Mehrizi-Sani, A. H. Etemadi, C. A. Cañizares, R. Iravani, M. Kazerani, A. H. Hajimiragha, O. Gomis-Bellmunt, M. Saeedifard, R. Palma-Behnke, G. A. Jiménez-Estévez, and N. D. Hatziargyriou, "Trends in microgrid control," *IEEE Transactions on Smart Grid*, vol. 5, pp. 1905–1919, July 2014.

[55] K. E. Yeager and J. R. Willis, "Modeling of emergency diesel generators in an 800 megawatt nuclear power plant," *IEEE Transactions on Energy Conversion*, vol. 8, pp. 433–441, Sep 1993.

[56] H. Bevrani, *Microgrid Dynamics and Control*. Hoboken, NJ: John Wiley & Sons, 2017.

[57] M. Farrokhabadi, S. König, C. A. Cañizares, K. Bhattacharya, and T. Leibfried, "Battery energy storage system models for microgrid stability analysis and dynamic simulation," *IEEE Transactions on Power Systems*, vol. 33, pp. 2301–2312, March 2018.

[58] B. V. Solanki, C. A. Cañizares, and K. Bhattacharya, "Practical energy management systems for isolated microgrids," *IEEE Transactions on Smart Grid*, vol. 10, no. 5, pp. 4762–4775, 2019.

[59] K. V. Vidyanandan and N. Senroy, "Primary frequency regulation by deloaded wind turbines using variable droop," *IEEE Transactions on Power Systems*, vol. 28, pp. 837–846, May 2013.

[60] C. Li, P. Rakhra, P. Norman, G. Burt, and P. Clarkson, "Metrology requirements of state-of-the-art protection schemes for dc microgrids," *The Journal of Engineering*, vol. 2018, no. 15, pp. 987–992, 2018.

[61] Mathworks.com, "Average-Value DC-DC Converter." 2019. [Online]. Available: https://www.mathworks.com/help/physmod/sps/ref/averagevaluedcdcconverter.html [Accessed: 01- Apr-2019].

[62] H. Bevrani, T. Ise, and Y. Miura, "Virtual synchronous generators: A survey and new perspectives," *International Journal of Electrical Power Energy Systems*, vol. 54, pp. 244 – 254, 2014.

[63] S. D'Arco, J. A. Suul, and O. B. Fosso, "Small-signal modelling and parametric sensitivity of a virtual synchronous machine," in *PSCC*, pp. 1–9, 2014.

[64] S. D'Arco, J. A. Suul, and O. B. Fosso, "A virtual synchronous machine implementation for distributed control of power converters in smartgrids," *Electric Power Systems Research*, vol. 122, pp. 180 – 197, 2015.

[65] A. Yazdani, *Voltage-sourced Converters in Power Systems: Modeling, Control, and Applications*. Hoboken, N.J: IEEE Press/John Wiley, 2010.

[66] F. Zhang, C. Meng, Y. Yang, C. Sun, C. Ji, Y. Chen, W. Wei, H. Qiu, and G. Yang, "Advantages and challenges of dc microgrid for commercial building a case study from Xiamen University dc microgrid," in *2015 IEEE 1st Int. Conf. DC Microgrids (ICDCM)*, pp. 355–358, June 2015.

[67] X. Wang, P. Wilson, and D. Woodford, "Interfacing transient stability program to emtdc program," in *Proceedings. International Conference on Power System Technology*, vol. 2, pp. 1264–1269, 2002.

[68] M. Arriaga and C. A. Cañizares, "Overview and Analysis of Data for Microgrid at Kasabonika Lake First Nation (KLFN)," *Hatch Project Report, University of Waterloo*, p. 148, Sept 2015.

[69] P. Kansal and A. Bose, "Bandwidth and latency requirements for smart transmission grid applications," *IEEE Trans. Smart Grid*, vol. 3, pp. 1344–1352, Sep. 2012.

[70] A. M. Gole, S. Filizadeh, R. W. Menzies, and P. L. Wilson, "Optimization-enabled electromagnetic transient simulation," *IEEE Transactions on Power Delivery*, vol. 20, no. 1, pp. 512–518, 2005.

[71] R. Teodorescu, *Grid Converters for Photovoltaic and Wind Power Systems*. Piscataway, New Jersey Chichester, West Sussex: IEEE Wiley, 2011.

[72] J. Alipoor, *Study on stabilization of power system with distributed generations using virtual synchronous generator*. PhD thesis, Osaka University, 2015.

[73] "IEEE Standard for Interconnection and Interoperability of Distributed Energy Resources with Associated Electric Power Systems Interfaces," *IEEE Std 1547-2018 (Revision of IEEE Std 1547-2003)*, pp. 1–138, 2018.

[74] "IEC 60038 standard voltages, defines a set of standard voltages for use in low voltage and high voltage AC and DC electricity supply systems. ," *IEC 60038 std voltages*, pp. 1–26, 2009.

[75] B. Alghamdi, K. Wieninger, and C. A. Cañizares, "Distributed voltage control of dc microgrids," in *2020 AEIT International Annual Conference (AEIT)*, pp. 1–6, 2020.

[76] B. Alghamdi and C. A. Cañizares, "Frequency and voltage coordinated control of a grid of microgrids." *IEEE Transactions on Smart Grid*, submitted Dec 2020, 8 pages.

[77] B. V. Solanki, A. Raghurajan, K. Bhattacharya, and C. A. Cañizares, "Including smart loads for optimal demand response in integrated energy management systems for isolated microgrids," *IEEE Transactions on Smart Grid*, vol. 8, no. 4, pp. 1739–1748, 2017.

[78] M. Farrokhabadi, C. A. Cañizares, and K. Bhattacharya, "Unit commitment for isolated microgrids considering frequency control," *IEEE Transactions on Smart Grid*, vol. 9, pp. 3270–3280, Jul. 2018.

[79] P. Kundur, *Power system stability and control*. New York: McGraw-Hill, 1994.

[80] "Distributed Generation Technical Interconnection Requirements: Interconnections at Voltages 50kV and Below." Hydro One Networks Inc., Toronto, ON, Canada, Tech. Rep. DT-10-015 R3, Mar. 2013.

[81] H. Bevrani, M. R. Feizi, and S. Ataee, "Robust frequency control in an islanded microgrid: H_∞ and μ-Synthesis Approaches," *IEEE Transactions on Smart Grid*, vol. 7, no. 2, pp. 706–717, 2016.

[82] B. V. Solanki, K. Bhattacharya, and C. A. Cañizares, "A sustainable energy management system for isolated microgrids," *IEEE Transactions on Sustainable Energy*, vol. 8, pp. 1507–1517, Oct 2017.

[83] M. Farrokhabadi, C. Cañizares, and K. Bhattacharya, "A voltage-based frequency controller for inverter-based systems in microgrids," in *2016 IEEE Power and Energy Society General Meeting (PESGM)*, pp. 1–5, July 2016.

[84] C. Ahumada, R. Cárdenas, D. Sáez, and J. M. Guerrero, "Secondary control strategies for frequency restoration in islanded microgrids with consideration of communication delays," *IEEE Transactions on Smart Grid*, vol. 7, no. 3, pp. 1430–1441, 2016.

[85] B. Alghamdi and C. A. Cañizares, "Frequency regulation in isolated microgrids through optimal droop gain and voltage control," *IEEE Transactions on Smart Grid*, pp. 1–11, 2020.

APPENDICES

Appendix A

Relevant data for the dc test MG based on a dc MG in Xiamen University, China, are presented here.

Table 5.1: Main parameters.

Parameter	**Value**
DC microgrid voltage	380 V_{dc}
LED load	20 kW
EV load	40 kW
A-C load	30 kW
PV	150 kW
Grid interface	160 kW
BESS 1	33.6 kW
BESS 2	33.6 kW
BESS 1 max SOC	38 kWh
BESS 2 max SOC	38 kWh
Lines resistances	5 mΩ
K_{P_V}	1
K_{I_V}	7
Distributed controller time constant	0.15 s

Table 5.2: BESS parameters.

Parameter	**Value**
Rated voltage	430 V
Switching frequency	25 kHz
C_{dc}	175.7859 μF
L_{dc}	0.168 mH
K_{P_I}	2
K_{I_I}	12

Table 5.3: PV parameters.

Parameter	**Value**
Rated voltage	430 V
Switching frequency	25 kHz
C_{dc}	527.9471 μF
L_{dc}	100 μH
K_{P_I}	2
K_{I_I}	8

Table 5.4: Load converter parameters.

Parameter	**Value**
Rated voltage	430 V
Switching frequency	25 kHz
C_{dc}	130 μF
L_{dc}	0.125 mH
K_{P_V}	2
K_{I_V}	4
K_{P_I}	2
K_{I_I}	10

Appendix B

The data for the MMG test system and associated VSGs are provided here.

Table 5.5: VSG interface parameters.

Parameter	**Value**
S_b	1.65 MVA
V_{base}	12.45 kV
V_{dc}	2.5 kV_{dc}
H	4.31 s
J_o	0.0001 s^2
D_o	1 s
ω_n	376.992 rad/s
K_{P_Q}	5
K_{I_Q}	10
K_{P_V}	6
K_{I_V}	7.6923
AC Current controller K_{P_I}	3
AC Current controller K_{I_I}	15
DC controller K_{P_I}	10
DC controller K_{I_I}	15
K_{Pdc}	20
K_{Idc}	10
L_f	1.65 mH
R_f	20 mΩ
C_f	220 μF

Table 5.6: B2B VSG adaptive inertia controller parameters.

Parameter	Value
J_{big}	0.01 s^2
J_{small}	$5*10^{-5} s^2$
D_o	1 s
D_{big}	3 s
τ_{AI1}	0.25 s
τ_{AI2}	0.25 s
τ_{AI3}	0.35 s
K_{AI}	1

Table 5.7: DC-AC VSG adaptive damping controller parameters.

Parameter	Value
K_{dc}	0.3
τ_{dc}	0.35 s
$\tau_{1_{dc}}$	0.01 s
$\tau_{2_{dc}}$	0.25 s
D_o	1 s

Table 5.8: MGs load parameters.

MG	Phase A (kVA)		Phase B (kVA)		Phase C (kVA)		PF	
	Res.	Com.	Res.	Com.	Res.	Com.	Res.	Com.
AC MG 1	361	95	210	175	250	175	0.9	0.85
AC MG 2	220	235	351	120	85	80	0.95	0.8
AC MG 3	322	160	233	90	345	110	0.9	0.9
Host grid	100	25	250	60	50	15	0.95	0.8
DC MG 1	1151 kW							
DC MG 2	1391 kW							

Table 5.9: AC BESS and WG parameters.

Parameters	**BESS**	**WG**
Switching frequency	5 kHz	5 kHz
L_f	3 mH	1.5
R_f	30 mΩ	15 mΩ
C_f	100 μF	200 μF
K_{P_I}	5	5
K_{I_I}	25	25

Table 5.10: DC BESS parameters.

Parameter	**Value**
Rated voltage	825 V
Switching frequency	25 kHz
C_{dc}	550 μF
L_{dc}	2.5 mH
K_{P_I}	1
K_{I_I}	10

Table 5.11: Governor data.

Parameters	**Value**
τ_{SG_1}	0.01 s
τ_{SG_2}	0.02 s
τ_{SG_3}	0.2 s
τ_{SG_4}	0.25 s
τ_{SG_5}	0.009 s
τ_{SG_6}	0.0384 s
K_{SG}	31
τ_D	0.024 s

Table 5.12: Diesel generators and AVRs.

Parameter	**Value**
R_a	0.0051716 pu
X_l	0.14 pu
X_d	1.014 pu
X_q	0.77 pu
X'_d	0.314 pu
X'_q	0.375 pu
$X"_d$	0.28 pu
$X"_q$	0.375 pu
T'_d0	6.55 s
T'_q0	0.85 s
$T"_{d0}$	0.039 s
$T"_{q0}$	0.071 s
ω_n	376.992 rad/s
H	0.5134 s
K_F	0.03 pu
τ_{SG_7}	0.025 s
τ_{SG_8}	0.1 s
τ_{SG_9}	0.8 s
τ_F	1.0 s
K_{SG}	1 pu

Appendix C

The data for the modified CIGRE benchmark test system are provided here.

Table 5.13: CIGRE test system line parameters.

From Bus	**To Bus**	$\boldsymbol{R_{ph}}$ $\boldsymbol{\Omega/km}$	$\boldsymbol{X_{ph}}$ $\boldsymbol{\Omega/km}$	$\boldsymbol{B_{ph}}$ $\boldsymbol{\mu S/km}$	$\boldsymbol{R_0}$ $\boldsymbol{\Omega/km}$	$\boldsymbol{X_0}$ $\boldsymbol{\Omega/km}$	$\boldsymbol{B_{ph}}$ $\boldsymbol{\mu S/km}$	**Length km**
1	2	0.173	0.432	3.83	0.351	1.8	1.57	1.2
2	3	0.173	0.432	3.83	0.351	1.8	1.57	1
3	4	0.173	0.432	3.83	0.351	1.8	1.57	0.61
4	5	0.173	0.432	3.83	0.351	1.8	1.57	0.56
5	6	0.173	0.432	3.83	0.351	1.8	1.57	1.54
6	7	0.173	0.432	3.83	0.351	1.8	1.57	0.24
7	8	0.173	0.432	3.83	0.351	1.8	1.57	1.67
8	9	0.173	0.432	3.83	0.351	1.8	1.57	0.32
9	10	0.173	0.432	3.83	0.351	1.8	1.57	0.77
10	11	0.173	0.432	3.83	0.351	1.8	1.57	0.33
11	4	0.173	0.432	3.83	0.351	1.8	1.57	0.49
3	8	0.173	0.432	3.83	0.351	1.8	1.57	1.3
12	13	0.173	0.432	3.83	0.351	1.8	1.57	4.89
13	14	0.173	0.432	3.83	0.351	1.8	1.57	2.99
14	8	0.173	0.432	3.83	0.351	1.8	1.57	2

Table 5.14: Governor data.

Parameters	**Value**
τ_{SG_1}	0.01 s
τ_{SG_2}	0.02 s
τ_{SG_3}	0.2 s
τ_{SG_4}	0.25 s
τ_{SG_5}	0.009 s
τ_{SG_6}	0.0384 s
K_{SG}	31
τ_D	0.024 s

Table 5.15: Diesel generators and AVRs.

Parameter	**Value**
R_a	0.0051716 pu
X_l	0.14 pu
X_d	1.014 pu
X_q	0.77 pu
X'_d	0.314 pu
X'_q	0.375 pu
$X"_d$	0.28 pu
$X"_q$	0.375 pu
T'_d0	6.55 s
T'_q0	0.85 s
$T"_{d0}$	0.039 s
$T"_{q0}$	0.071 s
ω_n	376.992 rad/s
H	0.5134 s
K_F	0.03 pu
τ_{SG_7}	0.025 s
τ_{SG_8}	0.1 s
τ_{SG_9}	0.8 s
τ_F	1.0 s
K_{SG}	1 pu

Table 5.16: Loads apparent power.

Bus	Phase A (kVA)		Phase B (kVA)		Phase C (kVA)		PF		
	Res.	Com.	Res.	Com.	Res.	Com.	Res.	Com.	Res.*
1	223.6*	–	–	130	260	130	0.9	0.8	0.95
2	130	260	650	260	–	260	0.95	0.85	–
3	–	104	260	104	65	104	0.9	0.8	–
4	260	–	130	–	130	–	0.9	–	–
5	260	65	223.6*	260	–	65	0.95	0.85	0.95
6	65	–	130	–	223.6*	–	0.95	–	0.95
7	–	130	130	130	–	130	0.95	0.95	–
8	130	–	195	–	–	260	0.9	0.9	–
9	130	–	195	–	130	–	0.95	–	–
10	195	–	130	–	325	–	0.9	–	–
11	65	195	65	195	–	195	0.95	0.85	–
12	223.6*	104	223.6*	104	–	104	0.9	0.8	0.95
13	–	188.5	–	188.5	–	188.5	0.95	0.85	–
14	–	117	–	117	223.6*	117	0.9	0.9	0.95

Table 5.17: BESS and WG parameters.

Parameters	BESS	WG
Switching frequency	5 kHz	5 kHz
L_f	3 mH	1.5 mH
R_f	30 mΩ	15 mΩ
C_f	100 μF	200 μF
K_{P_I}	5	5
K_{I_I}	25	25